Master's thesis

NTNU
Norwegian University of Science and Technology
Faculty of Information Technology and Electrical Engineering
Department of Electric Power Engineering

Anette Solheim

Incorporating Demand Side Response in Power System Adequacy Studies

Master's thesis in Energy and Environmental Engineering
Supervisor: Vijay Venu Vadlamudi
June 2019

NTNU
Norwegian University of Science and Technology

Anette Solheim

Incorporating Demand Side Response in Power System Adequacy Studies

Master's thesis in Energy and Environmental Engineering
Supervisor: Vijay Venu Vadlamudi
June 2019

Norwegian University of Science and Technology
Faculty of Information Technology and Electrical Engineering
Department of Electric Power Engineering

NTNU
Norwegian University of
Science and Technology

Abstract

The objective of this thesis is to incorporate demand side response (DSR) in power system adequacy assessment. Today, the power system is experiencing changes that can challenge the system's adequacy. As a result of the rising share of intermittent renewable production it is expected that there will be a growth in flexibility needs. Further, the widespread implementation of power demanding devices introduces grid supply challenges. A responsive demand side that shifts load from peak hours to off-peak hours can relieve some of these flexibility needs and contribute to improvement of the system's adequacy.

The main adequacy indices used in this thesis are Loss of Load Expectation (LOLE) and Expected Energy Not Supplied (EENS). The DSR models consist of two methods for load shifting, referred to as load shifting method (LSM)1 and LSM2, and a model for price-responsive demand, real-time pricing (RTP) model. LSM1 is based on a model found in literature which has a load recovery procedure that can create spikes in the load profile for greater amount of shifted load. Such spikes can illustrate rebound effects that can appear when loads are reconnected after a disconnection period. Thus, in LSM2, a uniformly distributed load level in the valleys is proposed. Effective Load Carrying Capability (ELCC) is chosen as the capacity credit and existing software that calculates the ELCC at hierarchical level (HL)I for other types of resources is extended to handle DSR resources available for load shifting modelled by LSM2 for both HLI and HLII evaluations. The generation- and composite system assessment, and ELCC calculations are performed on two standard test systems, the Roy Billinton Test System (RBTS) and the IEEE-Reliability Test System (RTS).

The main results for the assessment reveal that load shifting performed by LSM1 and LSM2 has a positive influence on system indices. Bus indices that experience most improvement in index values are buses with lowest curtailment costs. Bus indices of buses that are less connected, e.g. radial connections, appear to have little improvement with increased amount of shifted load. It is observed that indices obtained with LSM2 are lower than the indices obtained with LSM1 at

higher load shifting percentages due to the different valley filling procedures of these methods. The results obtained with the RTP model show that higher price differences, especially in high demand periods, give greater load responses which improve the adequacy indices. Further, increased elasticity coefficients are shown to improve the indices until a self-elasticity coefficient of -0.4 for the case studied. An increase in the index values is observed with this elasticity coefficient since load spikes are introduced in the load recovery period.

The ELCC results show that the procedure is dependent upon the system size and configuration, and which index that is used in the evaluation. The EENS index yields in general higher ELCC values than the LOLE index. The ELCC for increasing amount of DSR resources is investigated and the main observations are a declining increase in ELCC for the RBTS, and little difference between the ELCC at HLI and HLII for the RTS due to a reliable transmission grid in this network. A fixed amount of energy demand available for load shifting is evaluated at each bus in the RTS. The results show that the ELCC is differing among the buses.

Sammendrag

Formålet med denne avhandlingen er å innlemme forbrukerfleksibilitet i pålitelighetsstudier for kraftsystemet. I disse dager opplever kraftsystemet endringer som kan svekke leveringspåliteligheten. Som et resultat av økende andel fornybar produksjon er det forventet at det vil være et voksende behov for fleksibilitet. Videre kan den utbredte bruken av effektkrevende enheter og apparater bidra til å svekke forsyningspåliteligheten til nettet. Forbrukere som kan respondere ved å flytte last fra topplasttimer til timer med lavere forbruk, kan lette på noe av fleksibilitetsbehovet og bidra til å forbedre systemets pålitelighet.

Pålitelighetsindeksene som hovedsakelig brukes i analysene er Loss of Load Expectation (LOLE) og Expected Energy Not Supplied (EENS). Forbrukerfleksibilitetsmodellene består av to modeller for lastflytting, referert til som LSM1 og LSM2, og en modell for last som responderer på spotpriser (RTP-modell). LSM1 er basert på en modell funnet i litteraturen der det kan oppstå høye lastverdier i enkelte av timene lasten flyttes til ved større mengder flyttet energiforbruk. Dette kan illustrere effekttopper som kan oppstå når last gjeninnkobles etter en utkoblingsperiode. LSM2 er derfor implementert for å lage en helt flat profil i timene lasten flyttes til. Effective Load Carrying Capability (ELCC) er valgt som mål for kapasitetsverdien av forbrukerfleksibilitet og eksisterende programvare er utvidet til å håndtere forbrukerfleksibilitetsressurser i form av lastflytting modellert ved LSM2. Studiene for produksjons- og transmisjonssystemet, samt ELCC-beregningene er utført på to standard testsystemer, Roy Billinton Test System (RBTS) og IEEE-Reliability Test System (RTS).

Hovedresultatene fra studiene avslører at lastflytting har en positiv innvirkning på pålitelighetsindeksene. Nodeindeksene som opplever størst forbedring i indeksverdier tilhører noder med lavest kostnad for å kutte betjeningen til lasten. Nodeindekser for noder som er dårligere forbundet, f.eks. radielle forbindelser, viser seg å oppnå liten forbedring i indeksverdier med økende mengde flyttet last. Det observeres at indekser beregnet med LSM2 ved større mengder flyttet last er

lavere enn indeksene beregnet med LSM1 på grunn av de ulike strategiene for å gjenvinne last i timene med lavere forbruk. Resultatene fra RTP-modellen viser at høyere prisforskjeller, særlig i periodene med høy last, gir økt lastflytting som observeres å være positivt for påliteligheten. Økende priselastisitetskoeffisienter forbedrer indeksene inntil en selvelastisitetskoeffisient lik -0.4 for casen som studeres. En økning observeres ved denne elastisitetskoeffisienten fordi høye lastverdier opptrer når mye last flyttes til enkelte timer.

Resultatene fra ELCC-beregningene viser at prosedyren er avhengig av størrelsen og konfigurasjonen til systemet, i tillegg til hvilken indeks som brukes i evalueringen. EENS-indeksen gir generelt høyere ELCC-verdier enn LOLE-indeksen. ELCC for økende mengde av forbrukerfleksibilitetsressurser undersøkes og hovedobservasjonene er en avtakende stigning i verdi for RBTS, samt at det er lite forskjell mellom ELCC-verdiene for hierarkisk nivå (HL)I og HLII for RTS grunnet et svært pålitelig nett i det sistnevnte systemet. En gitt mengde forbrukerfleksibilitetsressurser evalueres for hver node i RTS. Resultatene viser at ELCC-verdiene varierer mellom nodene.

Acknowledgement

This thesis concludes my Master of Science (MSc) degree in Energy and Environmental Engineering at the Department of Electric Power Engineering at the Norwegian University of Science and Technology (NTNU). I am truly grateful for everything I have learned during the thesis work and for all my years in Trondheim.

I would like to thank my supervisor, Associate Professor Vijay Venu Vadlamudi at the Department of Electric Power Engineering, NTNU, for great guidance and good discussions throughout the semester. Your inputs, availability and burning commitment for power system reliability and research in general are highly appreciated.

Lastly, I would like to express gratitude towards my family and friends for all your love and support. You have always believed in me, and for that I am sincerely grateful.

Trondheim, June 2019

Anette Solheim

Contents

Abbreviations

BRP	Balance Responsible Party
CIGRE	International Council on Large Electric Systems
COPT	Capacity Outage Probability Table
CPP	Critical Peak Pricing
CV	Coefficient of Variation
DPL	Daily Peak Load
DSM	Demand Side Management
DSO	Distribution System Operator
DSR	Demand Side Response
ECC	Equivalent Conventional Capacity
EENS	Expected Energy Not Supplied
EEU	Expected Energy Unserved
EFC	Equivalent Firm Capacity
ELCC	Effective Load Carrying Capability
ENC	Equivalent Network Capacity
EUE	Expected Unserved Energy

FOR	Forced Outage Rate
HL	Hierarchical Level
HPL	Hourly Peak Load
IBP	Incentive Based Program
ICT	Information and Communication Technology
IEEE	Institute of Electrical and Electronics Engineers
LDC	Load Duration Curve
LOEE	Loss of Energy Expectation
LOL	Loss of Load
LOLE	Loss of Load Expectation
LOLP	Loss of Load Probability
LSM1	Load Shifting Method 1
LSM2	Load Shifting Method 2
MCS	Monte Carlo Simulation
MDT	Mean Down Time
MTTF	Mean Time to Failure
MTTR	Mean Time to Repair
OPF	Optimal Power Flow
PBP	Price Based Program
PEM	Price Elasticity Matrix
RBTS	Roy Billinton Test System
RTP	Real-Time Pricing

RTS	IEEE-Reliability Test System
TOU	Time of Use
TSO	Transmission System Operator
TTF	Time to Failure
TTR	Time to Repair
WPL	Weekly Peak Load
YPL	Yearly Peak Load

Nomenclature

Common

ΔT	Duration of time increment
λ	Expected failure rate
μ	Expected repair rate
p_i	Probability of compoment being in derated state i

Analytical Framework

C	Total installed capacity of system [MW]
g	Capacity of generating unit being added to the COPT as a two-state unit [MW]
g_i	Capacity of derated state i for a generating unit being added to the COPT as a multi-state unit
$LOLP_t$	The LOLP value in time increment t
n	Total amount of derated states for a generating unit
$P'(X)$	Cumulative probability of event X before addition of a new generating unit
$P(X \geq x_j)$	Cumulative probability of capacity outage
$p(X)$	Individual probability of event X
x_j	Capacity outage in state j [MW]

Simulation Framework

β	Coefficient of variation
$EENS^{MCS}$	EENS calculated by Monte Carlo simulation
$LOLE^{MCS}$	LOLE calculated by Monte Carlo simulation
$LOLP^{MCS}$	LOLP calculated by Monte Carlo simulation
M	Amount of time increments in the simulation
m	Amount of transition rates for a system
N	Amount of simulation years in the simulation
T	System transition time
x_j	System state variable for state j
Z	Energy deficit in loss-of-load event

Load Model for Test Systems

$HPL_{h,d,w}$	Hourly peak load in hour h, day d and week w [MW]
l_d	Daily peak load as a percentage of weekly peak load
l_h	Hourly peak load as a percentage of daily peak load
l_w	Weekly peak load as a percentage of yearly peak load
YPL	Yearly peak load [MW]

Load Shifting Model

Ω	Set of on-peak hours where energy is shaved
$\overline{L(t)}$	Load shifted model [MW]
Ψ	Set of off-peak hours where energy is recovered
A	Amount of load added to each off-peak hour in Ψ [MWh/h]
a	Percentage of shaved energy that is recovered during off-peak hours

$L(t)$	Original load model [MW]
L_t	Load level in time increment t [MW]
N	Amount of off-peak hours in Ψ
P	System peak demand after implementation of DSR activities [MW]

Real-Time Pricing Model

Δd	Change in demand
Δp	Change in price
ε_{ii}	Self-elasticity
ε_{ij}	Cross-elasticity
d_0	Demand in equilibrium point/initial demand
p_0	Price in equilibrium point/initial price

Effective Load Carrying Capability

ΔL	The additional load that can be served by the system with DSR resources [MW]
$EENS^{DSR}$	The EENS value of the system with DSR resources
$EENS^{Org}$	The EENS value of the original system
$L_{new,max}$	System peak load of new time series [MW]
$L_{old,max}$	System peak load of old time series [MW]
L_t^{DSR}	Load level in time increment t for a load shifted curve [MW]
$LOLE^{DSR}$	The LOLE value of the system with DSR resources
$LOLE^{Org}$	The LOLE value of the original system

List of Figures

List of Tables

Chapter 1

Introduction

1.1 Background

Adequacy studies are an essential part when conducting planning and operational analysis for power systems. A wide range of adequacy indices are used to ensure that the power system satisfies the desired level of security of supply. Deterministic criteria such as the N-1 criterion and the reserve margin criteria have been frequently used in the past. These deterministic criteria are relatively easy to use and interpret, but they do not account for the uncertain behaviour of a power system. Probabilistic indices are necessary to be able to capture the stochastic nature of power systems [1].

Increased amount of intermittent renewable resources, phase-out of flexible coal and gas power plants, in addition to a changing energy demand at the consumer side with increased use of power demanding appliances such as electric car chargers, challenge the security of supply [2]. Due to these changes, the power system in Europe is expected to observe a rising scarcity of flexibility. Demand side response (DSR) programs are one type of resources that can offer flexibility and thus improve the system reliability. The Norwegian Transmission System Operator (TSO), Statnett, has found that there is a great potential for flexibility resources in the Nordic countries. Along with flexible production and energy storage, this also includes consumer flexibility and DSR programs [3]. The literature review conducted in [3] finds that the demand flexibility in the Nordics can be estimated to be 12 GW in 2040, where industry can contribute with 5 GW and residential heating can contribute with 6 GW.

With the introduction of the smart grid regime, smart meters and other smart house technologies,

the possibilities for DSR have gained a lot of attention recent years [4]. Smart meters and information and communication technology (ICT) that enable two-way communication between the consumer and the utility, are facilitating the possibility for load shifting at the demand side. Load shifting can help to reduce supply fluctuations and bottlenecks in the grid on an intra-hour and intra-day basis. The demand for electricity has traditionally had weak price elasticity, and there have been little incentives for the consumers to shift load. Until this point there has been low transparency in prices and no real-time monitoring of consumption leading to a consumer that neither knows when the prices are high, nor benefits from shifting load within the hours of the day since the consumption is not monitored in real-time [5]. Smart meters and real-time pricing (RTP) can change this. As stated in [5], it is likely that smart meters and RTP can shift the short-run price elasticity from almost inelastic demand, i.e. below 0.5 in absolute value, towards 1.0 in absolute value. In addition, ICT, automation and aggregator services can lower the transaction costs for the consumers and that will further increase the price elasticity of demand.

The influence of DSR on power system reliability is an evident topic of interest. Following this, for long-term planning analysis it can be advantageous to obtain a measure that quantifies the value of having available DSR resources in the system. Capacity credits, like Effective Load Carrying Capability (ELCC), enable the possibility to compare DSR resources with other resources such as additional generating and transmission capacity in a framework of reliability needs. Furthermore, obtaining a capacity value of DSR can give a better indication of the potential within different markets and sectors and provide a guide to the real cost of DSR [6].

1.2 Scope

The objective of this thesis is to incorporate DSR in power system adequacy studies. The studies concern generation and composite levels. The thesis focus on probabilistic methods that are well known within the field of power system reliability. The main concepts used are Loss of Load Probability (LOLP), Loss of Load Expectation (LOLE), Expected Energy Not Supplied (EENS) and ELCC. Software developed by previous Master students at the Department of Electric Power Engineering at NTNU [7, 8], are used to calculate indices by an analytical approach and a simulation approach, respectively. The software for ELCC calculations was originally developed by [7] and has now been modified to handle DSR resources at generation and composite levels. New software for the modelling of DSR is developed and listed under the contributions below.

The thesis focuses on presenting the methodology and explaining concepts in power system adequacy studies including DSR in a pedagogical and transparent manner. Thus, the thesis does not look into real-case scenarios or present results from real-life power systems. Standard reliability test systems are used in the case studies, namely the Roy Billinton Test System (RBTS) and the IEEE-Reliability Test System (RTS).

Contributions of the thesis' work:

1. Two methods for load shifting are implemented in this thesis, referred to as load shifting method (LSM)1 and LSM2. LSM1 is a standard method provided in literature which studies the impact of DSR on power system adequacy indices. LSM1 adds an equal amount of load to each valley hour in the load recovery period. For greater amounts of shifted load, spikes can be introduced in the profile. Such power spikes can occur when loads are reconnected after a disconnection period. A contribution of the thesis is the creation of a modified version of LSM1, named LSM2. In LSM2, an even load level in the valleys is proposed. The main objective by implementing LSM2 in addition to LSM1 is to investigate how the different valley filling procedures of the two methods affect the adequacy.

2. LSM1 and LSM2 are effective from a centralized authority's point of view. However, in a deregulated power system, DSR can be achieved with active participation of consumers responding to price signals. A real-time pricing (RTP) model is implemented based on literature of consumer modelling through price elasticity matrices and nodal price calculation by OPF. An OPF formulation is chosen such that nodal prices can correlate with load data of the test systems, system topology, system constraints and production costs. In addition, outage cases can be used to trigger higher prices that will correlate to the hours with highest load demand in the yearly load profiles. The model is incorporated into an existing simulation framework at hierarchical level (HL)II.

3. One way to measure the value of having DSR resources in a power system is through ELCC. A method to calculate the ELCC of DSR resources at HLI and HLII is presented. Few sources in literature deal with this concept for DSR resources, and it is difficult to find detailed explanations of the calculation method. Existing software that calculates the ELCC at HLI for other type of resources like additional generating units or interconnector capacity is extended to handle DSR resources available for load shifting for both HLI and HLII evaluations. Changes are made to LSM2 which allow the user of the software to specify the available amount of MWh

of energy that can be used for load shifting at system or bus loads in the ELCC calculations.

4. The existing indigenous software for power system adequacy studies is suitably extended to incorporate the DSR models, and released for further internal use and research at the Department of Electric Power Engineering at NTNU.

5. This thesis gives a pedagogical introduction to the field of power system reliability with a focus on generation and composite system adequacy. This includes detailed explanations of both an analytical method and a simulation approach that are used to obtain adequacy indices. The concept of DSR is also treated and presented with a view to pedagogical clarity. Possible benefits, barriers and future market solutions for DSR are also included.

1.3 Thesis Structure

The work conducted in this thesis builds on a specialization project undertaken during the autumn of 2018. The reader should note the following:

For establishing narrative clarity and with an aim to make this thesis a complete and independent unit in and of itself, much of the content from chapters 2 and some from chapter 3 and 4 is a replication of the specialization project work, with suitable extensions where deemed necessary. The specialization project work did concern generation system adequacy, while the master thesis has been extended to also include composite system adequacy.

Chapter 1 - *Introduction*, provides the context, scope and contributions of the thesis.

Chapter 2 - *Fundamental Concepts in Power System Reliability Studies*, gives an introduction to power system reliability with its definitions, classifications and categorization of power system reliability studies.

Chapter 3 - *Theory of HLI- and HLII Adequacy Assessment*, presents the division of methods in generation and composite system adequacy assessment. An analytical approach and a simulation technique are further described. The probabilistic indices chosen for the analysis in the thesis are presented.

Chapter 4 - *Theory of Demand Side Response*, introduces the reader to the concept of DSR and provides a selected sample of previous work done on DSR and power system adequacy. Further, the

chapter presents a model for load shifting on a demand curve, and a model considering RTP and price elasticity. Lastly, the chapter presents a method to evaluate the capacity value of DSR. The chosen measure is ELCC.

Chapter 5 - *Methodological Approach*, presents the implementation of two variations of the load shifting model, and the calculation procedure for the RTP model. A graphical method used for the capacity credit calculations is also presented.

Chapter 6 - *Case Study Results and Discussion*, presents and discusses the results obtained by utilizing methodological approaches for evaluating the impact of DSR on adequacy and calculates the capacity value of DSR for generation and composite system adequacy. Standard test systems are utilized in the case study.

Chapter 7 - *Conclusions and Future Work*, gives a summary of the main findings and results from Chapter 6. Suggestions for future work are also listed in this chapter.

Chapter 2

Fundamental Concepts in Power System Reliability Studies

This chapter introduces the reader to the fundamental concepts in power system reliability studies. The definition and classification of power system reliability are provided, along with the categorization of power system reliability studies.

2.1 Introduction

Electric power systems are known to be highly complex systems. Factors such that electricity has to be consumed the moment it is produced, that the flows of electric power follows physical laws rather than scheduled transmission routes and that a disturbance at one point in the system can have consequences at system points distant from the fault location, have been well known for power system planners and operators since the early start of electricity supply [1]. Today, the power system planners and operators are also facing new aspects in a changing power system. Some of these elements are a greater share of unpredictable renewable energy resources in the generation mix and a changing consumption pattern including the growth in electric vehicles and charging stations. In Europe, due to these changes it has become evident that there is a need for more flexibility in the power system. Further factors that challenge the security of supply in Europe are the reduced profitability of gas power plants leading to periods of mothballing and the shutdown of old nuclear and coal power plants in line with new climate and energy policies [9]. Thus, flexible power plants

are being phased out to meet the climate goals. In consequence, all these factors challenge the power system reliability.

To design and operate an adequate power system has become a great concern for the European TSOs after the introduction of more intermittent renewable energy resources, and also to avoid over-capacity and incorrect investment signals. In addition, power system adequacy has to a large extent been a national issue. This is not the case anymore as the power system becomes more interconnected and the exchange of power becomes more frequently. Europe has a transition towards a single electricity market, and the scope of the adequacy problem is no longer just a national issue [9].

Even though the structure of the power system is more complex and interconnected today, there has always been a need for reliability criteria. The first indices developed for planning and operation were deterministic. A widely known criteria for planning network capacity is the N-1 (or N-2) criterion. When this criterion is fulfilled, the loss of any single element (or two elements) in a circuit will not prevent the electric power from being supplied to the consumer. The criterion shall be satisfied even if the component with the largest capacity is lost [10]. For operating capacity it has been customary to have a spinning reserve equal to the peak load forecast plus additional capacity equal to one or more of the largest units. When planning generation capacity a normal requirement has been to use an installed capacity equal to the expected peak load in addition to a fixed percentage of the maximum load. These deterministic criteria are relatively easy to use and interpret, but they do not account for the uncertainty which is always present in a power system. Availability of intermittent resources such as solar radiation and wind, load demand and unit availability are examples of variables that are stochastic. For this reason, probabilistic indices are more advantageous in capturing the stochastic nature of power systems [1].

It is hard to imagine the modern society without reliable electricity supply. Therefore, methods and tools used to quantify the reliability are essential, and are a constantly evolving field of research. This introductory chapter will explain the classification of power system reliability and give a division of power system reliability studies.

2.2 Definition and Classification of Power System Reliability

Power system reliability can be defined as the [11] *"probability that an electric power system can perform a required function under given conditions for a given time interval."* It should be noted that reliability in this term is a measure related to the success of nearly continuously supplying adequate electric service over a prolonged time period [11]. This definition has a system point of view. However, reliability of supply is an expression that is commonly used for the end-user viewpoint as well [12]. The authors in [13] put forward that reliability relates to that the energy delivered to the consumer should fulfill the given standards and be the required amount. Frequency, duration and magnitude of disturbances affecting the consumer negatively, can be used as measures of reliability of supply in this context.

The term power system reliability can be divided into two terms, security and adequacy [13]. Furthermore, [13] defines security and adequacy as specified in a number of Institute of Electrical and Electronics Engineers (IEEE) and International Council on Large Electric Systems (CIGRE) documents:

1. *"Security – the ability of the power system to withstand sudden disturbances such as electric short circuits or non-anticipated loss of system components."*

2. *"Adequacy – the ability of the power system to supply the aggregate electric power and energy requirements of the customer at all times, taking into account scheduled and unscheduled outages of system components."*

The above definitions relate the term security to the system's dynamic conditions, or system behaviour during transient phenomena. The term adequacy is related to the static conditions, or the system behaviour in steady state. Both terms are essential to accomplish the task of having a reliable system. However, the mechanisms and instruments used to achieve a secure system on one hand and an adequate system on the other hand will often be different. Taking necessary reserve provision in a power system as an example, it should be distinguished between operational reserves and installed reserves. One part of the operational reserves will be the spinning reserves that are used during the dynamic responses in real-time operation. The installed reserve capacity on the other hand, is made up of the number and size of generating units to meet the expected system demand. Both types of reserves contribute to the reliability of the system. While the operating reserves are related to the security of the system, the installed reserves are connected to the adequacy

of the system [14].

Security and adequacy can be used to assign the state of a power system. A system state can be labeled as normal, alert, emergency, blackout or restoration state [15]. A state is said to be adequate if all system constraints are satisfied. These include the load requirements and all the operational constraints. If any of the constraints are violated the state will be inadequate. The adequate states can be described as a normal state and the inadequate states can be described as either an emergency, blackout or restoration state. However, a departure form an adequate state can lead to an inadequate state. This can for instance be if a contingency occurs and the available restoration actions are not sufficient to maintain a normal state. In this case, the state can be described as an alert state. The operation limits are satisfied at the moment, but the contingency and the following lack of response to keep the constraints within the limits will lead to an inadequate state [1].

Again it should be noted that the concept of adequacy views each state in isolation and does not consider the entries or departures between states. It is obvious that the transitions between states are important when deciding if the state is static or just temporary. Therefore, it is evident that the security aspect also is important for a complete picture. To sum up, a system state can be described as adequate/inadequate and secure/insecure, with the total of four combinations.

1. Secure and adequate: All system constraints are fulfilled and the system is in steady state.

2. Insecure and adequate: All system constraints are fulfilled, but the state has a transition to a new state that is inadequate, e.g. due to a contingency.

3. Secure and inadequate: One or more system constraints are violated, but remedial action is accomplished before departure to another state. This combination can also have another interpretation. The system can be secure in the sense that even though the state is inadequate the system can be at steady state, i.e. transient or dynamic phenomena are not present.

4. Insecure and inadequate: One or more system constraints are violated and remedial action takes longer time than the transition to a new state.

By remedial action is meant activities that are taken up by the system operator to restore an adequate operating condition. Load shedding and re-dispatch are examples of such actions. All the states that are either inadequate or insecure contribute to the system's unreliability [1]. Figure 2.1 shows the different states of a power system and the transitions between them.

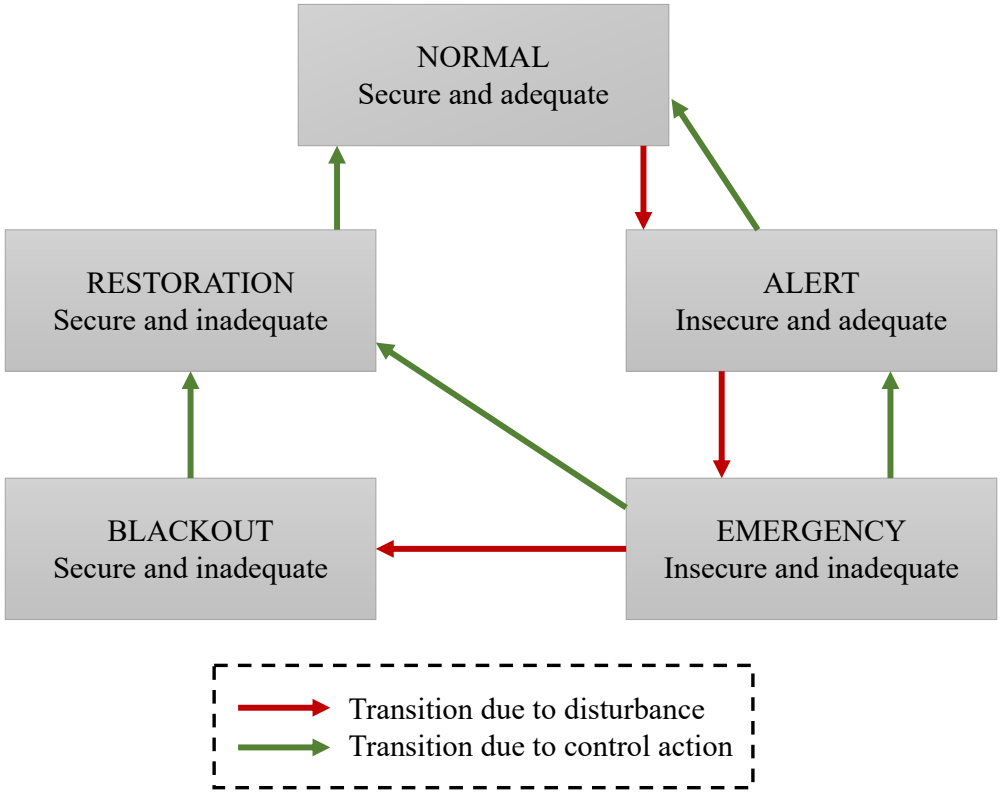

Figure 2.1: Power system state transition diagram, adapted from [16].

2.3 Categorization of Power System Reliability Studies

When analyzing power system reliability there can be computed a security assessment, an adequacy assessment or a combination of both. Power system reliability studies are also often categorized with reference to the main functional zones of a power system. These are the generation system, the bulk power system (combined generation and transmission system) and the distribution system [1].

Figure 2.2 shows this structuring by referring to different hierarchical levels (HLI, HLII and HLIII). HLI studies encompass the generation system and its capability to deliver enough energy to meet the system demand. HLII studies refer to the bulk power system and its ability to provide sufficient supply to the system load points. Lastly, HLIII studies cover all three levels, i.e. the system's ability to generate and transfer the energy to consumer load points. HLIII studies are difficult to conduct due to the large scale of the problem. Subsystems within the three HLs can also be

analyzed individually, e.g. substations, protection systems and generation plants [1]. This thesis is limited to adequacy assessment only. The reader can note that when the term 'reliability' is used in subsequent chapters it is always with a reference to 'adequacy' as defined in this chapter. Some of the main characteristics for conducting adequacy assessment for the three different levels of analysis will be given in the following subsections.

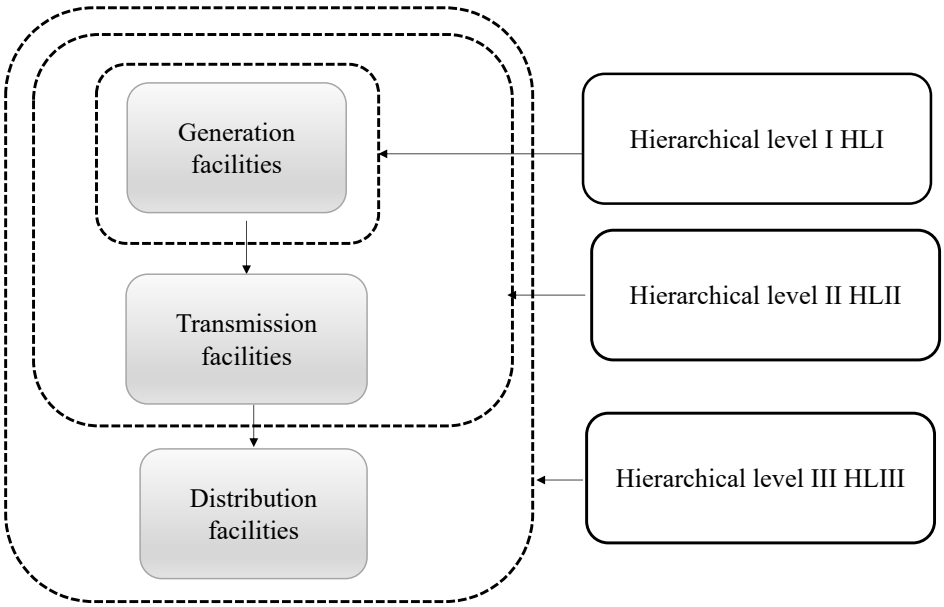

Figure 2.2: Hierarchical levels used in power system reliability studies, adapted from [1]

2.3.1 HLI Studies

HLI studies include the generation system only, and considers its capability to produce energy and meet the system demand. The components of interest in this case are the generating units and their available capacity. When conducting a HLI study, it is assumed that the other functional zones (transmission and distribution facilities) have a perfect reliability. Thus, this means that interrupted power supply to the consumers is only due to the generation system. This indicates that there exists no constraints with respect to the transferring and transformation of power to the consumer [14]. Figure 2.3 illustrates the system viewpoint in HLI studies. The load and the generation in the system is considered as total load and total generation. G_1 to G_n are the generating capacities of the n units and L is the demand in a given time instant. Analysis of interconnected power systems

can also be conducted as a HLI study since it is possible to evaluate each generation system and the tie line between them while ignoring the network in each system [1].

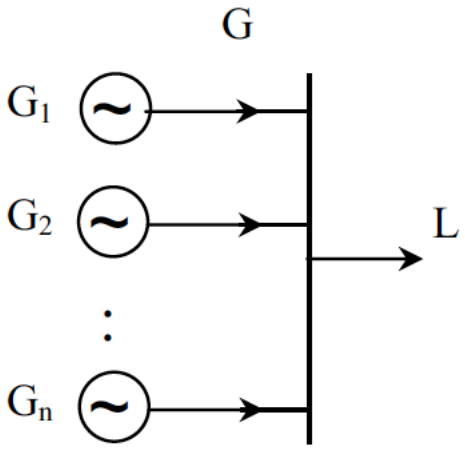

Figure 2.3: The system perspective used in HLI studies, taken from [14].

2.3.2 HLII Studies

In a HLII study a network model is combined with a generation model to produce a composite model for evaluation of load point indices or system indices [1]. An example of a five-bus composite system is shown in Figure 2.4. Load point and system indices are often expressed as expected, maximum or average values. An extensive literature review on different reliability indices can be found in [12].

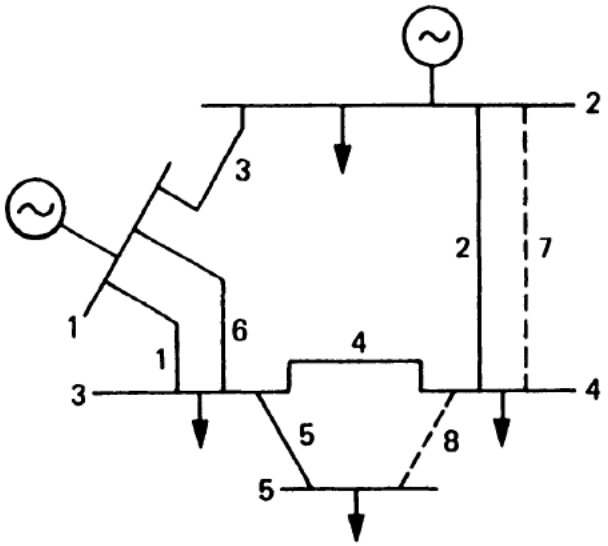

Figure 2.4: The system perspective in HLII studies, taken from [1].

The network model can be very complex due to the number of different components included and also due to the network configuration. Several constraints should be taken into account in the network model. This will be constraints such as voltage limits, maximum line loading and other steady-state stability limits. It is evident that the adequacy assessment performed in HLII studies significantly depends on the system configuration consisting of series- and parallel structures of components. Furthermore, in HLI studies events and components can be viewed as independent. The assumption about independent events is less valid in HLII studies due to the complex structure of the transmission grid and the interaction among the components. A more accurate assessment should account for possible common cause failures and cascading failures [1].

Another aspect that is different from a HLI study is the amount of data that is required to conduct a HLII study. A vast amount of both deterministic and stochastic data is needed. Deterministic data can be line impedances, current-carrying capabilities, voltage limits and other input parameters to a load flow analysis. Stochastic data include failure and repair rates of components. The possible number of outage events increases significantly compared to a HLI assessment [1].

2.3.3 HLIII Studies

As mentioned previously, HLIII studies are rarely performed due to the large scale of the problem. However, the distribution facilities are often analyzed as a separate functional zone. The connection to the transmission and generation facilities can be established by using load point indices from a HLII study as input values for the distribution system. The HLIII indices shall reflect the adequacy of the actual consumer load points. The severity of failure of the components in HLI and HLII is much greater than that for the distribution system. The consequences of faults are smaller and more localized in the distribution grid. However, the greatest share of failure events leading to inadequacy experienced at the load points are observed in the distribution system [17].

As for the modeling of the transmission system, the model of the distribution system can also become highly complex. The distribution system includes transmission lines, transformers, switches, fuses, breakers, etc. An important task in the analysis will be to find out which customer load points are affected during a specific component failure. In doing so the distribution system can be subdivided into a combination of main feeders and subfeeders [18].

2.3.4 Evolution of the HLs

Figure 2.5 shows the evolution of the HLs in relation to changes in the structure of the power system over the last 30 years. Figure 2.5 (a) represents the traditional representation explained earlier. This representation fits well for a vertically integrated structure and a centralized system. After liberalization of the electricity market, an open market structure was introduced with competition between producers and retailers. Transmission and distribution became operated by third party access. After competition was introduced between production companies, strategies for the use of primary energy resources became more significant. An example is optimal hydro production and scheduling. Hydro power producers that operate in a liberalized electricity market have mainly two options. They can bid a specific amount of production into the market or store the water for later use. This means that it is possible to optimize the production with respect to maximum income or minimum operation cost since the electricity price varies in the market and the water resources also have a value when they are stored and made available for later use. This optimization strategy for hydro power is often referred to as the water value method [19]. In Figure 2.5 (b) this strategy for optimal use of primary energy resources is represented by the added HL 0. The last important influencing structure change is shown in Figure 2.5 (c) as the increased use of distributed energy resources, i.e. small-scale generation and renewable resources located within the distribution systems which means that the transmission system is not considered for these resources [20].

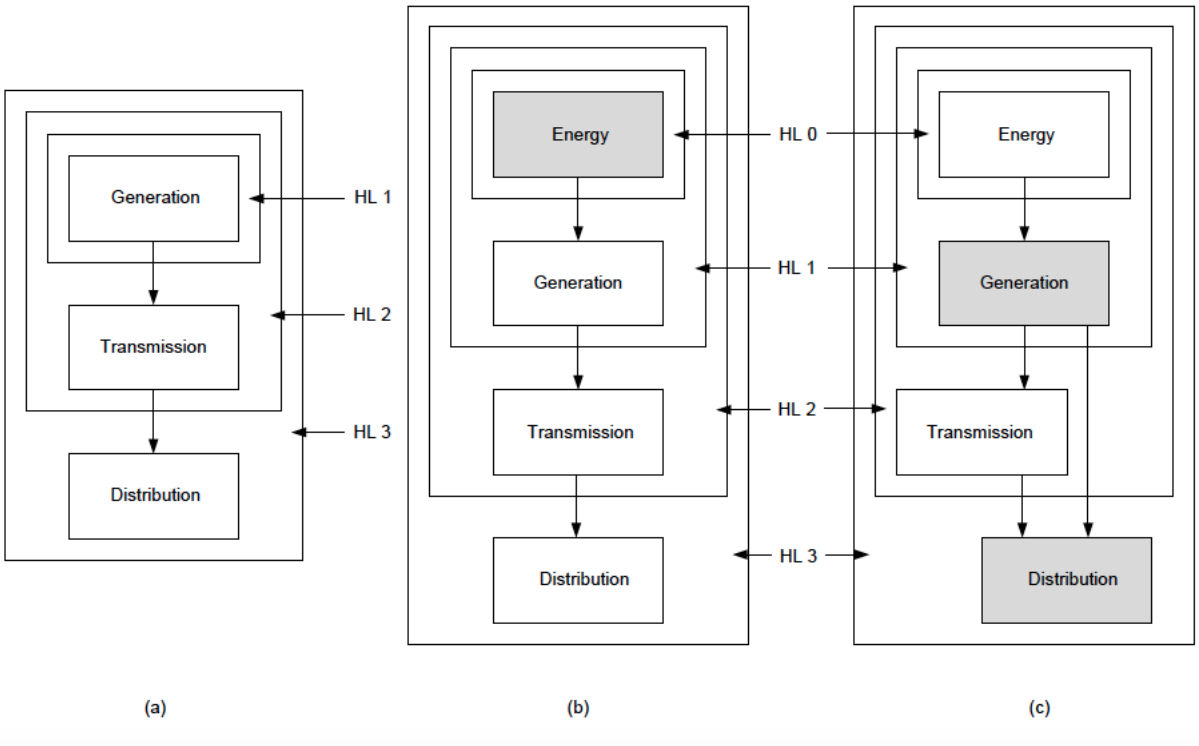

Figure 2.5: Evolution of the HLs used in power system reliability, taken from [20].

Chapter 3

Theory of HLI- and HLII Adequacy Assessment

This chapter presents the theory of generation and composite adequacy assessment. A general division of methodologies is given in the beginning. Theory and a detailed description of an analytical method and a simulation technique used in this thesis are provided afterwards. The adequacy indices chosen for this thesis are also provided in this chapter, and it is explained how these indices are calculated with the analytical method and with the simulation technique.

3.1 Division of Methodologies for HLI- and HLII Adequacy Assessment

The methodologies in generation- and composite adequacy assessment can be divided into deterministic and probabilistic techniques. The deterministic methods aim to give an estimation of the needed generation and network capacity based on deterministic criteria. These indices can be easy to use and interpret, but they do not account for the uncertainty present in the system. The probabilistic methods on the other hand try to capture the stochastic nature of the availability of the generating units and the transmission lines, and thereby calculate the probability that the system will not be able to meet the demand at a given instant in time [9].

The probabilistic methods can further be divided into analytical methods and simulation methods. The random variables of interest in an analytical approach are assigned to a fitting probability

distribution. Each system state has a probability of occurrence, called state probability. Adequacy indices are calculated based on these state probabilities. The other subdivision of probabilistic methods is simulation methods which simulate the random system behaviour. Although several simulation techniques exist, Monte Carlo simulation (MCS) is frequently used for reliability studies and is the chosen simulation technique in this thesis. MCS is a powerful tool as it is able to include a lot of details in the simulation process, e.g. weather dependencies and other correlations between load and generation [9].

An overview of the main subdivisions of power system reliability methods are displayed in Figure 3.1. Hybrid methods do also exist, but are not treated here. A further description of the methods will be given in the following. Probabilistic approaches are used in this thesis for conducting generation- and composite system adequacy assessment. Both an analytical and a simulation framework are presented in this thesis. A goal has been to present the theory about probabilistic methods in a pedagogical manner in this chapter.

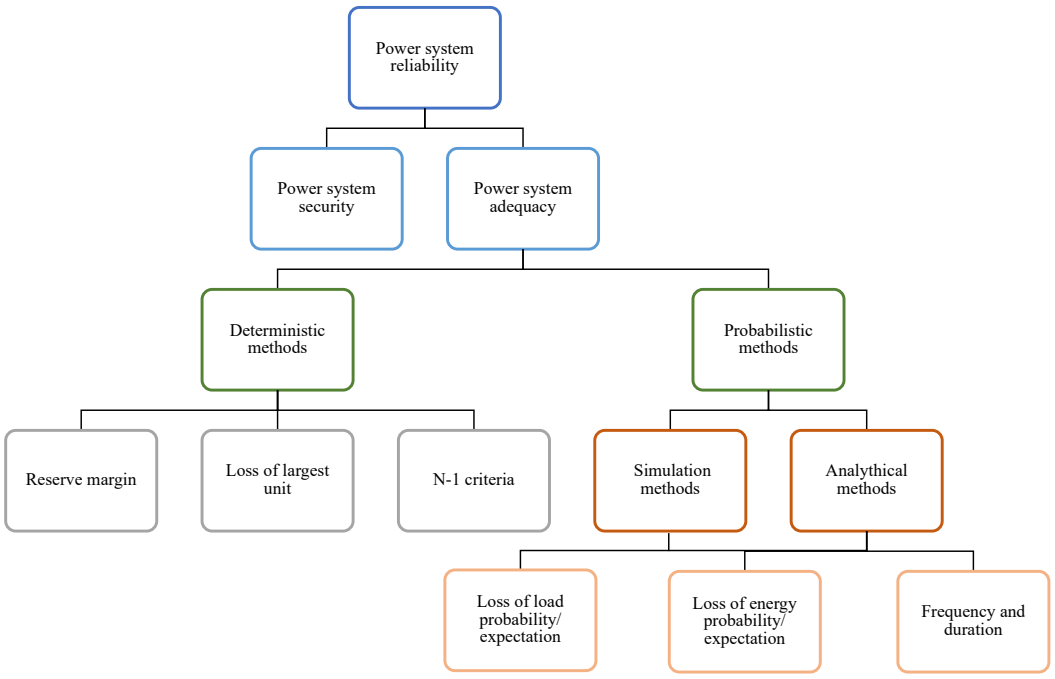

Figure 3.1: Main subdivision of power system reliability methods, based on [1].

3.2 Deterministic Methods

Deterministic methods will not be the focus of this thesis, but as they have been widely used for power system planning, some common deterministic adequacy indices will be explained in short here. Some of the shortcomings with a deterministic approach will be highlighted.

Generation reserve margin is a well known generation adequacy index. It describes the difference between the available generation capacity and the peak load. Generation reserve margin as a percentage value is given by Equation 3.2.1 [10].

$$\text{Generation reserve margin (\%)} = \frac{\text{Available capacity - Peak load}}{\text{Available capacity}} \cdot 100\% \tag{3.2.1}$$

The generation reserve margin index does not consider what kind of generation technology that is used, i.e if it is thermal, gas turbines, hydro, etc. Neither does it take into account the size of the generating units nor their reliability level. Consequently, two systems with dissimilar adequacy levels can have the same generation reserve margin. An example of two systems with the same installed capacity and the same peak load can illustrate this. If the first system has large generating units and the second has smaller generating units it is evident that the system with the smaller generating units has higher adequacy level when not considering differences in age or maintenance policies of the units. The probability of an outage of a large unit is greater than the probability of simultaneous outages of smaller units. Nevertheless, these two systems will have the same generation reserve margin [14].

The generation reserve margin index has been frequently used for generation capacity planning. This has been done by calculating the difference between the installed capacity that was available at peak load and the annual peak load. Usually, the resulting value had to fulfill a criterion based on past experience. It has been normal to require 15-25% reserve margins. Again it should be emphasized that such an approach does not considers the availability of the generators, their size or the load characteristics of the system. Since the index is easy to calculate it can provide a useful first step in capacity planning analysis. However, the accuracy of the information provided by the percentage reserve evolution is not satisfactory enough to give a trustworthy answer to how much installed generation capacity should be present to have an adequate system [10].

Another deterministic generation adequacy index that can be viewed as an extension of the reserve margin index is the loss of the largest generating unit method. In this approach the contribution from the loss of the largest generating unit is added to the already required reserve margin. The contribution will be the capacity of the largest unit divided by the peak load. To illustrate the approach, take a system with capacity of the largest unit equal to 200 MW and a peak load equal to 4000 MW. If the reserve margin is set to be 20% plus the contribution from the largest unit, this will be

$$20\% + \frac{200\ MW}{4000\ MW} \cdot 100\% = 25\%$$

The loss of the largest unit method is the simplest way of taking into account unit size on reserve capacity. This approach considers the impact of a single outage, namely the loss of the largest unit in the system. Probabilistic methods are needed if a greater variety of unit size unavailability is to be accounted for. Probabilistic methods can cover any combination of simultaneous outages in the system, and thereby provide a better estimate of sufficient installed generating capacity [10].

The N-1 criterion has been the favorable reliability criterion used for network planning. Based on this planning criterion a fixed set of contingencies considering the loss of single elements is evaluated. Thus, the reliability target is to maintain continuous supply in the presence of any outage of a single element. However, it is recognized that this deterministic approach does not capture the uncertainty that is present when power system management decisions are to be taken. To capture this uncertainty, any combination of contingencies with loss of N-1,N-2,...,N-N elements should actually be considered. Furthermore, the likeliness of the occurrences of these contingencies must be evaluated in order to take the best management decisions. Hence, the need for probabilistic methods is evident.

3.3 Probabilistic Methods for HLI- and HLII Adequacy Assessment

The analytical framework is only used for HLI assessment because the number of states to be evaluated and the following computation time will be immense in a HLII assessment. Thus, the analytical approach is only presented with respect to a generation system adequacy assessment.

MCS is used for both HLI- and HLII assessment, but the main focus has been on the application at HLII. The load model used for the analytical method and for the simulation method is the same. It will be presented after the sections concerning the theory about HLI- and HLII assessment. Lastly, the adequacy indices used in this thesis will be provided. The mathematical expressions for each index will be given in two formats, one that fits an analytical calculation method and one that suits a simulation framework.

3.3.1 Modeling of Component Availability

The modeling of component availability will be explained in the following. The components of interest are generators and transmission lines. The same model for component availability is used for both generators and transmission lines in this thesis. In system engineering the definition of unit availability is [21]: *"The ability of an item to perform its required function at a stated instant of time or over a stated period of time."* It is often practical to distinguish between the availability of a component, $A(t)$, at a given time t and the average or steady state availability, A. The steady state availability denotes the mean proportion of time the item is operative. The steady state availability based on a two-state model is given in Equation 3.3.1 [1].

$$A = \frac{\sum[\text{up time}]}{\sum[\text{down time}] + \sum[\text{up time}]} = \frac{\mu}{\lambda + \mu} = \frac{\text{MTTF}}{\text{MTTF} + \text{MTTR}} \tag{3.3.1}$$

where
λ = the expected failure rate of the component,
μ = the expected repair rate of the component,
MTTF = mean time to failure,
MTTR = mean time to repair.

More precisely, MTTF denotes the mean functioning time of the component and MTTR denotes the mean downtime after a failure. MTTR is often also denoted as MTD (mean downtime) [21].

The complement of availability is unavailability. Component unavailability is in power system engineering known as unit forced outage rate (FOR). The mathematical expression for the FOR is given in Equation 3.3.2 [1].

$$FOR = \frac{\sum[\text{down time}]}{\sum[\text{down time}] + \sum[\text{up time}]} = \frac{\lambda}{\lambda + \mu} = \frac{\text{MTTR}}{\text{MTTF + MTTR}} \tag{3.3.2}$$

The FOR given in Equation 3.3.2 is also a two-state model where the unit is classified as either working (up) or not working (down). More advanced modelling of system states, called derated states, can be achieved by Markov modelling. Derated states refer to a multi-state representation where the component can be classified into more states than "fully" working and "fully" down. For example, a derated state can be that 50% of the capacity is down. The derated states of the components can be found by applying Markov state equations. Hence, a component can be represented by several FOR values indicating the possible derated states. In addition, the FOR values represent steady-state unavailability of the components, i.e. they describe the unavailability of the components in the long-run. As such, the FOR given by a two-state model is an appropriate estimator for the unavailability of generating units with long operating cycles, like base load units. For generating units with shorter operating intervals, like peaking units, the FOR represented by a two-state model is not an adequate estimator of unit unavailability due to more frequent start-ups and shut-downs of the units. The probability of failure is higher during start-up of a generating unit, and this should be accounted for. Using a model with more possible states and transitions can better cover such aspects [1]. Transmission lines are always assumed to have a two-state model in this thesis.

A last remark is that the failure rate and the repair rate are given by a constant. It can be mathematically shown that a component with constant failure function has an exponential life distribution, i.e the probability density function is given by $\lambda e^{-\lambda t}$ [21]. A constant failure rate is a good approximation for the normal life period of a component, indicated by the constant part of the widely used bathtub curve in system engineering. The bathtub curve is a typical model used for representing the failure rate of a component and it is named after its characteristic shape. The probability of failure will be highest in the start and end of the life period due to undiscovered defects and wear out effects, respectively. The failure rate is nearly constant in the normal or useful life period. An illustration of the bathtub curve is given in Figure 3.2. As observed, it should be noted that a constant failure rate might not be a valid approximation for old components. However, what kind of maintenance policy that is used will affect how long a component is considered to be in the useful life period.

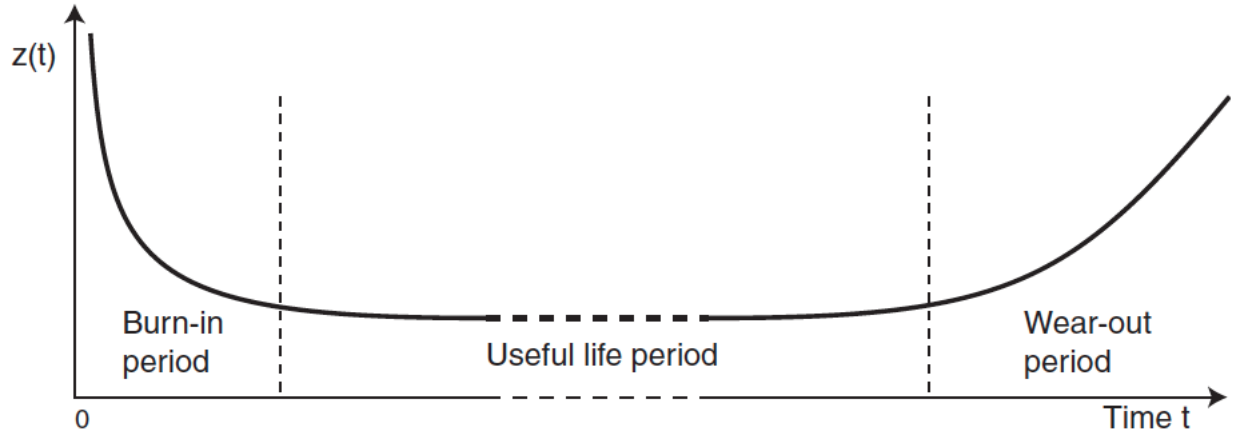

Figure 3.2: The bathtub curve illustrating the failure rate of a component as a function of time, taken from [21].

3.3.2 Elements of a HLI Adequacy Assessment

The main elements of a generation adequacy assessment are a generation model, a load model and a risk model [9, 22]. Essential for the generation model are the operating characteristics of the generating units which are used to model the available capacity. The operating characteristics will differ depending on if it is a base load or a peaking unit, a conventional or a renewable unit, etc. The load model aims at presenting the changes in load demand based on forecasts and additional assessment of variables that influence the consumer trend of electric energy. The weather condition is an example of a variable that has an effect on the demand. The generator model and the load model are combined to form a third model, which is a risk model. The risk model is used to calculate adequacy indices[1] [9]. Figure 3.3 illustrates the three main parts of a generation adequacy assessment.

It is important to realize that a single index cannot quantify all aspects of the system's adequacy performance. Therefore, it is important to be aware of the limitations of the individual indices. It is common to calculate several indices to strengthen the credibility of the assessment. The calculated indices are then compared to a threshold value which specifies the boundary between an adequate an inadequate system [9]. This threshold value can be decided based on prior experience,

[1]In literature there is a variety of terms used when referring to an adequacy measure. The most common are 'adequacy metric(s)', 'adequacy indicator(s)' and 'adequacy index/indices'. To not confuse the reader and to be consistent, adequacy index/indices will be used in this thesis when referring to the different measures used to quantify the level of adequacy.

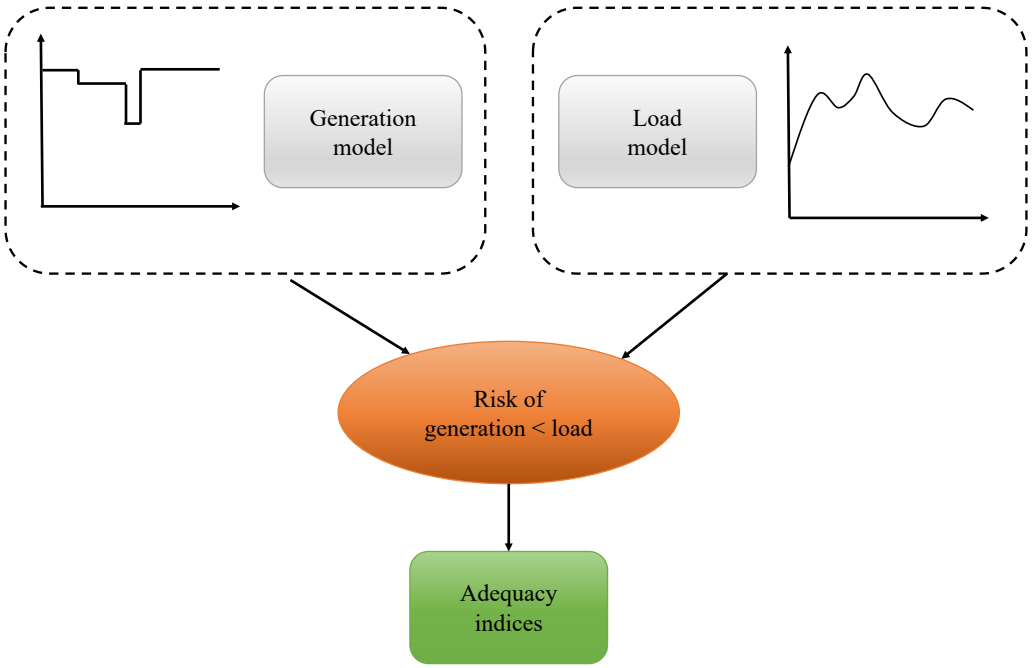

Figure 3.3: The models used in a generation adequacy assessment for calculation of risk indices, adapted from [9].

by comparison with existing criteria or by conducting a cost-benefit analysis [14]. Furthermore, it should be emphasized that the calculated indices are highly influenced by the assumptions and input data used in the generation and load models. This implies that the validity of the indices is directly linked to the validity of the models. This highlights that detailed knowledge about the system's generating units and load demand are crucial for calculating justifiable index values [10].

3.3.3 Analytical Enumeration Method for HLI Adequacy Assessment

The analytical method used in this thesis for HLI assessment is an enumeration method where the probability of having a given amount of capacity on outage is calculated. The procedure of combining the generator and the load model is a convolution process. Generally, random variables can be given by probability distributions. The sum/difference of random variables that have probability functions that are continuous can be found by using a convolution integral. To solve this integral can be time consuming and there might not exists an analytical solution. Approximate methods are then often needed. An example of such a method is the cumulant method [22].

On the other hand, if the probability density functions are discrete the convolution approach be-

comes considerably easier. Recursive unit addition and the equivalent load method are two discrete methods that are commonly used in analytical adequacy assessment [22]. The recursive algorithm for unit addition, also known as a Capacity Outage Probability Table (COPT), is chosen as the analytical generator model in this thesis.

The discrete convolution procedure has much faster computation time than Monte Carlo simulations. Analytical methods can therefore be useful for single- and two-area evaluations. The problem becomes more difficult to solve analytically if multiple areas shall be included in the analysis due to higher problem dimension as well as increasing amount of transmission constraints between the subareas. MCS is therefore more suited when conducting multi-area and also composite system adequacy assessment [1, 22, 23].

3.3.3.1 Generation Model: Capacity Outage Probability Table

The construction of a COPT will now be explained. The table consists of capacity levels with associated probabilities of occurrence. The capacity levels usually represent the capacity that is on outage. The various levels are obtained through a state enumeration of the generators in the system. An example of a COPT is shown in Table 3.1. The example system taken from [1] consist of two 3 MW units and one 5 MW unit. All units have a FOR equal to 0.02. The state space for the three generating units is shown in Figure 3.4.

The probability that a unit is down is 0.02 and the probability that the unit up is then 0.98. The failure behaviour of the generators is assumed to be independent. G_1 and G_2 have capacity 3 MW each and G_3 has capacity 5 MW. Superscript *'U'* and *'D'* indicate if the unit is up or down, respectively. Generally, for a two-state model there exist 2^n possible states. For a system with three generating units, there are in total 8 states. However, as observed in Table 3.1 the number of capacity outage states are less since some states in the state space contribute to the same capacity outage level. This is indicated by the red numbers in Figure 3.4.

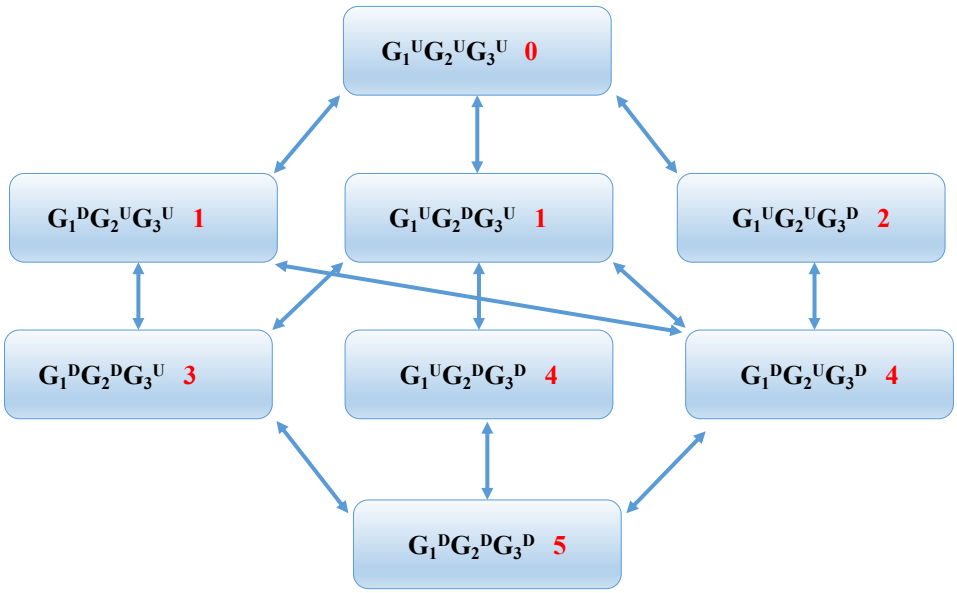

Figure 3.4: The state space for three generating units.

Table 3.1: Example of a COPT, adapted from [1].

State j	Capacity outage x_j [MW]	Individual prob. $p(X = x_j)$	Cumulative prob. $P(X \geq x_j)$
0	0	0.941192	1.000000
1	3	0.038416	0.058808
2	5	0.019208	0.020392
3	6	0.000392	0.001184
4	8	0.000784	0.000792
5	11	0.000008	0.000008

Each row in Table 3.1 shows the state, j, the capacity outage in MW in that state, x_j, the individual probability, $p(X = x_j)$ and the cumulative probability, $P(X \geq x_j)$. The individual probability is the probability that exactly x_j MW capacity is out. The cumulative probability is the probability that an amount equal to or greater than x_j MW capacity is out. The cumulative probability is also shown in Equation 3.3.3 [7].

$$P(X \geq x_j) = \sum_{X=x_j}^{C} p(X) \tag{3.3.3}$$

The cumulative probability is obtained as the sum of the individual probabilities over all capacity outage levels up to the total installed capacity in the system, denoted by C. For large systems there will be numerous capacity outage levels. A reduction of the number of states can be achieved by truncating states that correspond to low probabilities, typically in the range of $10^{-6} - 10^{-8}$. A rounding process can also be used to reduce the number of discrete capacity outage levels. This approach is described more in detail in [1].

The individual probabilities need to be calculated before obtaining the cumulative probabilities when using Equation 3.3.3. By using a recursive algorithm the cumulative probabilities can be calculated directly. This algorithm adds each generator one by one [1]. The algorithm will be given and calculations shown for the two-state system already used. Equation 3.3.4 shows how the recursive algorithm is used to obtain the cumulative probability of a capacity outage state $P(X \geq x_j)$ after a unit of capacity g is added.

$$P(X \geq x_j) = (1 - FOR) \cdot P'(X \geq x_j) + FOR \cdot P'(X \geq x_j - g) \tag{3.3.4}$$

$P'(X)$ is the cumulative probability from the old COPT table. The algorithm is initialized by Equation 3.3.5. Table 3.2 shows the calculations for recursive unit addition for the example system of three generating units.

$$P'(X \geq x_j) = 1 \text{ for } \begin{cases} x_j \leq 0 \\ x_j - g \leq 0 \end{cases} \tag{3.3.5}$$

Equation 3.3.4 can be modified to include a derated system representation. Equation 3.3.6 shows the recursive algorithm when a multi-state unit is added.

$$P(X \geq x_j) = \sum_{i=1}^{n} p_i \cdot P'(X \geq x_j - g_i) \tag{3.3.6}$$

Table 3.2: Calculations for the COPT of the example system.

Add first unit of 3 MW
$P(0) = (1 - 0.02) \cdot 1 + 0.02 \cdot 1 = 1.000000$
$P(3) = (1 - 0.02) \cdot 0 + 0.02 \cdot 1 = 0.020000$
Add second unit of 3 MW
$P(0) = (1 - 0.02) \cdot 1 + 0.02 \cdot 1 = 1.000000$
$P(3) = (1 - 0.02) \cdot 0.02 + 0.02 \cdot 1 = 0.039600$
$P(6) = (1 - 0.02) \cdot 0 + 0.02 \cdot 1 = 0.000400$
Add third unit of 5 MW
$P(0) = (1 - 0.02) \cdot 1 + 0.02 \cdot 1 = 1.000000$
$P(3) = (1 - 0.02) \cdot 0.00396 + 0.02 \cdot 1 = 0.058808$
$P(5) = (1 - 0.02) \cdot 0.0004 + 0.02 \cdot 1 = 0.020392$
$P(6) = (1 - 0.02) \cdot 0.0004 + 0.02 \cdot 0.0396 = 0.001184$
$P(8) = (1 - 0.02) \cdot 0 + 0.02 \cdot 0.0396 = 0.000792$
$P(11) = (1 - 0.02) \cdot 0 + 0.02 \cdot 0.0004 = 0.000008$

where

p_i = the probability of generating unit being in state i,

n = total amount of derated states for the generating unit.

3.3.4 The Basics of Monte Carlo Simulation

MCS is a technique where histories or scenarios are developed through sampling of random numbers from probability distributions. The random numbers are used to classify the state of the components in the system. In addition, random numbers are used to classify the transitions to other states. The system state can be expressed by a state vector, **S**, where each component in the system is represented by a state value, S_i. The number '1' is used in this thesis to indicate that the component is down and a '0' indicates that the component is up [2]. For example, for a system with four components the state vector in a particular history can be $\mathbf{S} = \{0\ 0\ 1\ 0\}$, indicating that one of the components is down. This binary representation reflect a two-state model for the components. Derated states can be included by representing component states with a value in the range [0,1].

In the context of power system reliability assessment, indices that are loss-of-load (LOL)-based can

[2]The opposite representation can often be found in literature.

be calculated by counting the number of LOL events in the histories and dividing by the number of histories generated, often denoted as the sample size N. The sampling and state classification procedure continues until a convergence criteria is met, i.e. the accuracy of the obtained reliability indices satisfies a desired threshold value [24].

As indicated, the sampling of random numbers is an essential part of the MCS method. Examples of random number generators used for this purpose are the multiplicative and mixed congruential generators. It should be noted that mathematical number generators or computational algorithms, as the two congruential generators mentioned, are only able to provide pseudo random numbers due to their deterministic features. Nevertheless, a random number generator is normally aiming at sampling numbers that are uniformly distributed in the range between [0,1]. For this purpose the uniform distribution can be used directly. However, for generating units and transmission lines, time to failure (TTF) and time to repair (TTR) are often assumed to follow the exponential distribution. Other techniques are needed to provide random numbers from nonuniform distributions like the exponential distribution. The inverse transform method is an example of an approach that is used to obtain random numbers that follow another distribution than the uniform [24].

It is common to divide MCS into non-sequential and sequential simulation processes. The difference between these two simulation processes is how the simulation moves in time. The system state in a non-sequential simulation is sampled in each time step, but the system states are not chronologically or sequentially dependent. A sequential simulation on the other hand, moves to the next steps chronologically. In this way the system state of a component will be dependent on its status in adjacent time steps. Hence, a sequential simulation process accounts for the failure and repair histories of the components [22]. The simulation framework used in this thesis is based on the work of [8]. Three different simulation methods are presented in [8]. These are the state sampling method, which is a non-sequential method, and the state duration method and the state transition method, which are sequential methods. Only the state sampling and the state transition method are used for HLII analysis in the framework of [8]. Thus, it is also chosen to focus on these two simulation processes in this thesis. The basic concept of the state sampling and the state transition method will be explained in the following.

3.3.4.1 The State Sampling Method

The state sampling method generates a random number, U, for each component in the system. As an example, consider generator unavailability as the random variable of interest. A random number between 0 and 1 can be generated for each unit. All units have data on their average unit unavailability or FOR. This can be, for example, 10% for a particular unit. The unit will be out of service in this history if the generated number is less than 0.1. Otherwise, the component is available. Derated states can also be included as shown in Table 3.3, where the component of interest has n possible states with a probability p_i to be in derated state i. A system state is obtained by comparing random numbers for all system components against their respective FOR values or derated state probabilities. Furthermore, the state sampling method is a non-sequential method and thus the previous component states are not affecting the outcome of the current component states. It is a "memory less" simulation process. Due to this fact, random numbers can be drawn directly from the uniform distribution as transition times are not considered. One evident shortcoming with the state sampling method is that it cannot be used to obtain frequency and duration indices. Also, it is not suited to account for correlation effects [24].

Table 3.3: Example of probability table of component with derated states.

Component state	Probability table
Up	$U \geq p_n$
.	.
.	.
.	.
State i	$p_i \leq U < p_{i+1}$
.	.
.	.
.	.
Down	$U < p_1$

3.3.4.2 The State Transition Method

As denoted earlier, the state transition method is a sequential simulation process. An example of a simple sequential state diagram of a system is shown in Figure 3.5. The state transition method considers the state transitions of the system as a whole and not transitions at component level. The method is only valid if all probability distributions follow an exponential distribution. As stated in [24], it can be proved that when all transition times follows an exponential distribution, the system transition time, T, will also follow an exponential distribution. The shape parameter of T, will be the sum of all m transition rates out of the current system state as shown in Equation 3.3.7. These m transitions include the transition rates of all components out of the current system state, also taking into account possible derated states of the components.

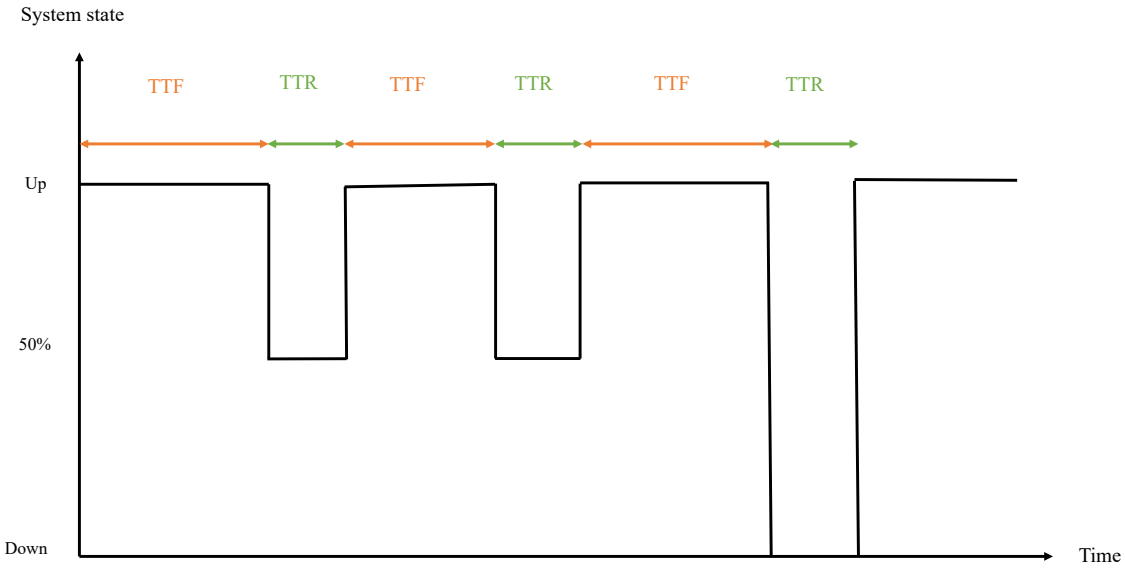

Figure 3.5: A sequential state diagram for a system.

$$\lambda = \sum_{i=1}^{m} \lambda_i \tag{3.3.7}$$

The system transition time, T, can also be viewed as the minimum of all the components' time to transition, as seen in Equation 3.3.8. This indicates that the departure from the current system

state is set by the component with the lowest state duration time with respect to the current state.

$$T = \min\{T_1, T_2, ..., T_m\} \tag{3.3.8}$$

Denote t_0 as the time the next system transition takes place. The probability that this transition is a result of state j determining the transition from the current state is given by the conditional probability $P_j = P(T_j = t_0 \mid T = t_0)$. Since T and T_j follow an exponential distribution, it can be mathematically shown that the conditional probability can be given as displayed in Equation 3.3.9 [24].

$$P_j = P(T_j = t_0 \mid T = t_0) = \frac{P(T_j = t_0 \cap T = t_0)}{P(T = t_0)} = \frac{\lambda_j}{\sum_{i=1}^{m} \lambda_i} \tag{3.3.9}$$

In addition, any of the m transition rates can lead to the next system state. Hence, the sum of all system state probabilities must equal one, as shown in Equation 3.3.10.

$$\sum_{i=1}^{m} P_i = 1 \tag{3.3.10}$$

The simulation process builds on essentially two steps. Firstly, generate a random number, U_1, that is uniformly distributed in the range [0,1]. This number gives the next system state. The system state probabilities, calculated by Equation 3.3.9, can be indicated by a given segment in the range of [0,1] as illustrated in Figure 3.6. The segment U_1 falls in between decides the next system state. In this case U_1 falls into the segment of P_j, which means that the next system state is a result of state j determining the transition from the current state. Secondly, obtain a new random number, U_2, to decide the time to the next event. The total transition rate given in Equation 3.3.7 must be used when calculating the time to the next transition.

As the state transition method is a sequential method, it enables the possibility to obtain frequency and duration indices. In addition, a sequential simulation approach makes it possible to obtain the probability distributions of the reliability indices and not just the expected values, which is not achievable with the state sampling method and an analytical approach [24].

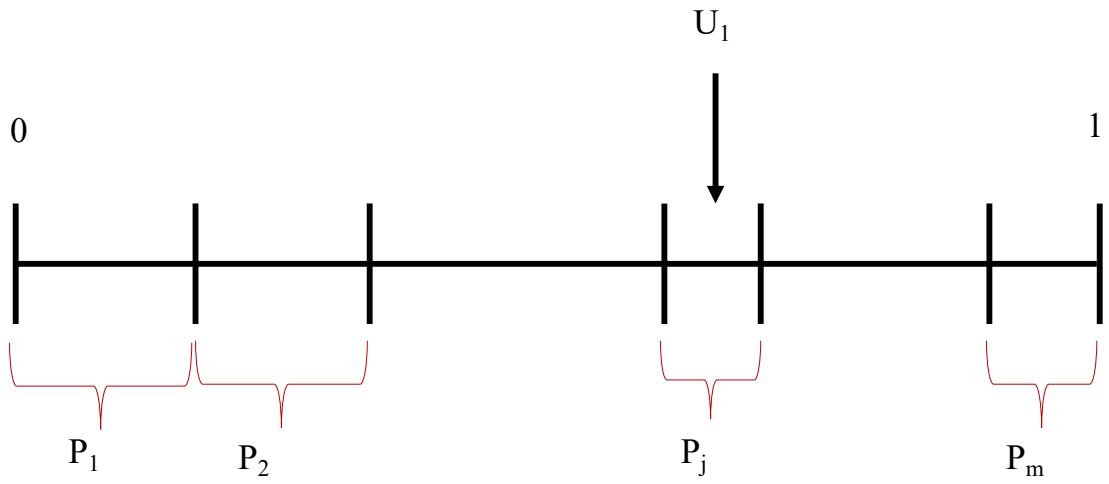

Figure 3.6: Decision of the next system state for the state transition method.

3.3.4.3 The Statistical Foundation of Monte Carlo Simulation

The statistical inference obtained from MCS builds on sampling distribution theory. The sample mean and sample variance are two important measures in this frame of reference, measuring the average and the variability of the observations in a sample. The sample mean and sample variance[3] are shown in Equation 3.3.11 and Equation 3.3.12 [25]. In statistics theory, a sample is referred to as a subset of the population [25]. The population is the totality of observations which can be made. The population with respect to a power system reliability evaluation consists of the totality of observations that can be made for an index. Each simulation year in a sample provides an observation X_i, i.e. a reliability index value. A sample that consists of N simulated years yields N observations for the index.

The accuracy of an estimate obtained trough a MCS is high if the sample mean, $\overline{X}$, is close to the true mean of the population's distribution[4]. Furthermore, the precision of an estimate obtained

[3]Note that the term 'sample mean' and 'sample variance' are used both for the statistics $\overline{X}$ and S^2, and the computed values $\overline{x}$ and s^2.

[4]The true mean of the population's distribution is often denoted μ , and the variance of the population's distribution is often denoted σ^2.

trough a MCS is high if the variance of the sampling distribution is low [8]. A low variance indicates that the dispersion of the observations from the mean is low. Next, it should be pointed out that a statistic computed from a sample, such as the the sample mean, is a random variable that follows a probability distribution called the sampling distribution [25]. The variance of the sampling distribution of the mean can be calculated with the formula given by Equation 3.3.13 [24]. The variance of the sample mean's distribution gives information about the variability of the sample means around the population mean. The sample mean distribution can be thought of as the distribution that results when a sample of size N is sampled from a population over and over again, yielding the many values of $\overline{X}$ [25].

$$E(X) = \overline{X} = \frac{1}{N}\sum_{i=1}^{N} X_i \tag{3.3.11}$$

$$S^2 = \mathrm{Var}(X) = \frac{1}{N-1}\sum_{i=1}^{N}(X_i - \overline{X})^2 \tag{3.3.12}$$

$$\mathrm{Var}(\overline{X}) = \frac{1}{N}\mathrm{Var}(X) = \frac{1}{N}\left(\frac{1}{N-1}\sum_{i=1}^{N}(X_i - \overline{X})^2\right) \tag{3.3.13}$$

The different simulation approaches, e.g. state sampling or state transition, aim at providing random samples that are representative of the population. This is essential if conclusions drawn from the sample about the population are to be valid. If the sampling procedure consistently overestimates or underestimates the observations, the process is biased and the conclusions drawn from the samples will be misleading. Consequently, it becomes evident that the accuracy and the precision of estimates obtained from MCS samples are key concerns. With respect to this fact, two statistical theorems constitute the foundation for the MCS method, namely the law of large numbers and the central limit theorem [26]. The law of large numbers says that the sample mean as displayed in Equation 3.3.11, approaches the true mean of the population when the sample size tends towards infinity. This theorem indicates that if N is large enough, the mean obtained from a MCS will be a good estimation of the population mean. However, the theorem does not give any information about the uncertainty of the estimate provided by a MCS. This particular knowledge can be provided by the central limit theorem. The central limit theorem proclaims that the sampling

distribution of the mean, whether it stems from a population with unknown distribution or another than the normal distribution, will be approximately normal, with mean μ and variance σ^2/N, provided that the sample size is sufficiently large. Thus, the central limit theorem provides an estimate of the variability of the estimated expected value. The variance of the sample distribution can be approximated by Equation 3.3.13 when N is sufficiently large. It can also be observed that when the sample size increases the variance of the estimated expected value will decrease.

Next, it should be noted that MCS has a fluctuating convergence process. This means that adding a few more observations to the the sample does not necessarily provide a more precise estimate compared to the current estimate [24]. However, as just reviewed, the variance of the sample mean distribution will decrease with increasing sample size. Also, the sample mean will tend towards the true mean of the population with increasing sample size. Consequently, the uncertainty in the estimate, i.e. the variance, can indicate a converging criteria for a MCS. The coefficient of variation (CV) is often used in MCS to indicate the convergence criteria of the simulation process. The simulation stops when the CV reaches a specified threshold value [24]. The coefficient of variation, denoted β, is unitless and displayed in Equation 3.3.14. The CV is the ratio between the sample's standard deviation, denoted s(X), and the sample's mean. The sample's standard deviation is calculated based on the variance of the sample mean distribution in Equation 3.3.13. As stated in [24] the CV of the EENS index converges slower than the CVs of other LOL-based indices. Hence, the CV of the EENS index should then be used when setting the stopping rule in the case of using the same sample to calculate different indices. The reader can also note that increasing the sample size to reduce the variance will increase the computation time. Accordingly, there exists various variance reduction techniques that can make the MCS more efficient.

$$\beta = \frac{s(X)}{\sqrt{N} \cdot E(X)} \tag{3.3.14}$$

Figure 3.7 sums up this section about the fundamental statistic theory of MCS. It illustrates that the MCS method is a technique that uses the sample mean to give an estimation of the population mean. The law of large numbers and the central limit theorem constitute the foundation of the validity of the method. The sample together with inferential statistics makes it possible to draw conclusions about the population. The desired information about the population in the context of power system reliability is the various reliability indices of the system.

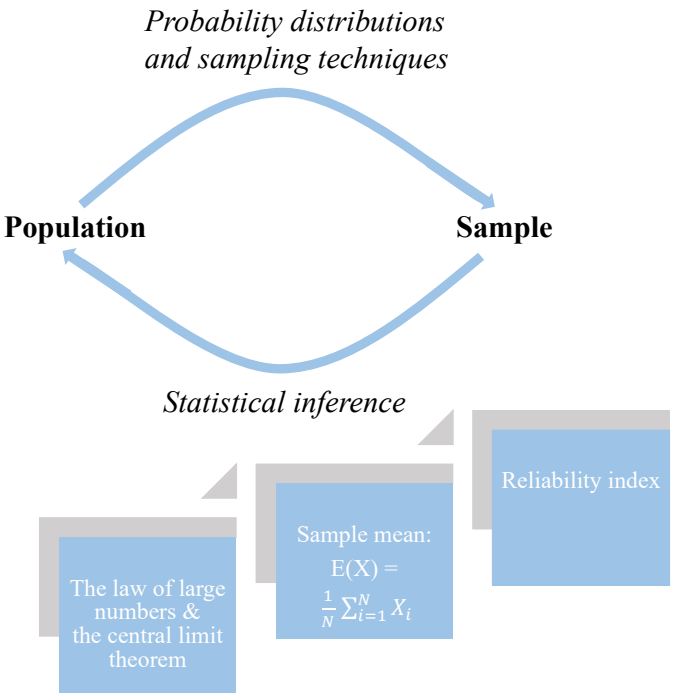

Figure 3.7: Fundamental relationships of the Monte Carlo method.

3.3.5 Application of Monte Carlo Simulation to HLI Adequacy Assessment

MCS applied to generation system adequacy assessment can be summarized in three steps:

1. Generator states are sampled through generation of random numbers. An additional random number is generated if a sequential method is used, determining the time to next event. Generator data requirements are capacity ratings, in addition to FOR values (non-sequential method) or failure and repair rates (sequential method).

2. The sampled states determines the system state which is classified as a 'success' or a 'failure'. A failure state occurs when total available capacity is less than the system demand in the time increment being evaluated. All failure states are recorded and the severity of the capacity deficit is calculated. The mathematical expressions of the reliability indices are explained in detail in Section 3.5.

3. The sampling and classification procedure are usually performed till a satisfactory convergence is reached. The reliability indices of the sample are calculated as an average of all the observations.

3.3.6 Elements of a HLII Adequacy Assessment

Composite system analysis, or sometimes referred to as bulk system analysis, includes the network configuration of the transmission system in the assessment. Full enumeration of system states becomes extremely tedious with the inclusion of the transmission grid in the analysis. Although an analytical approach is possible, simulation techniques fit better for this purpose. It is not only the amount of system states that is larger compared to a HLI analysis. As stated in [24], several other aspects and considerations should be included in a HLII assessment. These aspects will be the same for both analytical and simulation-based approaches, and include load flow and contingency analysis, rescheduling options for generators, control actions for overload situations, load shedding prioritizing, etc. The load flow problem and contingency solver, formulated as an optimal power flow (OPF) problem, can be either a DC model or an AC model. The DC model is a simplified approach where only active power flows are considered. The reader is referred to see Appendix D and Appendix E for the full DC and AC model descriptions, respectively. The DC and AC model descriptions are taken from [8], and these are the models used in the software. The power flow equations for the DC and AC models are also given in the appendices to highlight the difference between the two OPF problems, namely the linearity of the DC formulation and the non-linearity of the AC formulation.

The working of both contingency solvers is the same. In the case of a contingency, the solvers seek to find a feasible state of operation. That is, none of the constraints in the OPF formulation are violated. If a constraint violation occurs, control actions are performed to obtain a feasible operating point. These actions are rescheduling of generators and load curtailments in that priority order. By default the cost of rescheduling is set to zero and hence rescheduling actions are always performed first. If rescheduling is not sufficient to obtain a feasible operating point, load curtailments are carried out. The curtailment cost is varying among buses leading to a prioritization of load curtailments, where load at buses with lower curtailment costs is shed first.

Additional data that is required when conducting a HLII assessment compared to a HLI assessment, includes FORs or failure and repair rates of transmission lines, network topology, line impedances

and current limits of lines. At each bus it is necessary to specify load requirements and load curtailment costs. If an AC model is used, minimum and maximum reactive power limits for generators are needed, in addition to minimum and maximum voltage limits at buses. Due to the load flow problem there is also a need to incorporate a tool to handle the cases of isolated buses that might occur in the presence of multiple line outages.

Figure 3.8 gives an overview of the elements of a composite system adequacy assessment. A system state is obtained by the generation and the network model, accounting for the status of all generators and transmission lines in the system at each time increment. This system state, in addition to the load demand at the given time increment, is combined in a risk model where it is checked if available capacity is less than the load requirement. As indicated, if this is the case, the contingency solver will try to find a new feasible operating point through rescheduling and load curtailments. Curtailed load, or load lost due to isolation of buses will contribute to the adequacy indices.

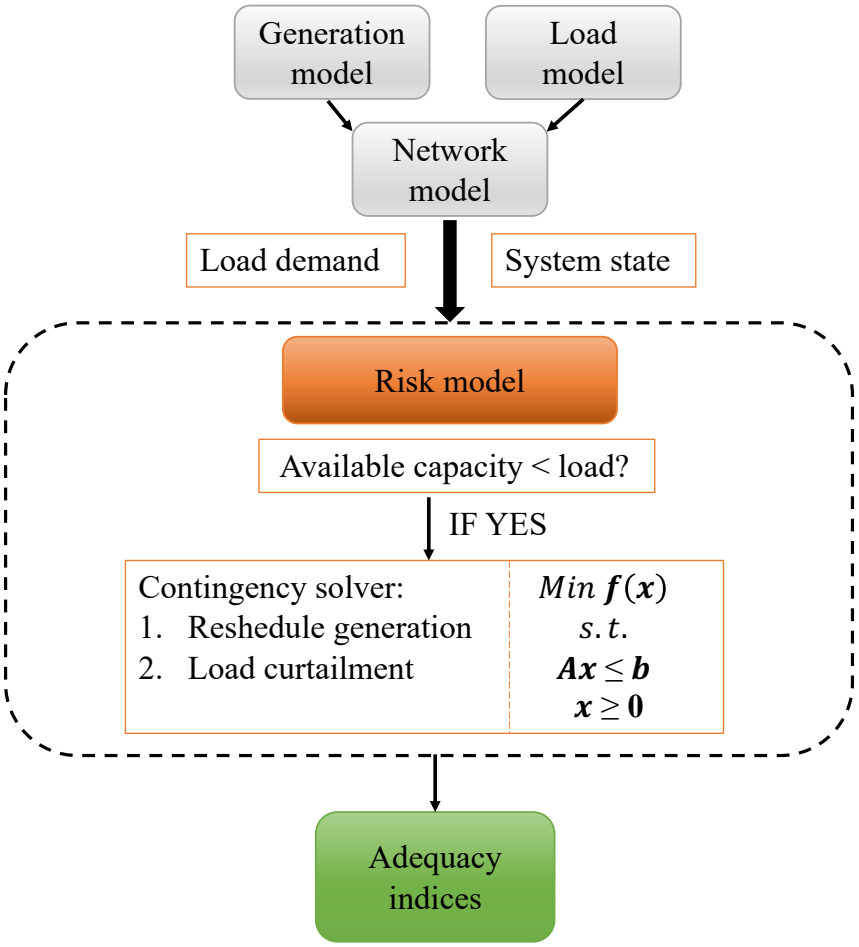

Figure 3.8: Elements of a composite system adequacy assessment.

3.3.7 Application of Monte Carlo Simulation to HLII Adequacy Assessment

The needed data and special features of a HLII adequacy assessment were outlined in the previous section. The flowchart in Figure 3.9 illustrates how MCS can be applied to HLII adequacy assessment. The contingency solver can be a DC or AC OPF model. Figure 3.9 indicates the simulation process when a non-sequential method is used. The sampling and classification procedure is repeated for each time increment. When a sequential method is to be utilized, like the state transition method, a random number giving the time to next event must also be generated. In this case, note that the time increment is not updated if the time to next event is less than the duration of the time increment. Thus, there can be more than one event happening inside a single time increment for a sequential method.

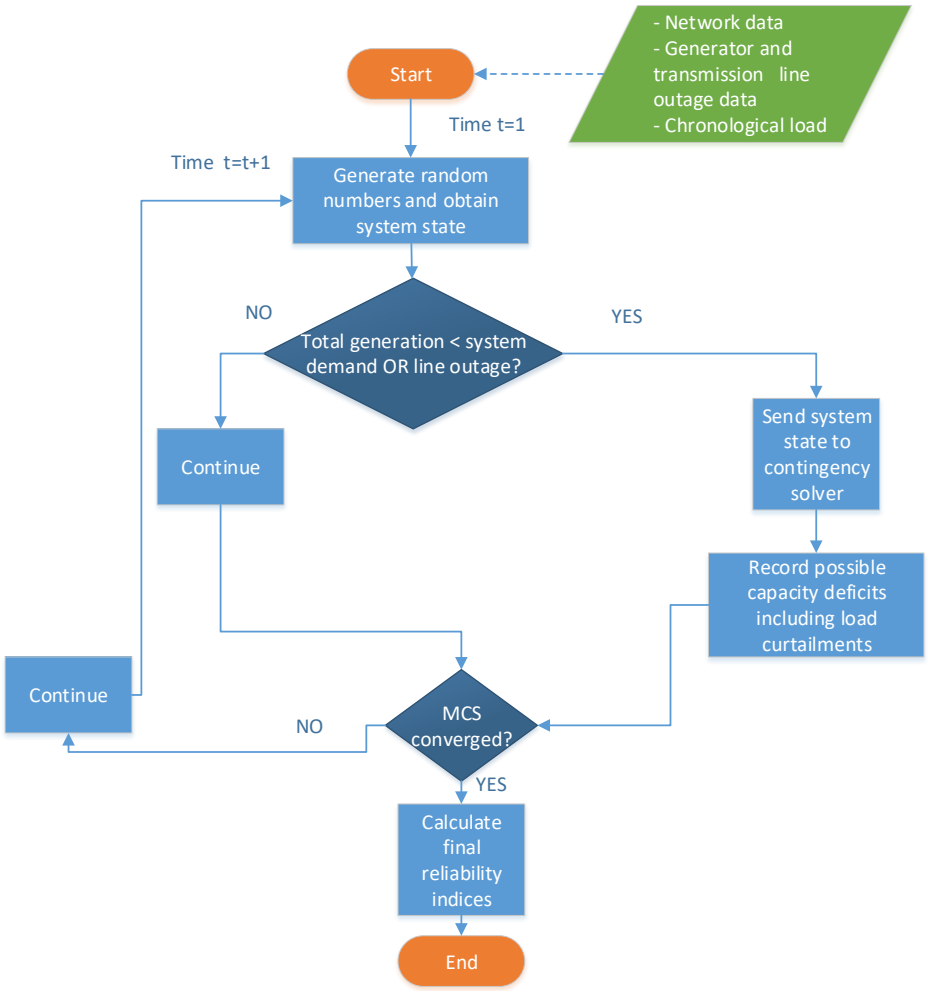

Figure 3.9: Flowchart showing the application of Monte Carlo simulation and state sampling to calculate adequacy indices at HLII.

3.4 Load Model

The load model presents the system load variations over a given time horizon, e.g. one year. The length of the time increment is a determining factor for the accuracy of the model. The most simple model will be a load model given by the yearly peak load (YPL). This would be a very pessimistic model as only a few hours of the year are representative for this value. A less pessimistic load model would then be the weekly peak loads (WPLs) which consists of 52 time increments through a year. Further on, more accurate models would be load models represented by daily peak loads (DPLs), hourly peak loads (HPLs), or even models with finer time resolution. Consequently, the load model becomes less pessimistic with finer time resolution. An HPL model is used for both HLI- and HLII assessment in this thesis.

The peak loads can be given in a chronological representation or arranged in descending order. The latter is usually referred to as a load duration curve (LDC). Figure 3.10 shows examples of chronological peak load curves. Examples of LDCs are given in Figure 3.11. It should be mentioned that these load models are forecasts of future load usually based on historical data. Load forecast uncertainty can be included in the modelling. An approach using a discrete approximation of the normal distribution for load uncertainty is described in [1]. Load forecast uncertainty is not considered in this thesis.

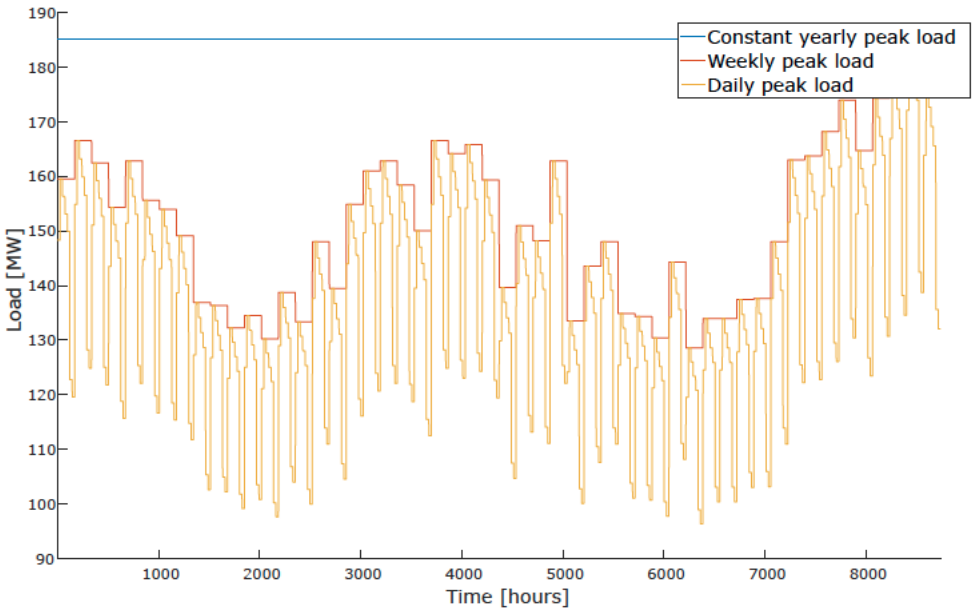

Figure 3.10: Examples of chronological peak load curves, based on data from [27, 28].

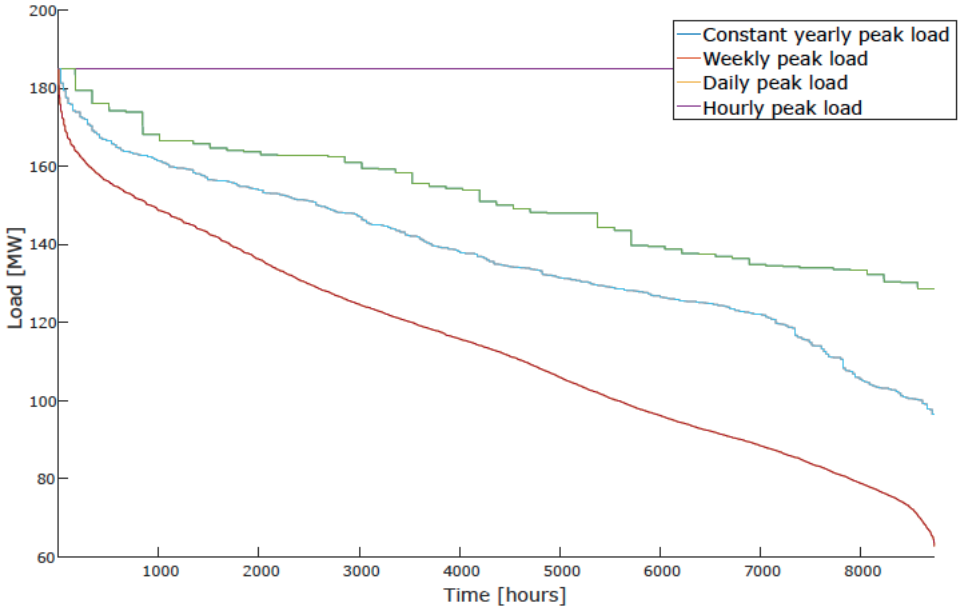

Figure 3.11: Examples of load duration curves, based on data from [27, 28].

3.5 Probabilistic Indices

Several probabilistic risk indices can be calculated from the risk models for HLI- and HLII assessment. The most common LOL indices that are applicable for both HLI- and HLII assessment are Loss of Load Probability (LOLP), Loss of Load Expectation (LOLE) and Expected Energy Not Supplied (EENS)[5]. Only system indices can be obtained for HLI, whereas bus indices can also be calculated for HLII. Furthermore, the probabilistic indices presented in this section will be given in two different formats, one that fits the analytical approach and one that fits a simulation framework. This is because the calculation procedure for the indices is dependent on the probabilistic method used. In the following, superscript *'MCS'* denotes that the index is in a MCS format, and no superscript denotes that the index is in an analytical format. Nevertheless, the general interpretation of the indices is the same whether it stems from an analytical method or a MCS.

As indicated, LOLP, LOLE and EENS are the three main indices chosen for this thesis. It should be noted that frequency and duration indices can easily be calculated from the state transition method for MCS. Frequency and duration indices can also be calculated through extensions of the recursive algorithm used in the analytical approach, as shown in [1]. Anyhow, frequency and duration indices

[5]Other indices that reflect the composite system features can be useful for HLII analysis. Examples of such can be found in e.g. [24].

have not been the focus of this thesis.

3.5.1 Reliability Indices: LOLP, LOLE and EENS

The software used for the analytical method is based on the work of [7], whereas the software used for MCS is based on the work of [8]. Thus, the mathematical formulae displayed for the indices are gained from an understanding of these sources. Suitable explanations, comparisons and clarifications are added where necessary. It should be noted that the formulae used for the analytical method are formulated with respect to a HLI analysis, and use notation and expressions related to the COPT. The formulae used for the MCS framework are more generally formulated. They are based on the outcome of system states which can include status of generators and also status of transmission lines.

The first index that will be explained is LOLP which is the probability that the demand is exceeding the available capacity during a certain time period. The name of the index can be misleading in the sense that load is not lost. A LOL situation in this context is a deficiency of generation capacity in service to meet the load demand at both HLI and HLII. For HLII the consideration of insufficient transfer capacity to meet the demand is also included. The reader should note that the interpretation and the use of the LOLP index in this thesis is slightly different for the analytical and the simulation method. LOLP values are calculated for each time increment for the analytical method. These values are then used to calculate the LOLE index. This interpretation of LOLP was found to be convenient because of the enumeration approach used in the analytical method. The LOLP index is a "re-engineered" version of the LOLE index for the MCS approach. Thus, it is an average value obtained from all time increments in all simulation years. Nevertheless, both interpretations are dependent on the load model used. A LOLP value calculated by a DPL curve may differ from one calculated by an HPL curve.

The LOLP value in time increment t can be mathematically represented by Equation 3.5.1 for the analytical method.

$$LOLP_t = P(L_t > C - X) = P(X > C - L_t) \tag{3.5.1}$$

where X is the the outage capacity, C is the installed capacity of the system that is not on scheduled

outage and L_t is the load at a specific time increment. $P(L_t > C - X)$ represents the above-mentioned definition, i.e. that the demand is exceeding the available capacity. Equation 3.5.1 shows that this will be the same as the probability of having an outage capacity greater than the installed capacity less the load at that particular time increment. Both of these interpretations can be found in literature.

The formula for the LOLP index in MCS format will be given after the LOLE index is displayed, because it is a "re-engineered" version of the LOLE index. However, there is a general way to think of LOLP in a MCS framework, that is not "re-engineered". The generated system states all have a probability of occurrence. The sum of the probabilities for system states that causes a LOL event will be the LOLP.

The indices LOLE and LOLP are closely related and often mixed up in literature. First of all, LOLP is defined as a probability and hence it is a unit-less quantity. LOLE on the other hand, is defined as an expected number of occurrences of a particular event during a time period. More specifically, the expected number of a capacity shortage in serving the demand in the time period. The unit for the LOLE index is consequently dependent on the study period and the resolution of the the load model. The study period could be a week, a month or a year, though a year is often chosen. If the daily peak curve is used for a year the value of LOLE would be in days/year. Similarly, if the hourly peak curve is used for a year the value of LOLE would be in hours/year. For the analytical method, the definition of LOLE can be mathematically shown in Equation 3.5.2 and Equation 3.5.3, using a DPL curve and an HPL curve, respectively.

$$LOLE = \sum_{t=1}^{t=365} P(X > C - L_t) \cdot \Delta T = \sum_{t=1}^{t=365} LOLP_t \cdot \Delta T \ [days/year] \tag{3.5.2}$$

$$LOLE = \sum_{t=1}^{t=8760} P(X > C - L_t) \cdot \Delta T = \sum_{t=1}^{t=8760} LOLP_t \cdot \Delta T \ [hours/year] \tag{3.5.3}$$

$P(X > C - L_t)$ can be recognized as the $LOLP_t$ at a given time increment. It can be noted that the LOLE calculations will consist of the summation of all the $LOLP_t$ values over the desired time period if the time increment, ΔT, is equal to one day for Equation 3.5.2 and one hour for Equation 3.5.3.

System states are sampled for each time increment in a year in a MCS framework. The unit of

the LOLE index is dependent on the length of the time increments in the same manner as for the analytical method. Usually, hourly time increments are used. In general, the simulation year is divided into M time increments, for which each system state will have an outcome, x_j. This variable will be equal to 1 if the system state has a LOL event and zero otherwise. The outcome of each trial is multiplied with the duration of the given time increment, ΔT. N simulation years are simulated in a sample. A LOLE value is calculated by the end of each simulation year, and the final value is an average of all N simulation years. Thus, the LOLE index obtained from a MCS can be mathematically shown as in Equation 3.5.4.

$$LOLE^{MCS} = \frac{\sum_{i=1}^{N} \left(\sum_{j=1}^{M} x_j \cdot \Delta T \right)}{N} \tag{3.5.4}$$

As mentioned, a "re-engineered" version of the LOLP index can be calculated from the LOLE index. A unitless index is obtained by dividing the LOLE index displayed in Equation 3.5.4 by the number of time increments. The "re-engineered" version of the LOLP index used in this thesis is shown in Equation 3.5.5.

$$LOLP^{MCS} = \frac{\sum_{i=1}^{N} \left(\sum_{j=1}^{M} x_j \cdot \Delta T \right)}{N \cdot M} \tag{3.5.5}$$

The last index included in this thesis is EENS. In HLI assessment this index is also known as Expected Energy Unserved (EEU), Loss of Energy Expectation (LOEE) and Expected Unserved Energy (EUE). The EENS index also accounts for expected number of LOL events. In addition, EENS recognizes the severity of the LOL events. Thus, the EENS index provides the expected number of megawatt hours of demand that cannot be served during a given time period as a consequence of generation and/or transfer capacity deficits. Firstly, the approach to calculate EENS for the analytical method is given. The expected number of MW not served is obtained as the probability of having a specific number of MW on outage, $p(X = x_j)$, multiplied with the the energy that is curtailed at that specific number of MW outage capacity, $x_j - (C - L_t)$. To obtain EENS there will be a summation over all capacity outage states that give a capacity deficit and a summation over all time increments, usually all hours in a year. EENS is mathematically represented by Equation 3.5.6.

$$EENS = \sum_{t=1}^{t=8760} \sum_{x_j=C-L_t}^{C} [x_j - (C - L_t)] \cdot p(X = x_j)[MWh/year] \tag{3.5.6}$$

The expression for EENS in MCS format is shown in Equation 3.5.7. The outcome of a trial, x_j, is multiplied with the amount of energy deficit, Z_j, for that trial and the time duration of the time increment, ΔT. Correspondingly, if there is no LOL event, x_j is zero and the energy deficit is also zero.

$$EENS^{MCS} = \frac{\sum_{i=1}^{N} \left(\sum_{j=1}^{M} x_j \cdot Z_j \cdot \Delta T \right)}{N} \tag{3.5.7}$$

3.5.2 Remarks About the Indices

There are a few important remarks considering the interpretation of these indices. First of all, the indices are expected values. This means that they cannot be interpreted as values that will occur every year, but they indicate the behaviour in the long-run[6]. It should be emphasized that the calculated indices indicate neither frequency nor duration of the capacity shortages. In addition, LOLP, LOLE and EENS are based on static considerations. Their computations are made from information of unit size, availability and load demand. Consequently, the indices do not contain information based on operating conditions, i.e. dynamic responses and operating reserves necessities. It is also evident that the calculated indices are much dependent on the models that are used in the calculation or simulation procedure. Influencing aspects in the models can be how detailed the generator and transmission line state representation is, the modeling of uncertainty, if maintenance is considered or not and also the type of load model used [1].

EENS is the only index that considers the size of the capacity outage. In the evaluation of LOLE all shortages are equally accounted for, e.g. a 10 MW shortage is treated the same as a 100 MW shortage. Hence, EENS can be better suited for power system planners to estimate the cost and impact of LOL events since the index recognizes the size of the event [22].

[6]The distribution of the reliability indices can be obtained by MCS and the state transition method.

Chapter 4

Theory of Demand Side Response

The objective of this chapter is to give the reader an introduction to demand side response (DSR) with a description of its potential as a flexibility resource and its role in the future electricity market. A classification of DSR with its division of different programs is provided in this chapter. Thereafter a literature study on previous work conducted on DSR and power system adequacy is displayed. Based on the literature study the chapter presents a basic model for load shifting, a model for demand side response based on real-time pricing (RTP) and price elasticity, and lastly a method to measure the capacity value of DSR resources with respect to power system adequacy.

4.1 Conceptual Background

The structure of the power system is changing in Europe. One of the changes with significant impact on the reliability is the introduction of more renewable resources into the generation mix. These intermittent resources are substituting base load generation and flexible power plants [2]. As a result of the increasing share of renewable production it is expected that there will be a rising scarcity of flexibility in the power system, both in Europe and in the Nordics [3]. This will lead to more frequent situations with a shortage of available production and a challenging balancing task, but also periods with surplus production. This again will affect the electricity prices in the spot market, which will become more volatile. The Norwegian TSO, Statnett, puts forward that the increased price volatility can give higher profitability for utilization of existing or new flexibility resources [3]. Statnett has found that there is a great potential for flexibility resources in the Nordic countries. Along with flexible production and energy storage, this also includes consumer flexibility

and DSR programs. It is highlighted that these flexible resources are essential for facilitating more renewable production and maintaining a reliable power system.

With the introduction of the smart grid regime, smart meters and other new smart house technologies, the possibilities for DSR have gained a lot of attention recent years. Smart meters and RTP are widely accepted to be required for an efficient use of DSR resources [4]. Furthermore, future benefits of DSR could be numerous. The authors in [4, 29] put forward some of its potential benefits. These include reduction in generation margin and more cost-effective investments in the power system. An estimate found in [29] is that the top peak demand hours usually account for approximately 5% of the time in a yearly load cycle and consume about 1% of the total energy supplied over a year. Installing new generation to cover this peak demand is not economically profitable. DSR resources can substitute this peak demand and thereby postpone investments in new generation capacity, as well as needed upgrade of transmission and distribution facilities for handling grid congestions. Effective utilization of DSR resources would also lead to more cost-effective operation and needed provision of balancing reserves to ensure power balance, voltage and frequency stability. In addition, the authors in [30] highlight that a participating demand side in electricity markets encourages better allocation of economic resources from a socio-economic viewpoint. Improving the demand elasticity in power markets can help to avoid large price spikes in spot markets and lessen the possibilities for generating companies to exercise market power.

Potential barriers for utilization of DSR with respect to the Nordic countries is investigated in [5]. The authors highlight that smart meters and RTP are key concerns for enabling DSR. Real-time monitoring and prices will inform consumers about peak hours and critical events through higher prices. Consumers can be rewarded when there is real-time monitoring of consumption. If they lower their consumption in peak hours or move it to off-peak hours they can get reduced energy bills. Information and communication technology (ICT) and automation services are pointed out as measures that are needed to reduce the transaction cost and apprehension of realizing DSR. These technologies can be able to register prices and cut consumption automatically when prices are high. For instance, the future charging of the electrical car or usage of the water heater can be stopped when prices are above a certain limit. Thus, ICT and automation services can increase the price elasticity of demand. Aggregation services are another measure that is pointed out as required to make use of the potential flexibility DSR offers. Aggregation services help small consumers to react to price signals by management of their consumption. Aggregation services will increase the reliability of DSR resources since larger amounts of load can be aggregated and controlled. Also,

these services make it possible for DSR resources to participate in power markets. The authors in [5] argue that the present Nordic wholesale power market has some features that are not friendly for DSR resources. These are a too long settlement period and a too large minimum bid size. Reducing both the settlement period and the minimum bid size will enhance the potential for DSR in the power market.

Until now, smart meters and ICT are available technologies that can enable DSR resources. Though, it should be mentioned that there follows a cost-benefit analysis of whether there is a potential to save money for the consumers. Installing smart equipment and an ICT infrastructure implies additional costs for the consumers. Also, aggregation services, market design and other contractual settings are not well developed yet. Nevertheless, there is a great interest in DSR options due to the potential benefits mentioned above. There will be several actors involved in the realization of DSR resources, i.e. load providers, aggregators, balance responsible parties (BRPs), distribution system operators (DSOs), TSOs, and software and hardware providers. Communication, guidelines and roles of all parties must be clearly outlined to make use of the full potential of DSR. DSR resources in the future electricity market will be discussed in greater detail later on in this chapter. Firstly, the different features of DSR as flexible resources will be explained.

4.1.1 Demand Side Resources as Flexibility Resources

As mentioned, DSR can provide flexibility resources in a power system that is experiencing rising scarcity of flexible production. In this section the characteristics of flexibility will be explained in further detail. Examples of how DSR resources at end user level can contribute to flexibility will be provided. To begin with, flexibility can be divided into explicit and implicit flexibility [31]. Explicit flexibility is resources that can be mobilized by command, e.g. by a system operator. Most markets for flexibility today are concerning explicit flexibility and short-term operation. This can be balancing services such as primary, secondary and tertiary reserves. These reserves are necessary for handling real-time operation and are offered by generators and larger industrial customers. Implicit flexibility on the other hand, is connected to how consumers respond to price signals. In this case, there will be uncertainty connected to the the availability, mobilization time and volume of the DSR resource. Nevertheless, implicit flexibility can contribute to reduce the need for future explicit flexibility and lessen or postpone the need for capacity upgrades. Figure 4.1 illustrates the main features of explicit and implicit flexibility. The explicit DSR covers a smaller volume with shorter duration compared to the implicit DSR. However, the uncertainty of the implicit DSR is greater.

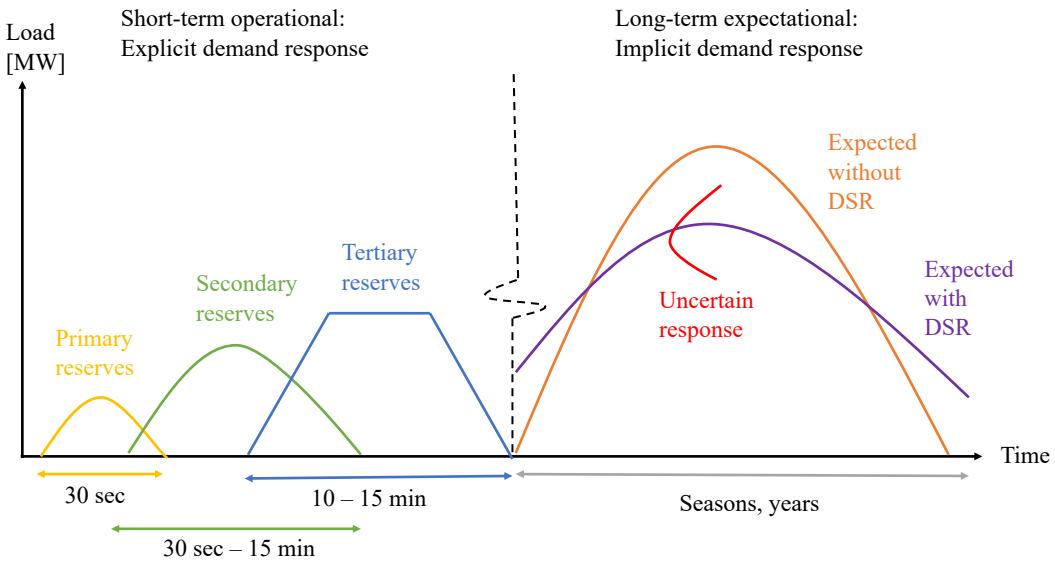

Figure 4.1: Characteristics of flexibility, adapted from [31].

End users can provide both explicit and implicit flexibility. As stated by the authors in [31] the introduction of "internet of things", i.e. smart loads, makes automated load management possible. These automation systems can for instance be responsive to price signals. Another option is that smart loads can be remotely controlled by an aggregator. Hence, the authors in [31] state that the type of flexibility offered by end users is much dependent upon the contractual settings. However, different household resources have different abilities to contribute to explicit and implicit flexibility. This can be due to both technical factors, e.g. load characteristics and human related factors, e.g. influence on comfort level. An example of household resources' possible contribution to both explicit and implicit flexibility is given in Table 4.1. In the examples down-regulation refers to reduced demand and up-regulation refers to increased demand.

Table 4.1: Example of household resources' contribution to flexibility, taken from [31].

Source	**Explicit Flexibility**	**Implicit Flexibility**
Heating (and cooling) system	Suitable for down-regulation for shorter periods, up to hours	Price signal to trigger substitution with other energy carriers, or to flatten demand curve over the day
Household appliances	Limited flexibility, except refrigeration that can provide down-regulation	Flatten demand curve with systematic shift in time-of-use of wet appliances
Local generation of electricity, like PV systems	Limited capability, may up-regulate (reduce generation)	May increase need for flexibility, but also reduce long term need for capacity depending on technology
Local storage, hot water or electricity (batteries)	May shift load from hours up to days. May provide both up- and down-regulation	Flatten demand curve for all usages (el or heating hot water)
Transportation, i.e. electrical vehicle (EV) charging	Suitable for down-regulation, may provide up-regulation (cost issue)	Flatten demand curve with controlled charging behaviour

4.1.2 Demand Side Resources in the Future Electricity Market

The current electricity business model in the Nordics consists of mainly large and centralized generators that sell production in a wholesale market. Retailers buy wholesale and sell to end users, while a system operator is responsible for the security of supply. System services and balancing reserves are in most cases provided by generating units and a small number of larger industry customers [31]. As mentioned, due to more renewable production and less flexibility in the the power system, both Europe and the Nordics will experience more frequently power imbalances. Hence, the question about generation adequacy is put on the agenda again. The authors in [2] address four concrete projects that the Nordic TSOs are focusing on to meet the generation adequacy challenge. These are finer time resolution in the power markets, incentives to provide full cost of balancing, establishing a common Nordic methodology for capacity calculation and empowering of consumers by demand response options that are market-based. All four projects have in common that a well-functioning power market is the solution to reassure generation adequacy. It is further highlighted that if the potential of DSR shall be realized there is a need for an aggregator role. This will permit third parties to aggregate loads from different bidders and offer it to a market as flexibility resources.

As an example, one residential water heater can provide only approximately 0.0005 MW of load reduction. On the other hand, an aggregation of 100 000 water heaters could yield 50 MW of load reduction [32].

Different options for market design incorporating DSR with respect to the current models in Europe and in the Nordics can be found in [33, 34]. It is put forward that there might not be a single solution for a fitting market design. In some cases bilateral agreements can be the best choice, in other cases integration with existing markets can be sufficient, while in other instances formation of separate markets for flexibility is the best choice. It is put forward by [34] that all relevant markets should be open for competition with DSR if a goal is to get the consumers to react to electricity prices. A much related concern is to decide which party that shall take the aggregator role. An integrated model suggests that retailers or BRPs take the role as aggregator. Other models recommend third party aggregators. A last suggestion is a regulated model where a DSO or a TSO takes the role as aggregator. Hence, market design and the aggregator role are topics that need to be further addressed before efficient use of DSR resources can take place. This thesis does not further deal with this matter, but recognizes the issue.

Figure 4.2 shows how the future value chain for a smart end user can look like. In addition to selling flexibility to an aggregator, there can be possibilities to sell surplus power to the grid, store own produced power for future use or flatten out the demand curve, sell power on a peer-to-peer foundation, etc. It is evident that a flexible consumer can be achieved in a variety of practices in the future. Figure 4.2 also indicates that not only the TSO, but also DSOs can make use of flexible resources. This suggests that flexibility should be priced correct for its local value when it is needed to solve local issues. One example of a local market platform for flexibility is NODES [35]. This is a market place where flexibility sources are linked to its placement in the grid, and bids and offers will also be linked to placements such that buyers can purchase flexibility where it is needed. It is evident that local flexibility has a very high value in some hours, but zero value in most hours. As suggested in [35], the marketplace for local flexibility should also function as a gateway to the other main electricity markets, like the intra-day market, when the value is higher there than at the local market. Thus, the future consumer can profit from being price responsive both at a local level and at a central level.

A consumer offering flexibility to a market will affect the demand-supply curve. Figure 4.3 shows an example of a demand-supply curve for today's case of almost inelastic demand and a hypothetical demand curve in the case where the demand side bids amounts of load as a function of price. A

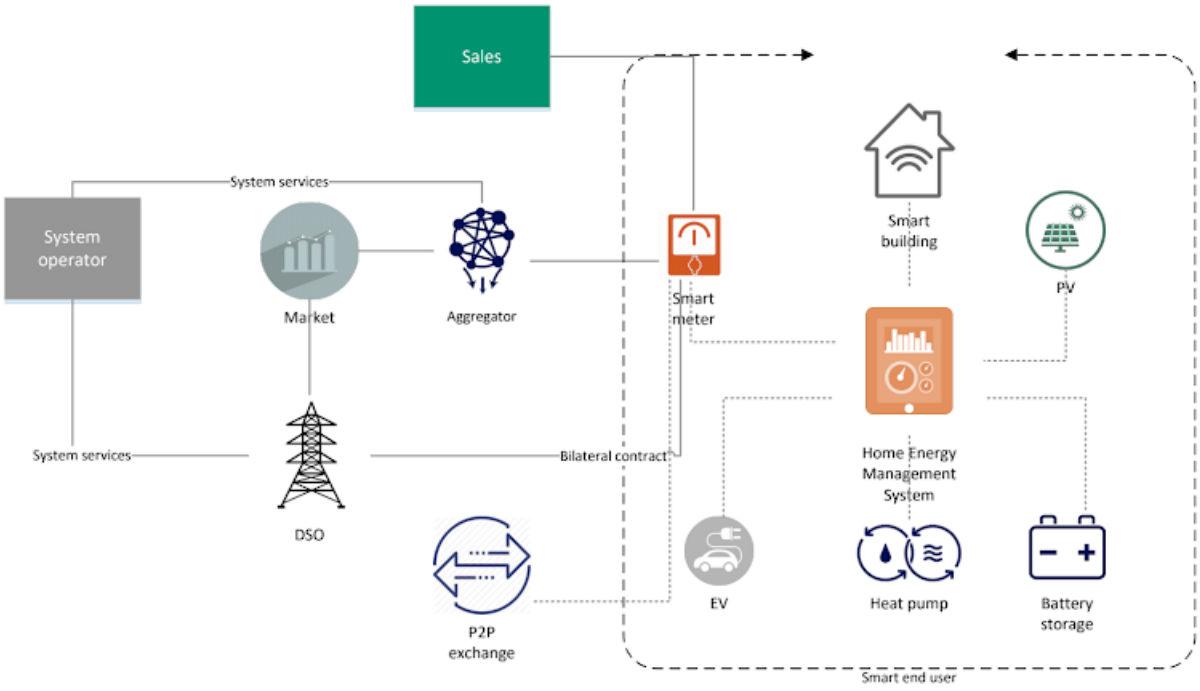

Figure 4.2: A future value chain for the smart end user, taken from [31].

market model would set the demand to be a fixed value in each hour when the demand curve is treated as inelastic. The optimization is then aimed at the generator bids only [32]. Conversely, the demand curve can be arranged in merit order as seen in Figure 4.3 when the demand side is able to bid into a wholesale day-ahead electricity market.

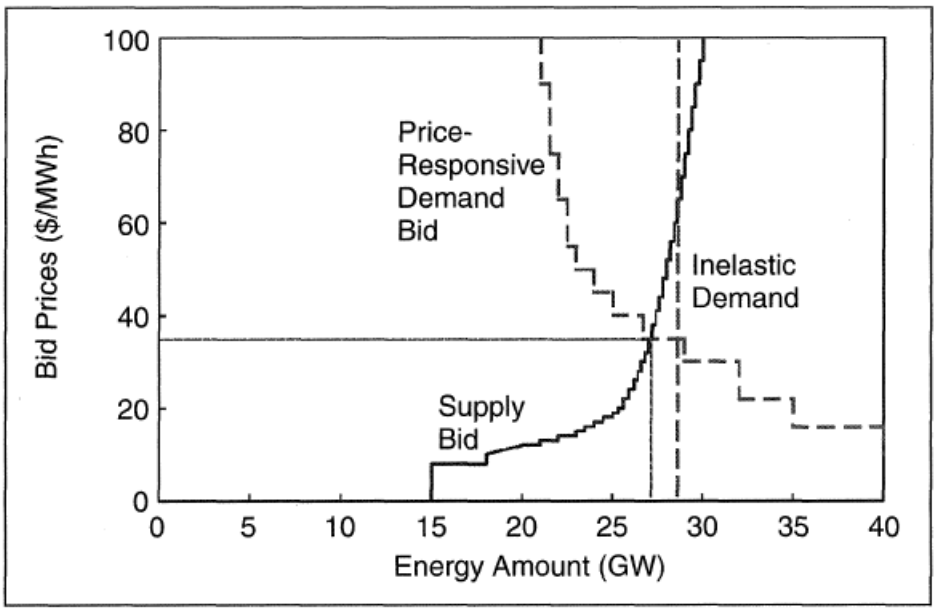

Figure 4.3: Demand-supply curves for inelastic demand and demand bidding, taken from [32].

4.2 Classification of Demand Side Response

This section will give a theoretical explanation and division of DSR programs. Firstly, DSR can be viewed as one of the divisions of demand side management (DSM). In literature, DSM and DSR are often used and referred to interchangeably. This section will therefore start by giving a definition of DSM and explain the activities it covers. DSM can be explained to be programs implemented by electric utilities to motivate consumers to adopt practices that are advantageous from both system and customer view points [36, 29]. These programs have the objective to affect the shape of the load curve. This is done by affecting the time pattern of the curve, the magnitude or a combination of both [29]. Figure 4.4 shows the main division of DSM activities. Energy efficiency and strategic load growth will be explained briefly in the following. DSR will be the main focus and the different DSR programs will be explained in more detail afterwards.

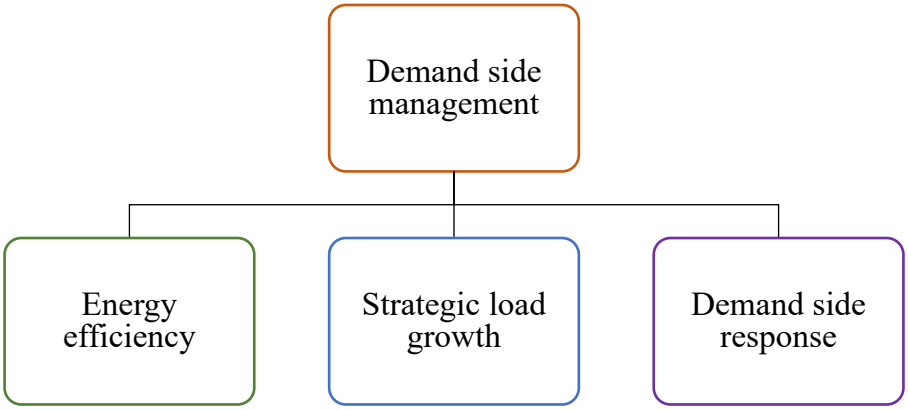

Figure 4.4: Division of demand side management activities, adapted from [29].

Energy efficiency strategies aim at reducing demand through energy-efficient practices or processes. This will lead to reduced energy demand. Examples of such strategies can be energy efficient buildings, using heat waste from industrial processes for heating purposes or improving the efficiency of the power grid by using low-loss transformers or advanced control systems [29].

Strategic load growth means an increased electrical load demand normally induced by incentives

from the utilities. An example is the substitution of fuel heating with electrical heat pumps [29]. Strategic load growth is also referred to as electrification [31]. This can be seen as increased electricity demand due to for example growth in electrical vehicles and charging stations.

DSR can be defined as the reaction encountered by end-use consumers in their electrical energy demand due to changes in electricity price, to incentive payments or signals from the system operator [6]. Figure 4.5 shows a division of DSR programs. The classification of DSR programs can differ in literature. The division in Figure 4.5 is between incentive-based programs (IBPs) and price-based programs (PBPs) [37]. As mentioned in [37], literature papers also classify the programs into system- and market-led, emergency- and economic-based, or stability- and economic-based. A short explanation of the programs displayed in Figure 4.5 will be given in the following.

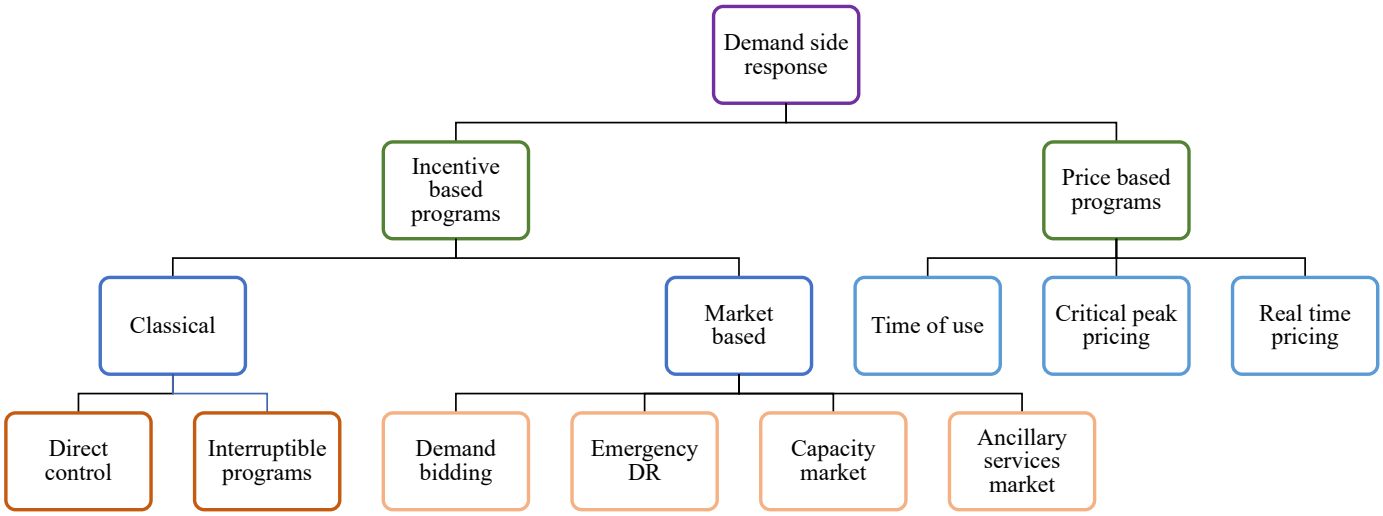

Figure 4.5: Division of DSR programs, adapted from [37].

Classical IBPs include direct load control and interruptible load programs. The participants in the classical IBPs usually receive discounted electricity rates or a reduced bill compensation for participating in the programs [29, 37]. The utility can control the load directly after consumers

are informed in direct load control programs. These programs aim at reduction in load demand in periods when security is jeopardized. Interruptible load programs are normally applied for large industrial and commercial consumers who are able to shut down their load for a short period. The consumers that are included in the program can be penalized if they do not reduce the load when required [29].

In market IBPs the participants will receive payments in line with their performance which depend on the amount of load reduction [37]. Demand bidding or sometimes referred to as buyback programs involves consumers bidding on load reductions in a wholesale market. It would be most beneficial for the consumer to bid for load reduction when the electricity prices are high, that is during the peak hours [37]. In emergency DR programs the participants receive incentives to reduce their load demand during critical situations such as system contingencies. In these programs there are no penalties if the costumer cannot participate [29]. Capacity market programs for DSR resources are usually intended for those consumers that are able to provide pre-specified load reductions when contingencies occurs. Ancillary service market programs for DSR involve participants that are allowed to bid on load reductions in the spot market and then function as an operating reserve. If their bids are accepted, participants get paid the spot price for being on stand-by and ready to curtail load [37].

PBPs are based on dynamic pricing schemes where the electricity price shall reflect the real cost of electricity and thereby try to flatten out the demand curve. This will involve a higher price during peak hours and a lower price during off-peak hours [37]. Some of the main PBPs are given in Figure 4.5. Time of use rates (TOU) are predefined price levels over given time periods. The time periods can be seasonal, monthly, weekly or daily [29]. The rates aim at reflecting the average cost of electricity during the given time period [37]. Critical peak pricing (CPP) reflects the actual spot price in the presence of critical events. Hence, CPP can initiate consumers to decrease load during stress events and thus contribute to improved system reliability [29]. RTP are programs where customers are charged with the actual market price. The prices are usually given on a day-ahead or hour-ahead basis [29, 37]. A model for price-responsive demand based on RTP is explained in greater detail later on in this chapter.

All DSM activities shown in Figure 4.4 have an effect on the shape of the load curve. Energy efficiency and strategic load growth have long-term effects on the load demand. DSR programs can have both long-term effects like PBP, and short-term effects like the short-term load manipulations initiated by IBPs. Anyhow, DSR can in general be viewed as a load shaping management process

which is performed through peak clipping, valley filling or load shifting [29]. These techniques are illustrated in Figure 4.6.

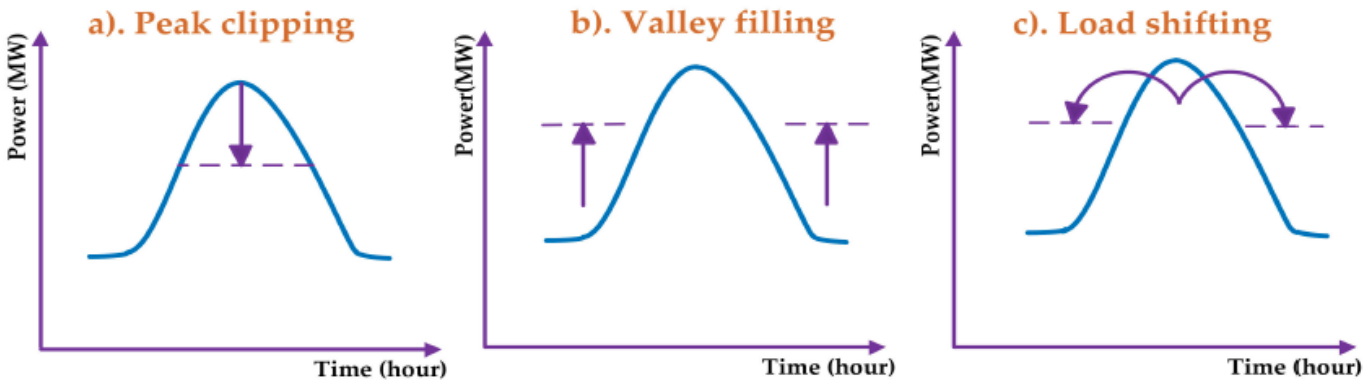

Figure 4.6: Load shaping techniques, taken from [38].

4.3 Previous Work on Demand Side Response and Power System Adequacy

This section provides a selected sample of previous work done on DSR and power system adequacy. The objective of the literature study is to find relevant literature for the modelling of DSR in adequacy assessment. It is chosen to focus on sources that model load shifting which is a main load shaping activity that can be initiated with DSR, and sources that model price responsive demand which link DSR activities to actual programs. The reader should note that it is not focused on sources that go into technical details concerning load shifting, e.g. which loads that suit to be used for load shifting, duration constraints, ect. The focus is rather on how load shifting can be modelled in the yearly load profiles used in power system adequacy assessment. In addition, literature that presents methods to evaluate the capacity value of DSR are covered. For a more comprehensive literature study on the topic of DSR and power system reliability in general, the reader is recommended to see [29].

4.3.1 Demand Side Response Modelled by Load Shifting

A basic load shifting model is used in a number of research papers for the evaluation of the impact of DSR on power system adequacy [36, 38, 39, 40, 41, 42, 43, 44]. The load shifting model consists

of the two elementary operations peak clipping and valley filling. Load is clipped at a pre-specified peak level and the clipped energy is recovered in the following off-peak hours. The recovered energy is added in equal proportions to each valley hour after the peak period. Several different studies are conducted using this load shifting model. The studies in [36, 39, 41, 43] are examples of HLII-studies using the described load shifting model. The authors in [36, 41] found that the load shifting had a positive effect on load point indices in the RTS. The authors in [43] included load forecast uncertainty in a similar study. Furthermore, [39] investigated the interaction between DSR and a thermal rating system for composite power system adequacy.

The study in [38] evaluated the impact of DSR on generation system adequacy. The authors differentiated between preventive load shifting and corrective load shifting. The preventive load shifting model is the same load shift model referred to above. This model shaves the peak load even though there is no generation capacity deficit. Thus, the load manipulations are performed in advance. Contrarily, the corrective load shifting model only clips the load when there is a deficiency of generation capacity. The authors in [40] also performed a study on the impact of DSR on generation adequacy. The authors used the basic load shifting model for modelling of DSR and divided the load into different load sectors. The effect of load shifting on the different load sector demand profiles was evaluated as well as the contribution to different generation adequacy indices. In addition, [42, 44] performed reliability cost/worth analysis for generation system in the presence of DSR programs modelled by peak clipping, valley filling and the basic load shifting model.

The basic load shifting model used in the previously mentioned literature utilizes a chronological load curve in the reliability evaluation. The studies in [45, 46] are examples of research papers that proposed methods to model the impact of DSR and DSM in general on a LDC. The authors in [45] presented a method to reflect the impact of DSM on a LDC by the change in three particular variables, change in peak load, change in base load and/or energy demand. Moreover, [46] utilized an eigenvector method to describe impacts of DSM on future electricity demand. These impacts were reflected in the LDC used in the calculation of adequacy indices.

4.3.2 Demand Side Response Considering Demand-Price Elasticity

The concept of cross-time elasticity was first explored in early papers from the late 80's and beginning of the 90's. Two examples of such papers are [47] and [48]. The authors of these research papers argued that a regular demand-elasticity model only considering self-elasticity, i.e. the response in

load to price changes in the same time interval, was inadequate. With the concept of cross-time elasticity, i.e the response in load due to price changes in other time intervals, it was shown that dynamic tariffs and load demand can be mutually influencing each other in an iterative solution procedure.

A demand-price model using both self- and cross-elasticities is often referred to as a price elasticity matrix (PEM) in literature. Several studies that cover DSR have used PEMs to model consumer behaviour and interaction with RTP schemes. The authors in [49] investigated how elasticity of demand could be taken into account when deciding the electricity price in a centralized competitive market. The authors showed how different structures, namely the arrangement of zero and non-zero values in the PEM, could model different consumer strategies.

The authors in [50] and [51] studied how demand-price elasticity affected the reliability in deregulated power systems. Demand response was modeled using PEMs. Nodal prices was calculated as Lagrange multipliers from OPF models. The RBTS was used as test system in [50], while the 24-bus RTS was used in [51].

In addition, PEMs have also been used in market models. The authors in [52] used PEMs to model consumer behavior in a market optimization model for a microgrid with demand side bidding. Furthermore, the authors in [53] used PEMs to model inter-hour shifting constraints in a model for a new wholesale bidding mechanism for demand response within a smart grid regime.

4.3.3 Methods for Evaluating the Capacity Value of Demand Side Response

Methods to evaluate the capacity value of DSR resources can be found in [6, 54, 55]. The authors in [6] used Effective Load Carrying Capability (ELCC) as the capacity credit for DSR in a HLI assessment. The study used demand response availability profiles and investigated the effect of energy constraints on the capacity value of the DSR resources. The authors used an analytical approach with a COPT for the index calculation. The study in [6] also mentioned Equivalent Conventional Capacity (ECC) and Equivalent Firm Capacity (EFC) as common metrics for capacity evaluations in adequacy assessment. Moreover, [54] utilized ELCC as the capacity credit in a HLI study evaluating different price-based DSR programs. The authors analyzed how increasing amount of available DSR resources affected their capacity value, how the flexibility and the design of the DSR program affected their capacity value as well as how uncertainty influenced the value of the ELCC. Lastly, [55] investigated the reliability of DSR technologies for handling congestion in distribution

grids. In addition to ELCC and EFC, Equivalent Network Capacity (ENC) was used to quantify the reliability contribution of different DSR technologies.

4.4 A Model for Load Shifting

The purpose of DSM techniques in general is to shape the load curve. As mentioned this is achieved by either reducing, increasing or shifting load. For DSR this is performed through incentive-based or price-based programs as shown in Figure 4.5. The effect of these programs can be modeled by three operations, namely peak clipping, valley filling or load shifting. The magnitude and duration of the characteristics will vary according to which type of program that is implemented. This section presents the model for load shifting in this thesis. The model is used to investigate the impact of load shifting on adequacy indices. The basic load shifting model found in [38, 36, 39, 40, 41, 42, 43, 44] is given in Equation 4.4.1. This model is applicable for a chronological load curve. The model is displayed for a load curve with units in MW, but it can also be used with a per unit notation.

$$\overline{L(t)} = \begin{cases} P, & t \in \Omega \\ L(t) + A, & t \in \Psi \end{cases} \tag{4.4.1}$$

where

$$A = a \cdot \frac{\sum_{t\in\Omega}(L(t) - P) \cdot \Delta T}{N},$$

$L(t)$: original load model in MW with time increments of duration ΔT,
$\overline{L(t)}$: modified load model in MW,
Ω: set of on-peak hours where the energy is shaved,
Ψ: set of off-peak hours where the energy is recovered,
P: system peak demand in MW after implementation of DSR activities,
A: amount of load in MWh/h added to each off-peak hour of Ψ,
$\sum_{t\in\Omega}(L(t) - P) \cdot \Delta T$: shaved energy in MWh for the peak hours in Ω,
N: amount of off-peak hours in Ψ,
a: percentage of the shaved energy that is recovered during off-peak hours.

The on-peak and off-peak hours can be determined by a pre-specified load level or be given by particular hours during the day. The load in on-peak hours are reduced to the new peak value P.

The energy that is clipped during on-peak hours is shifted to the immediately following off-peak hours. As can be seen from Equation 4.4.1, an equal amount of load is added to the following off-peak hours. If it is assumed that the DSR program will not contribute to decrease in the energy consumption throughout the day, but only shift the load, then it would mean that the energy recovery percentage is equal to 100%.

4.5 A Model for Demand Side Response Based on Real-Time Pricing and Price Elasticity

Smart meters and RTP permit transparency in prices as well as monitoring of consumption. This again enables the consumer to know when electricity prices are higher. Also, the consumers can be rewarded if they reduce their demand in these hours since the consumption is monitored in real-time. The authors in [5] have conducted a literature review on how smart metering can influence the price elasticity. They found that it is likely that smart meters and RTP can shift the short-run price elasticity from almost inelastic demand, i.e. below 0.5 in absolute value, towards 1.0 in absolute value. Although there is uncertainty in the studies the authors refer to, transaction costs can be lowered by ICT, automation and aggregator services and that will further increase the price elasticity of demand. This section presents a model for how a consumer can react to RTP depending on their price elasticity.

To begin with, the assumptions that are made for the RTP model are listed below:

1. An OPF formulation is used to calculate nodal prices that function as real-time prices for the tests systems used in the case study. With an OPF formulation, nodal prices can correlate to the load data of the test systems, system topology and constraints, and production costs. In addition, with an OPF formulation, outage cases can be used to trigger higher prices that will correlate to the hours with highest load demand in the yearly load profiles. This is a main reason to why an OPF formulation is used to calculate real-time prices.

2. Demand is taken as a constant and it is assumed that only the supply side sends bids of production to the operator.

3. The bids of the supply side reflect the generator production costs. Quadratic cost functions are used. All generating units at a bus have the same cost function.

4. Load forecast uncertainty is not considered in the analysis. It is assumed that the operator knows the initial demand for the next day.

5. The operator announces the prices for the following 24 hours based on initial load demand and the available generation and/or transmission capacity. The consumer can then react to these prices by changing their initial load demand over the 24 hour study period. This reaction is based on their price elasticity and the potential difference between the prices announced by the operator and the prices expected by the consumer.

6. Potential price changes are triggered by outage of generating units and/or transmission lines. An outage case is simulated for all hours in a year, yielding a price difference in most hours.

7. The consumers only reschedule their load, meaning that the total energy demand over the 24 hour study period is not reduced. Furthermore, it is assumed that all consumers react to high prices in the same way, i.e. the elasticity matrix is the same for all loads.

8. Only short-term responses to prices are considered in this model. Short-term is defined as the time that elapses between the announcement of the day-ahead prices and the actual demand period.

9. Only response to spot prices for electricity are accounted for. Other parts of a tariff are not regarded[1].

4.5.1 Price Elasticity of Load Demand

A typical price-demand curve is illustrated in Figure 4.7. In general, the demand decreases as the price of a commodity increases. It can be a hard task to quantify the actual price-demand curve of a commodity. Usually, the curve will not be linear. Hence, the curve can be linearized around an equilibrium point (d_0, p_0) as shown in Figure 4.7 [49]. In this thesis, the equilibrium point is defined as the price and demand of the original case, i.e. initial demand and price. The initial prices are calculated using the initial demand and a system with all components up. Further, one equilibrium point is chosen for each study period with equal time spacing, e.g. initial demand and price in hour 12, 36, 60, 84, ..., 8724. The price elasticity of demand is shown in Equation 4.5.1.

[1] If a power tariff is implemented this can give further incentives for the consumers to shift load from peak hours to off-peak hours [3]

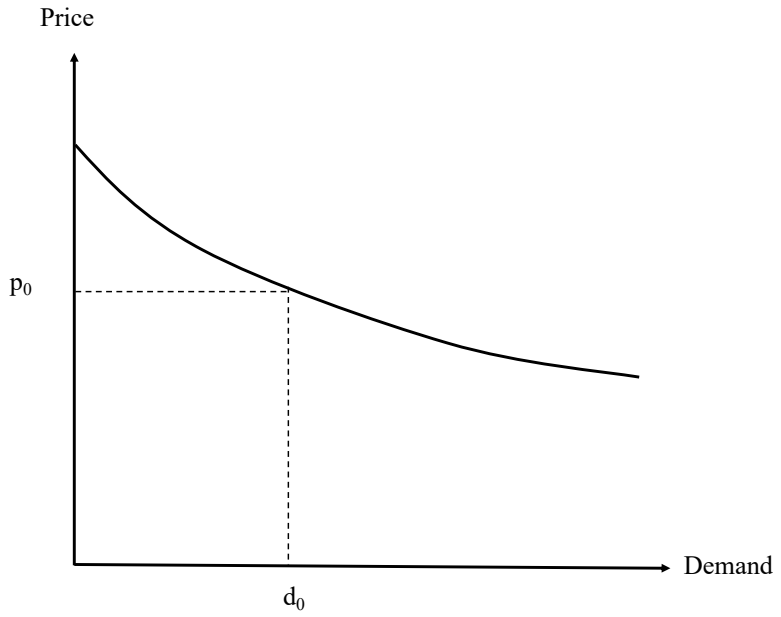

Figure 4.7: A typical price-demand curve, adapted from [49].

$$\varepsilon = \frac{\Delta d/d_0}{\Delta p/p_0} \tag{4.5.1}$$

where Δd and Δp are changes in demand and price with respect to the initial case, and d_0 and p_0 are the chosen equilibrium point.

Electrical demand and electricity prices are constantly changing through a day. As stated in the assumptions, only short term responses are considered in this thesis with a 24 hour study period.[2] Thus, prices and demand at different hours in a day are correlated for a price responsive load. This means that the elasticity changes form a single scalar value to an elasticity matrix consisting of 24x24 values if an hourly resolution is used. The PEM consists of two types of coefficients. These are self- and cross-elasticity. The self-elasticity coefficient, ε_{ii}, indicates the effect of price in hour i on demand in hour i. The cross-elasticity coefficient, ε_{ij}, indicates how demand in hour i changes with respect to the price in another hour j. Equations 4.5.2 and 4.5.3 show the formulae for the self- and cross-elasticity respectively. Normally, the self-elasticity coefficients are negative values

[2]Consumers with long-term responses would take into account all study periods when deciding their demand.

and the cross-elasticity coefficients are positive values [49].

$$\varepsilon_{ii} = \frac{\Delta d(i)/d_0}{\Delta p(i)/p_0} \tag{4.5.2}$$

$$\varepsilon_{ij} = \frac{\Delta d(i)/d_0}{\Delta p(j)/p_0} \tag{4.5.3}$$

The demand and price changes in this thesis are the differences between the prices announced by the operator and the expected prices by the consumers which are the prices from the initial case. How to calculate the demand changes from the elasticity matrix and the deviation between the announced prices and the expected prices is shown in Equation 4.5.4.

$$\begin{bmatrix} \Delta d(1) \\ \Delta d(2) \\ \dots \\ \Delta d(i) \\ \dots \\ \dots \\ \Delta d(24) \end{bmatrix} = \begin{bmatrix} \varepsilon_{1,1} & \varepsilon_{1,2} & \dots & \varepsilon_{1,24} \\ \varepsilon_{1,2} & \varepsilon_{2,2} & \dots & \varepsilon_{2,24} \\ \dots & \dots & \dots & .... \\ \dots & \dots & \varepsilon_{i,j} & \dots \\ \dots & \dots & \dots & \dots \\ \dots & \dots & \dots & \dots \\ \varepsilon_{24,1} & \varepsilon_{24,2} & \dots & \varepsilon_{24,24} \end{bmatrix} \cdot \begin{bmatrix} (\Delta p(1)/p_0) \cdot d_0 \\ (\Delta p(2)/p_0) \cdot d_0 \\ \dots \\ \dots \\ (\Delta p(j)/p_0) \cdot d_0 \\ \dots \\ (\Delta p(24)/p_0) \cdot d_0 \end{bmatrix} \tag{4.5.4}$$

Figure 4.8 shows how price elasticity together with a price deviation is used to modify the demand. The effect of DSR on nodal price volatility is not studied to any great extent in this thesis. Nevertheless, this can easily be implemented by running the OPF with the adjusted demand and obtaining the new nodal prices. Smart meters and ICT enable that demand and prices can interact mutually. The iterative procedure indicated by Figure 4.8 can be applied until the deviation between the announced prices and the expected prices is smaller than a set threshold value, i.e. the interaction between the utility and the consumers is dynamic. The authors in [53] show how this iterative procedure can be used in a market clearing algorithm with demand bidding. This can be an option if aggregation services emerge. For simplicity and illustrative purposes, only one iteration is considered in this thesis. As stated in the assumptions, a day-ahead tariff is used and consumers

can plan their demand based on the announced prices for the next 24 hours, their expected prices and their price elasticities.

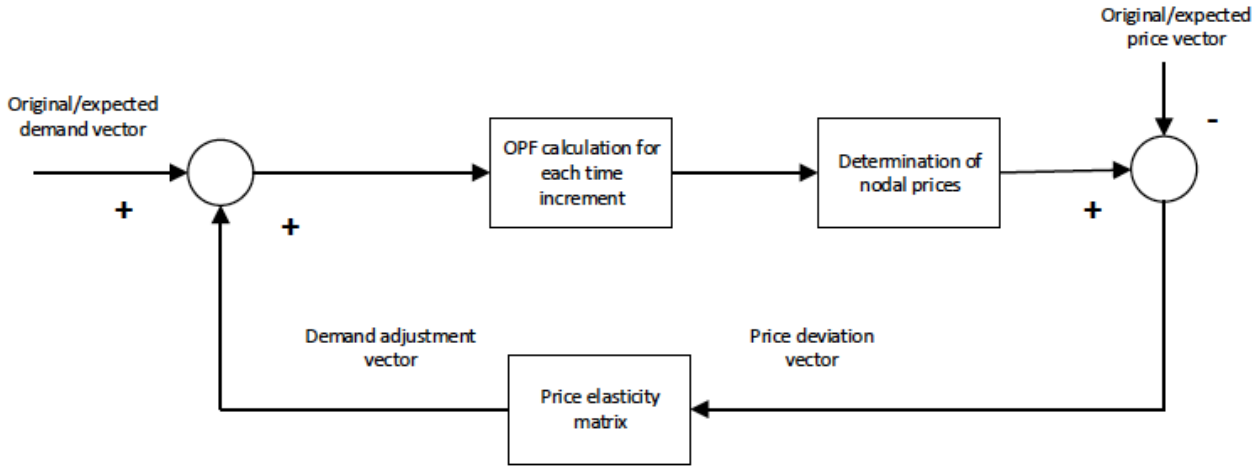

Figure 4.8: Interaction between price elasticity, price deviation and demand, adapted from [51].

4.5.2 Consumer Modelling by Price Elasticity Matrices

The structure of the coefficients in the PEM can be used to reflect different load types or consumer strategies. An understanding of how to model different consumer behavior was mainly gained from [49]. In addition, the reader can find illustrative examples of structures of PEMs that model early shifting, late shifting, forward shifting, backward shifting, flexible and real-world consumers in [52] and [53]. To begin with, column j in the PEM indicates how change in price in hour j affects the load in other hours. Correspondingly, row i in the PEM indicates how change in price at different hours affect the load in hour i. Non-zero values above the diagonal, the upper triangle of the PEM, can be used to model a consumer that brings forward its load demand when the prices are higher than expected prices in subsequent hours. If non-zero values are placed below the diagonal, the lower triangle of the PEM, this is an indication of a consumer that postpones load demand due to high prices in previous hours, i.e. the consumer postpones consumption to times when the prices are lower.

The placement of zeroes and non-zero values in the upper triangle is also reflecting the consumer's amount of information. An upper triangle of zeroes and a lower triangle of non-zero values reflects a consumer that only has access to prices of past and current time intervals. The consumer has not been given the prices for the next hours. On the other hand, if the consumer is given prices for the

subsequent hours non-zero values will also occur in the upper triangle.

The flexibility of a load, i.e. how long is the period a consumer can reschedule its consumption, is modeled by the length of non-zero values around the diagonal. If a load is totally inflexible all cross-elasticities will be zero. For a load with some flexibility the values will be clustered around the diagonal. A very flexible load has values spread over the whole column.

The consumer can both bring forward and postpone consumption with an economical optimal strategy. A smart or optimizing consumer will reschedule its consumption such that load is increased during low price periods and decreased during high price periods. Low price periods will usually be early in the morning and during night time and higher prices are expected during day time. Hence, the PEM will have non-zero values in the top and bottom rows for a smart consumer.

Furthermore, one of the assumptions made for the analysis is that the overall energy demand of the consumers is kept constant. A consumer that does not reduce, but only reschedules its consumption over the 24 hour study period is obtained if the relation given in Equation 4.5.5 holds for all columns in the PEM. Contrarily, if the overall demand is reduced during the study period, the sum of all ε_{ij} in a column would be less than zero.

$$\sum_{j=1}^{24} \varepsilon_{ij} = 0 \qquad \forall\ i \tag{4.5.5}$$

4.5.3 Calculation of Nodal Prices Using Optimal Power Flow

The theory behind nodal price calculations based on an OPF formulation can be found in textbooks such as [56]. The full AC OPF problem formulation and the associated Lagrangian function can be found in [50] and [51]. In this thesis, the OPF formulation described in [8] has been reformulated to be a minimization of generator production costs. Most of the constraints in the OPF will be the same as in [8]. The only difference is that load curtailments are not considered. Thus, these variables are fixed to zero in all constraints and in the final solution. The AC OPF problem given in [8] can be found in Appendix E.

The new objective function is given in Equation 4.5.6. Only the cost of active power production is considered.

$$\text{Min f} = \sum_{i}^{n} C_i(P_i) \tag{4.5.6}$$

where C_i is the generator cost function of node i. The generator cost functions are quadratic functions as shown in Equation 4.5.7.

$$C_i(P_i) = a + b \cdot P_i + c \cdot P_i^2 \tag{4.5.7}$$

The a-coefficients are set to zero for all generating units since they are not affecting the solution of the optimization problem.

The nodal prices are obtained as the shadow prices or Lagrange multipliers of the active power balance constraints at optimal solution. Hence, a nodal price at bus i is the marginal cost of supplying load at bus i, i.e. the cost of supplying one additional load unit to bus i. An unconstrained case that disregards grid losses yields equal prices at each node [56]. The nodal price model in this thesis uses an AC OPF formulation that accounts for grid losses. Hence, different nodal prices are obtained at the nodes regardless of whether there are binding transmission constraints or not. The solver used in MATLAB for the AC OPF model, *fmincon*, can return Lagrange multipliers for any constraint defined in the problem if specified.

As a concluding note, it can be put forward that in a decentralized system spot prices are calculated by finding the intersection between the aggregated sale and purchase curve of electric power [56]. Hence, this system price does not indicate transmission constraints between areas. As presented in [56], pooling institutions like Nord Pool use area prices for congestion management. This is a simpler price representation than nodal prices. Nodes are grouped into different price areas or zones, and if there is congestion between areas system prices are adjusted to relieve the congestion. Generally, produced power will flow from an area with lower price towards an area with higher price [56].

4.6 A Measure for the Capacity Value of Demand Side Response

The basic load shifting model and the RTP model presented in the previous sections can be used to analyze the effects of load shifting on the reliability of load buses and the system as a whole. However, for long-term planning it is needed more information than just the influence DSR resources have on the reliability level. The authors in [6] put forward that there is a need to measure the value of having available DSR resources in a power system. To be able to obtain a capacity value of DSR enables the possibility to compare the value of DSR resources with respect to other resources such as additional generating and transmission capacity. Also, obtaining a capacity value of DSR can give a better indication of the potential within different markets and sectors and provide a guide to the real cost of DSR.

Based on the literature review, ELCC was the capacity credit preferred by most authors that consider DSR resources. The procedure to obtain the ELCC is the same for both HLI- and HLII assessment. This metric will be explained in further detail, and ELCC is chosen as the method for evaluating the capacity value of DSR resources in this thesis. Nevertheless, the definitions of EFC and ECC will be given as well since those metrics also appear to be frequently used in adequacy evaluations. The authors in [6] define EFC as the capacity of a 100% reliable unit that can be replaced by the resource under investigation while maintaining the current reliability level. In case of DSR resources, EFC gives the amount of 100% available capacity which can replace the DSR resource while maintaining the given reliability level. ECC is similar to EFC except that the measure is in terms of conventional capacity and not 100% reliable capacity. ECC is defined by [6] as the capacity of a conventional unit, meaning not 100% reliable, that can be replaced by the resource while keeping the current reliability level.

ELCC, when the resource under investigation is a DSR resource, can be defined as the amount of load increase allowed in the presence of DSR resources while maintaining the original reliability level [55]. Most of the definitions, both ELCC and the other metrics, use the reliability level of the original system as reference. In principle this can be any desired reliability level. The desired reliability level is measured by an appropriate reliability index, and LOLE and EENS are often used.

Below follow the mathematical expressions for calculating ELCC in the presence of DSR resources by using these two indices. The analytical expressions for LOLE and EENS are used to illustrate the interpretation of the ELCC since those equations are found to be most suited for that purpose.

Equations 4.6.1-4.6.2 give the expression with LOLE as the reliability index and Equations 4.6.3-4.6.4 express the same by using EENS as reliability index. The notation is similar to that introduced in Section 3.5.

$$LOLE^{Org} = LOLE^{DSR} \tag{4.6.1}$$

$$\sum_{t=1}^{T} P(X > C - L_t) = \sum_{t=1}^{T} P(X > C - (L_t^{DSR} + \Delta L) \tag{4.6.2}$$

$$EENS^{Org} = EENS^{DSR} \tag{4.6.3}$$

$$\begin{aligned} &\sum_{t=1}^{T} \sum_{x_j=C-L_t}^{C} [x_j - (C - L_t)] \cdot p(X = x_j) \\ &= \sum_{t=1}^{T} \sum_{x_j=C-L_t^{DSR}}^{C} [x_j - (C - (L_t^{DSR} + \Delta L))] \cdot p(X = x_j) \end{aligned} \tag{4.6.4}$$

Superscript *'Org'* denotes the original system and superscript *'DSR'* indicates the system with DSR resources. With reference to the context of this thesis, L_t^{DSR} denotes the changed load curve after DSR has been implemented. Thus, the ΔL that satisfies the condition in Equation 4.6.1 or 4.6.3 is the ELCC for the DSR resource. Although the analytical equations are used to describe the ELCC, the general interpretation will be the same if MCS is used to obtain the indices. The methodological approach given in Section 5.4 is further illustrating the implementation of the ELCC calculations in this thesis. The reader should note that the ELCC calculation procedure is the same both for an analytical and for a simulation approach, and also for HLI- and HLII assessment. The input to the ELCC calculation procedure is vectors of index values. Hence, what type of assessment and approach that is used to obtain these vectors can differ, but not the calculation procedure to obtain the ELCC.

It is important to remark that ELCC as a capacity credit is a system dependent measure. When evaluating a specific system configuration, the ELCC obtained is representative for that specific system with its total installed capacity, a given number of generating units, its network topology,

the components' availability and its given load profile. Also, ELCC as a measure is dependent upon the reliability index used. The same system can have unequal values of ELCC if different indices are used.

Chapter 5

Methodological Approach

This chapter presents the methodological approach for the evaluation of the impact of DSR on power system adequacy indices and the calculation of the capacity value of DSR resources. DSR is modeled by two applications of the model for load shifting presented in Section 4.4, and the RTP model presented in Section 4.5. The two load shifting methods are abbreviated LSM1 and LSM2 in the following. This notation is also used in the case study. MATLAB-scripts for these models have been developed and a detailed description of the implementation will be given in this chapter. These models are utilized to modify the load curve before reliability indices are calculated, i.e. the modified load model is kept constant during the calculation procedure. Figure 5.1 gives an overview of the calculation procedure. The indices are calculated either by an analytical or a simulation approach as presented in Chapter 3. The software for the analytical approach is from the work of [7] and the software for the simulation approach is from the work of [8].

For the calculation of the capacity value, ELCC, modifications are made to the work of [7]. These MATLAB-scripts were originally made for evaluation of the ELCC of interconnectors and generating units, but are modified to calculate the ELCC of DSR resources instead based on the theory given in Section 4.6. As mentioned in [7], an iterative approach can give the exact solution for the ELCC, but as this can be computationally intensive, simplified methods like curve fitting can be applied. A simplified graphical method is presented in [7] and is the basis for the MATLAB-scripts utilized for the ELCC calculations. The graphical method used will be illustrated later in this chapter. Firstly, a description of the load model applied for the test systems in the case study will be provided. Following this comes the implementation of the different DSR models.

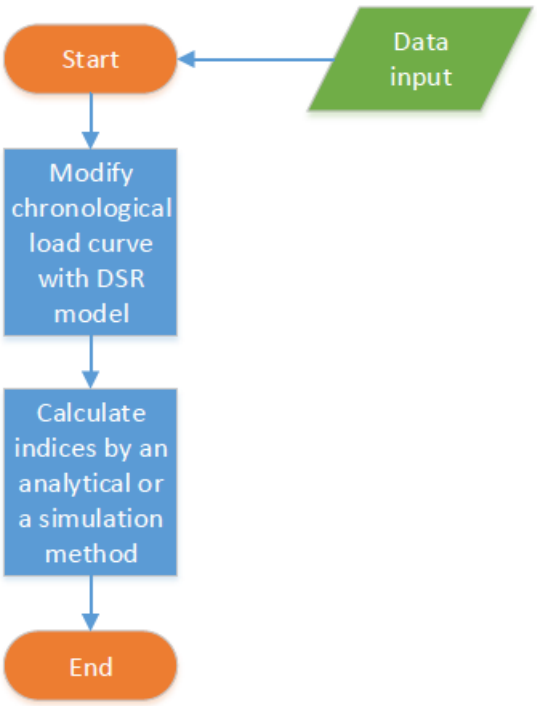

Figure 5.1: Overview of reliability index calculation procedure with demand side response models.

5.1 Description of Load Model Used in Case Study

The load model used in this thesis is a chronological load model. The same model is used for the two test systems in the case study, only scaled by the yearly peak load (YPL) of the system. The load model is based on the following approach: The weekly peak load (WPL) is given in percent of the YPL, the daily peak load (DPL) in percent of the WPL, and the hourly peak load (HPL) in percent of the DPL. Thus, these percentage values are the same for the two test systems and can be found in Appendix C. The HPLs are calculated by multiplying the YPL with the percentage values for the corresponding hour, day and week as shown in Equation 5.1.1. A HPL model is used for every assessment in the case study. When an AC model is used for HLII assessment it can be mentioned that the share of reactive load is set to be 20% of the active load at the given bus. However, the reader should also note that curtailments of reactive load do not contribute to the index values.

$$HPL_{h,d,w} = YPL \cdot l_h \cdot l_d \cdot l_w \tag{5.1.1}$$

where

$HPL_{h,d,w}$ = hourly peak load in hour h, day d and week w [MW],
YPL = yearly peak load [MW],
l_w = weekly peak load as a percentage of yearly peak load,
l_d = daily peak load as a percentage of weekly peak load,
l_h = hourly peak load as a percentage of daily peak load.

The software developed by [7] and [8] reads the load with the above-mentioned representation. The obtained load curve has repeating patterns for weekdays, week-ends and seasons. The load curve is given as a chronological vector as input to other scripts and functions in the software. Other load data that is chronological, e.g. real load data, can be used. The HPL model described above has 8736 load values (52x7x24). Hence, the software loops though all load points in a year when calculating an annual reliability index. Another amount of load points can easily be used by specifying this in the beginning of the simulation/calculation. However, if the spacing between load points is different, this gives a more complicated calculation as the duration of each time step will differ and must be accounted for in the calculation of the indices.

5.2 Load Shifting Models

5.2.1 LSM1: Using the Original Load Shifting Model

The first method for load shifting uses the model from Section 4.4 as it is presented. This method is found in several sources listed in the literature review in Section 4.3. In this method, shaved load is transferred to the corresponding valley hours by an equal amount. How the load modifications are performed will be described in the following. An example of a load modified curve will also be provided.

Based on Equation 4.4.1, the input for calculating the load shifted curve will be an original load curve, a pre-specified peak value, a time interval for valley hours and an energy recovery percentage. The pre-specified peak value will be the upper limit for the peak load in the modified curve. This pre-specified load level is chosen to be determined as a percentage of the peak load in the system or at a particular bus. For example, if the peak load is 185 MW, the peak load of the modified curve can be chosen to be 90% of this value, i.e. 166.5 MW.

The off-peak hours or valley hours are determined within a time interval given by a start and stop

value with the last peak hour as reference, e.g. from 2 hours after the last peak hour and ranging to 10 hours after the last peak hour has occurred. Several of the sources in the literature specify a given load level as a limit for the determination of valley hours e.g. 50% of the peak value. This approach is not chosen because of the unsymmetrical load pattern and magnitudes throughout the year. It is found more convenient to transfer the shaved energy to the closest valley hours by specifying an interval. In addition, it is easy for the user to change the interval if time constraints are to be modelled. The energy recovery percentage variable will be set equal to 1 if all load that is shaved is transferred to valley hours. This however, can also be changed by the user in the software.

Figure 5.2 shows an original load curve compared to a load shifted curve obtained with LSM1. In this example, the original load curve is the system load curve from the RBTS with an annual peak load of 185 MW. The pre-specified peak level of the modified curve is in this case set to be 80% of the peak load. All the shaved energy is recovered during off-peak hours. Off-peak hours are ranging from 2 hours after the last peak hour to 10 hours after the last peak hour. As can be seen in Figure 5.2 some of the valley hours will get a total load value that is higher than the pre-specified peak limit after the load modification since an equal amount of load is added to each valley hour. An assumption that all load can be shifted is applied for the case in Figure 5.2, which means that the energy recovery percentage is 100%.

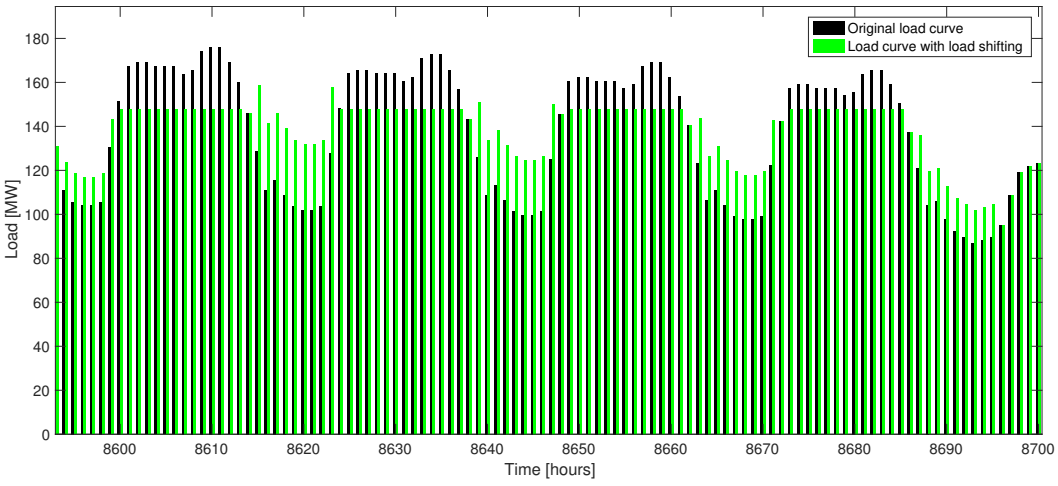

Figure 5.2: Example of a load shifted curve using LSM1.

5.2.2 LSM2: Uniform Filling of Load Valleys

LSM2 is a modified version of LSM1 to obtain an even load level in the valleys. By applying Equation 4.4.1 in an iterative framework the valleys in the load curve will be filled to a uniform

level. If the pre-specified peak level is set to be 80% of the annual peak as in the example in Figure 5.2, the peak clipping and valley filling for LSM2 will occur in a number of incremental steps starting from the original peak load level and shaving the curve in small steps to a final peak load level equal to 80% of the original peak load. In this way, the amount of shaved energy in each iteration will be incremental, and this load amount is added to the lowest of the immediate following valley hours. This results in valleys that are filled more uniformly and not following the shape of the curve as is the result with LSM1. Figure 5.3 illustrates the result of the approach for LSM2 for the same case as shown in Figure 5.2.

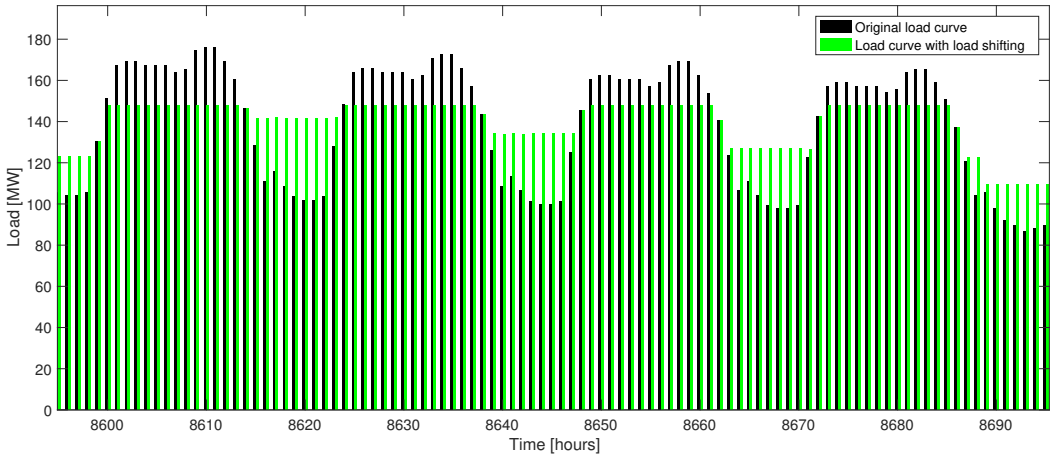

Figure 5.3: Example of a load shifted curve using LSM2.

5.3 Real-Time Pricing Model

The method for modeling DSR by RTP and price elasticity will now be explained. This model is applied for composite level. The theory behind the model is presented in Section 4.5. Equation 4.5.4 displays how the load change is initiated by this model. The load change is dependent on the structure of the PEM and the difference between the announced prices and the price expected by the consumer at each node. Thus, the load response can differ among buses. An AC OPF is used to calculate the nodal prices. The calculations for the RTP model can be summarized with the following steps:

1. Decide the structure of the PEM as described in Section 4.5.2 depending on the consumer strategy and load type. In this thesis, all buses have the same PEM.

2. Calculate nodal prices for all hours in a year when all components in the system are up. Use the original load curve in this calculation. The nodal prices obtained from this calculation are the prices expected by the consumers. The nodal prices are calculated as described in Section 4.5.3 using an AC OPF formulation.

3. Calculate nodal prices for an outage case for all hours in a year. An outage will trigger higher nodal prices. The outage case can be generating units and/or transmission lines that are down. Remember that the OPF must have a solution in all hours. Thus, there must still be enough generating and transfer capacity to cover the load in all hours.

4. Choose an equilibrium point, (d_0, p_0), from the original load curve and the nodal prices expected by the consumers for all buses. Any known point on these curves can be used[1]. One equilibrium point is chosen for each study period from the load and price curve at each bus with equal time spacing, e.g. initial demand and price in hour 12, 36, 60, 84, ..., 8724 at the load buses.

5. Calculate the change in demand by Equation 4.5.4. Add this change to the original load curve and obtain the price responsive demand.

Figure 5.4 and Figure 5.5 provide an illustrative example of the RTP model. Figure 5.4 shows an example of nodal prices when all components are up, and when there is a generator outage. The prices are shown for bus 13 in the RTS. As observed, the nodal prices become higher in case of an outage. In addition, price spikes are introduced when generating capacity is down. This is due to the fact that more expensive generators must produce to cover the peak load. As observed from Figure 5.4 there will be a difference between the announced price (generator on outage) and the expected price by the consumers (all components up). Further, Figure 5.5 illustrates the difference between the original load demand of bus 13 in the RTS, and its price responsive load demand due to the observed price difference. A smart consumer, i.e. a consumer that shifts load from hours with high prices to hours with lower prices, is assumed for the PEM in this example.

As a last remark, the reader can note that during the thesis work it is found that the solver in MATLAB, *fmincon*, returns solutions that match nodal prices obtained with the MATPOWER software [57] when the *'sqp'*-algorithm[2] is chosen instead of the default *'interior-point'*-algorithm.

[1] During the thesis work it is found that there are only minor changes in load response with different equilibrium points.

[2] 'sqp' stands for sequential quadratic programming.

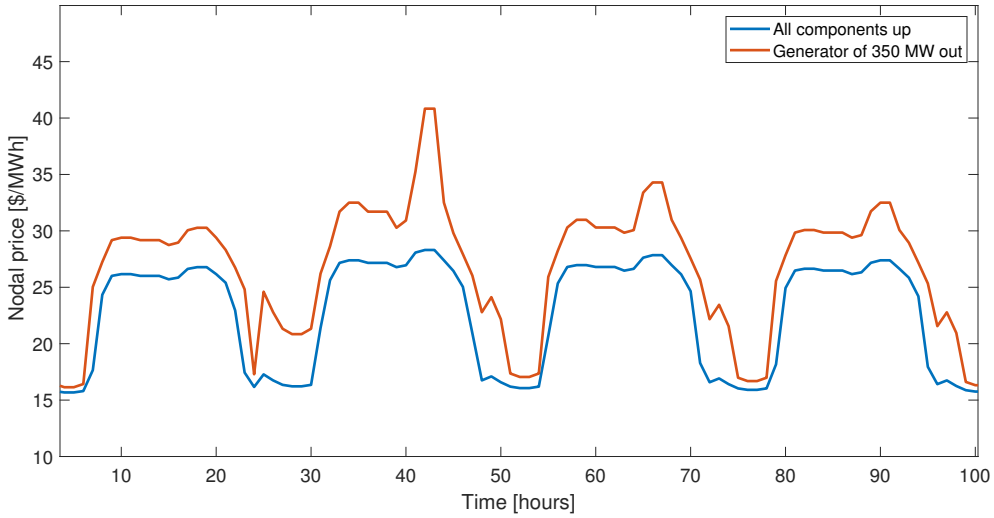

Figure 5.4: Nodal prices for bus 13 in the RTS when all components are up, and when a generator of 350 MW at bus 23 is down.

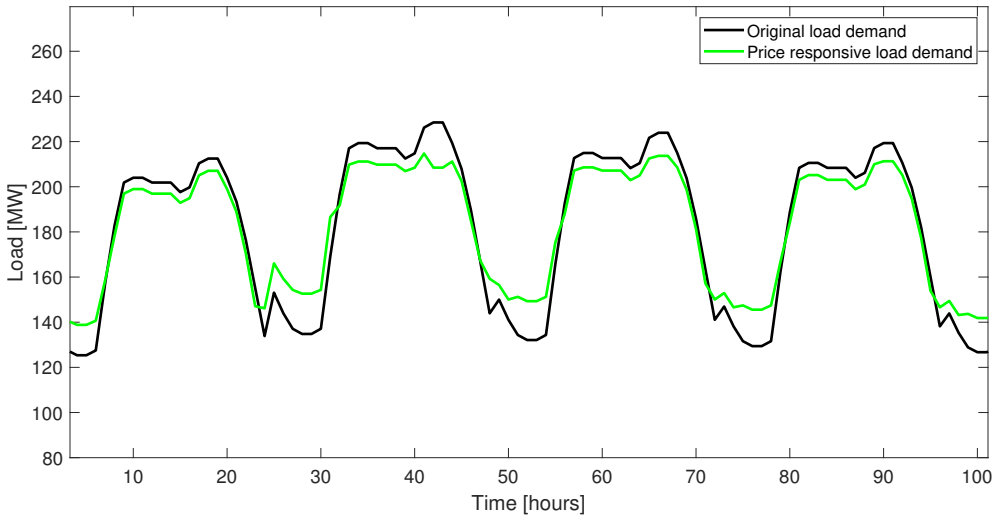

Figure 5.5: Original load demand and price responsive load demand for bus 1 in the RTS.

Any particular reasons for this could not be found. However, maximum function evaluations are kept the same as in the contingency solvers, which can be an influencing element. As stated in [58], the *'sqp'*-algorithm can in certain cases be faster and more accurate than the *'interior-point'*-algorithm for solving non-linear problems. The reader is referred to see [58] if a description of the solver and the available solution algorithms is needed.

5.4 Graphical Method for ELCC Calculations

The graphical method for ELCC calculations will be explained in this section. An overview of the calculation procedure is given in Figure 5.6. Index values are calculated for increasing peak load demand. All points on the load curve are scaled by an equal factor in each increment. In this way the load profile is maintained. It can be noted that the scaling of the load curve is always performed on the original load profile for every increment. The methodology is applicable to both HLI- and HLII assessment. The method is further explained by three steps and an illustrative example is given in Figure 5.7.

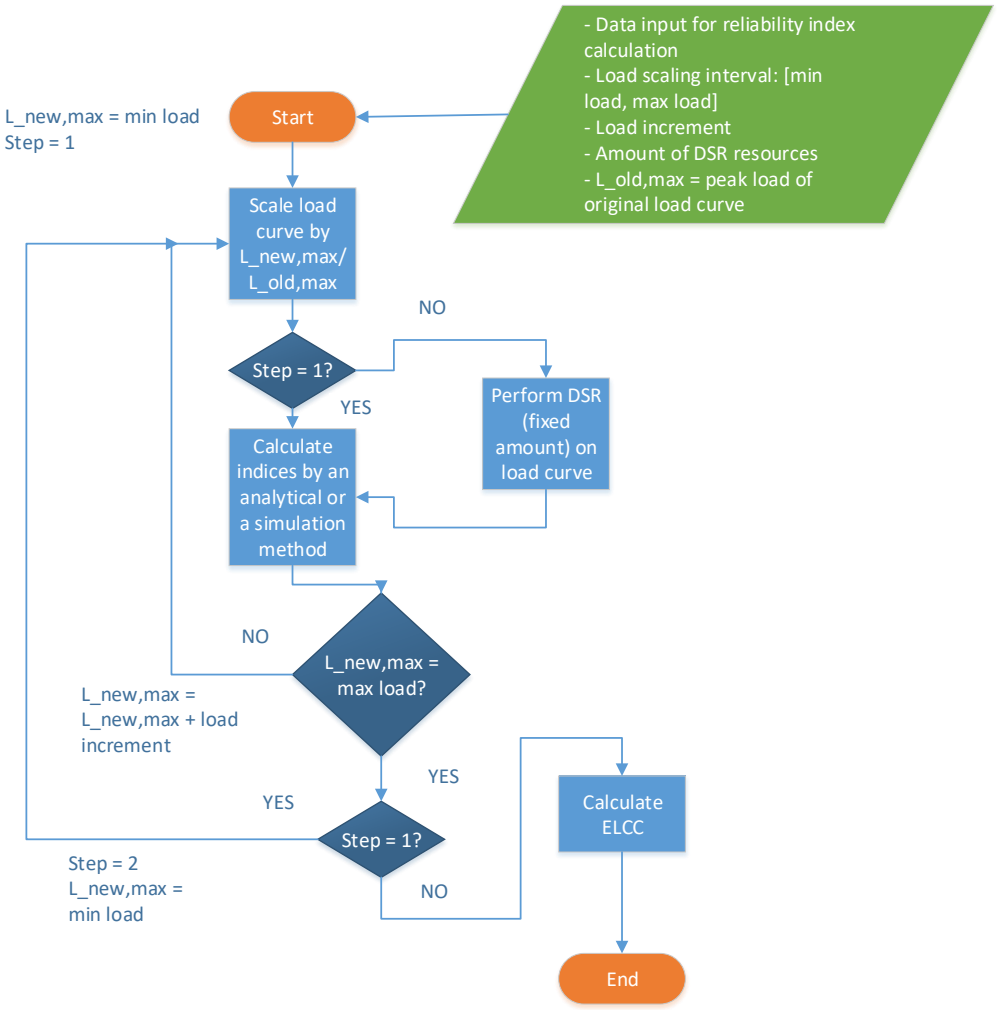

Figure 5.6: Overview of ELCC calculation procedure.

Step 1:

The first curve plotted is for the original system, i.e. the system without DSR resources. A

reliability index, LOLE or EENS, is plotted with respect to increasing load. The loads of the time series are scaled by multiplying each load value with the same factor, which is $L_{new,max}/L_{old,max}$. The $L_{new,max}$ value is the peak load of the new time series and the $L_{old,max}$ value is the peak load of the old time series. The $L_{new,max}$ value is increased in incremental steps. By scaling each hourly load by the same factor, the shape of the load curve is maintained. The index values are plotted for the new peak loads, i.e. the maximum load in the new time series. The blue line in Figure 5.7 represents the curve showing EENS for the original system with respect to increasing peak load, here system peak load. A semi-logarithmic scale is used and the curve is approximated to be linear between the index value points.

Step 2:

The next curve to be plotted is for the system with DSR resources. This corresponds to the red curve in Figure 5.7. In this case the amount of available DSR resources is 3000 MWh. LSM2 for load shifting, presented in Section 5.2.2, is used to achieve a curve with shaved energy equal to this amount. A modified version of the MATLAB-script for LSM2 is utilized. Instead of incrementally increasing the shaved energy up til the given percentage, the peak clipping and valley filling continue until the total shaved energy reaches the specified amount, e.g. 3000 MWh, which is kept constant as the peak load increases.

Step 3:

As seen in Figure 5.7 the horizontal line between the curves represents the ELCC, in this case for 3000 MWh available DSR resources. The ELCC is Figure 5.7 can be interpreted as the amount the system peak load can increase by, which is 6.08 MW, when 3000 MWh DSR resources are available for load shifting and given that the reliability level shall be maintained. It is common to use the reliability level of the original system as reference, but any pre-defined level can be chosen.

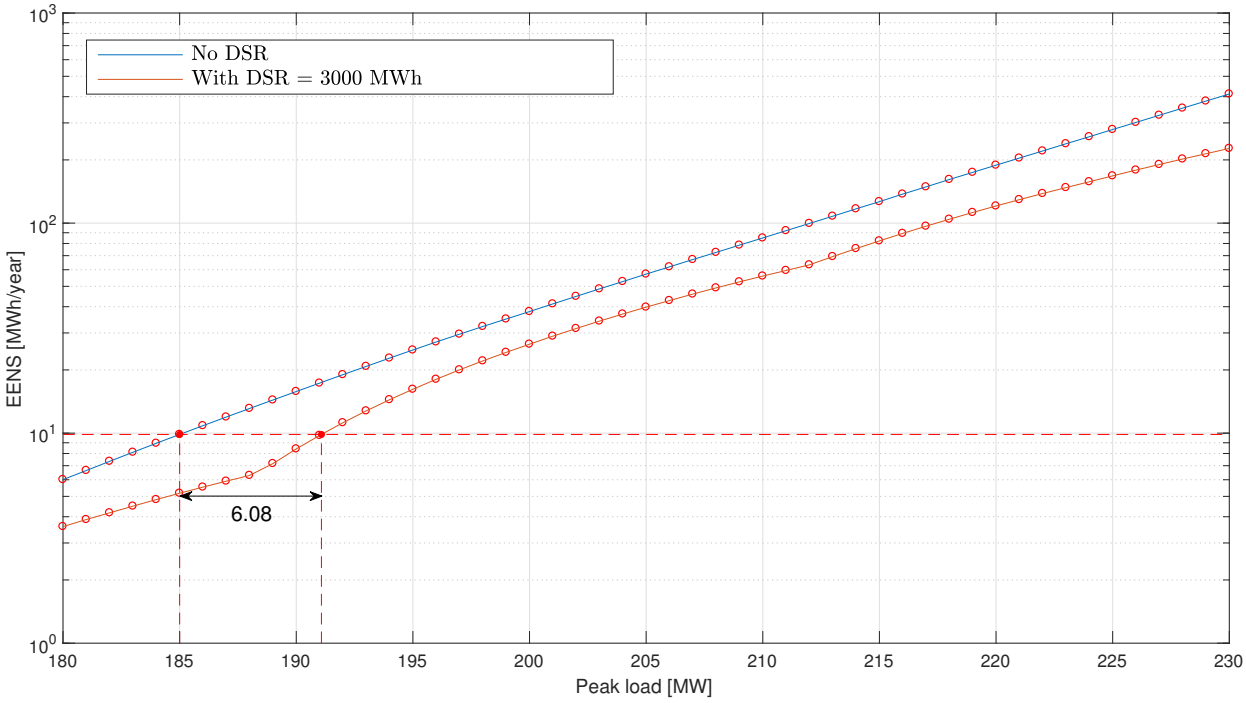

Figure 5.7: Example of approximate solution of ELCC by graphical method.

Chapter 6

Case Study Results and Discussion

6.1 Structure of the Case Study

There are several methods and models presented in this thesis. The list below provides the general structure of the case study and informs the reader about which test systems, DSR models and calculation methods that are used for each assessment. The results are analyzed and discussed continuously as they are presented.

1. *HLI assessment: impact on system indices*
   (a) Test system: RBTS
   (b) DSR model: LSM1 and LSM2
   (c) Calculation method: analytical method and MSC
2. *HLII assessment: impact on system and bus indices*
   (a) Test system: RBTS and RTS
   (b) DSR model: LSM1 and LSM2, and RTP model
   (c) Calculation method: MCS (DC and AC models)
3. *ELCC calculations*
   (a) Test system: RBTS and RTS

(b) DSR model: LSM2

(c) Calculation method: analytical and MCS for HLI, and MCS for HLII (DC model)

6.2 Test Systems

The test systems chosen for this thesis are the Roy Billinton Test System (RBTS) [27] and the IEEE-Reliability Test System (RTS) [28]. These test systems are frequently used in reliability analysis, both for generation system and composite system evaluations. The RBTS has 6 buses, 11 generating units and 9 transmission lines. The total installed capacity is equal to 240 MW and the YPL of this system is 185 MW. The RTS is a larger test system with a total of 24 buses, 32 generators, 38 transmission lines, a total installed capacity of 3405 MW and a YPL of 2850 MW. A detailed description of the RBTS and the RTS is provided in Appendix A and B, respectively. This include generator and network data, bus specifications and line diagrams. The COPT for the RBTS is also provided in Appendix A. The reader should note that a renumbering of the buses in the RTS is used in the calculations to get the slack bus as bus 1. This renumbering is applied in the software, but the results are provided with the original numbering. The renumbering of the buses used in the software for the RTS are displayed in the last column of Table B.6.

The load model used for the two test systems is the same, only scaled by the YPL of the system. A chronological and hourly peak load model is used for every assessment. The description of the load model is given in Section 5.1 and the load data given as percentage values are provided in Appendix C.

6.3 Demand Side Response Models

The theory and the methodological approach, with a general description of the models, are given in Chapter 4 and Chapter 5. This section gives specifications and illustrations of the DSR models used in the case study.

6.3.1 Load Shifting Models

The peak clipping for LSM1 and LSM2 is varied by percentage values with reference to the original peak level when studying the impact on the indices. The following notation is used in the result section: 100% load shifting refers to the original peak value and hence a load curve with no load shifting. 90% load shifting indicates that load values exceeding 90% of the original peak value get clipped and the shaved energy is transferred to the nearest valley hours. When referring to the peak value in this context it is always meant the YPL of the system load or bus load profile. The valley filling for LSM1 ranges from 2-10 hours after the last peak hour. This time interval is chosen since it gives a low number of MW, in the valley hour interval, exceeding the new pre-specified peak value. Recall that an equal amount of load is added to each valley hour for LSM1. A shorter interval gives more energy that needs to be recovered in each hour. However, the interval chosen also results in some high load values for larger amount of shaved energy which can illustrate unwanted rebound effects. For LSM2, it is applied that valley hours are ranging from the last peak hour until 10 hours after the last peak hour. The delta increment applied for LSM2 used in the HLI and HLII assessment is 0.00025. Hence, the iteration interval starts at 100% peak level and shaves the peak load by a proportion of 0.00025 in each increment. Furthermore, it is assumed an energy recovery percentage of 100% for all cases with load shifting, i.e. the load is only shifted and not increased or reduced.

Figure 6.1 and Figure 6.2 show the different load shifting levels used in this thesis with the specifications mentioned above for LSM1 and LSM2, respectively. The load curves displayed are for the system load in the RBTS. The same load profile are used in all cases, both as system loads and bus loads. Bus loads are given as a percentage share of the system load, and can be found in Appendices A and B for the two tests systems. It can be observed from Figure 6.1a that for 80% and 75% load shifting some of the valley hour loads are ranging higher than the peak load of the original load profile. This is also shown for a section of the load profile with high load demand in Figure 6.1b. Figure 6.2 on the other hand, illustrates that utilizing LSM2 gives a load profile that flattens out as the load shifting percentage increases. In Figure 6.2b this is illustrated for the same section of the load profile. The load shifting percentage is varied between 100%-75% with increments of 5% in the HLI assessment. Only load shifting levels of 100%, 90% and 80% are evaluated in the HLII assessment due to longer computation time.

LSM2 can be stated to be an optimistic method with respect to a real case. Rebound effects

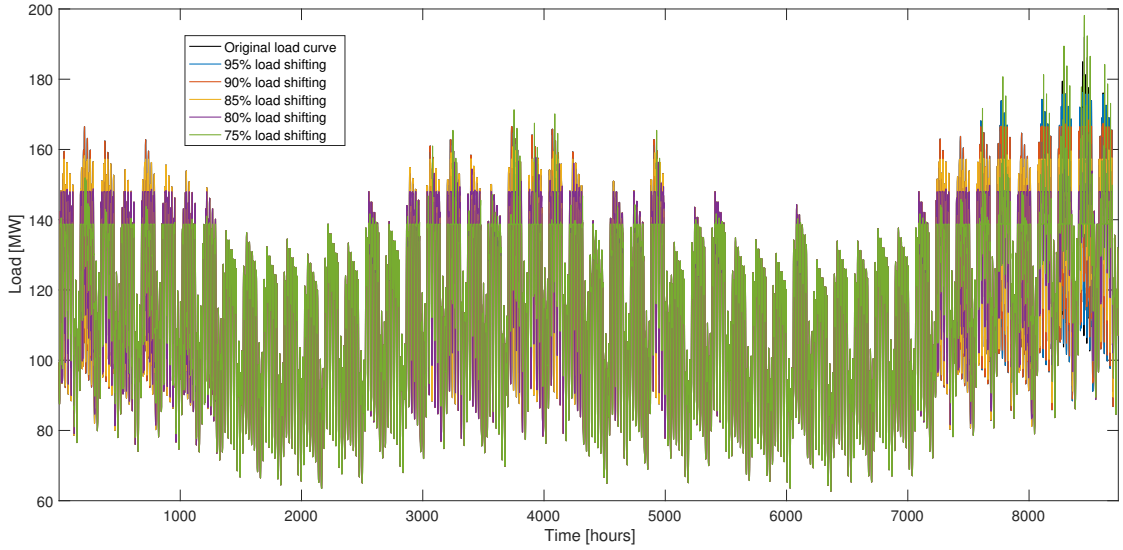

(a) Load shifting levels displayed for the whole load profile.

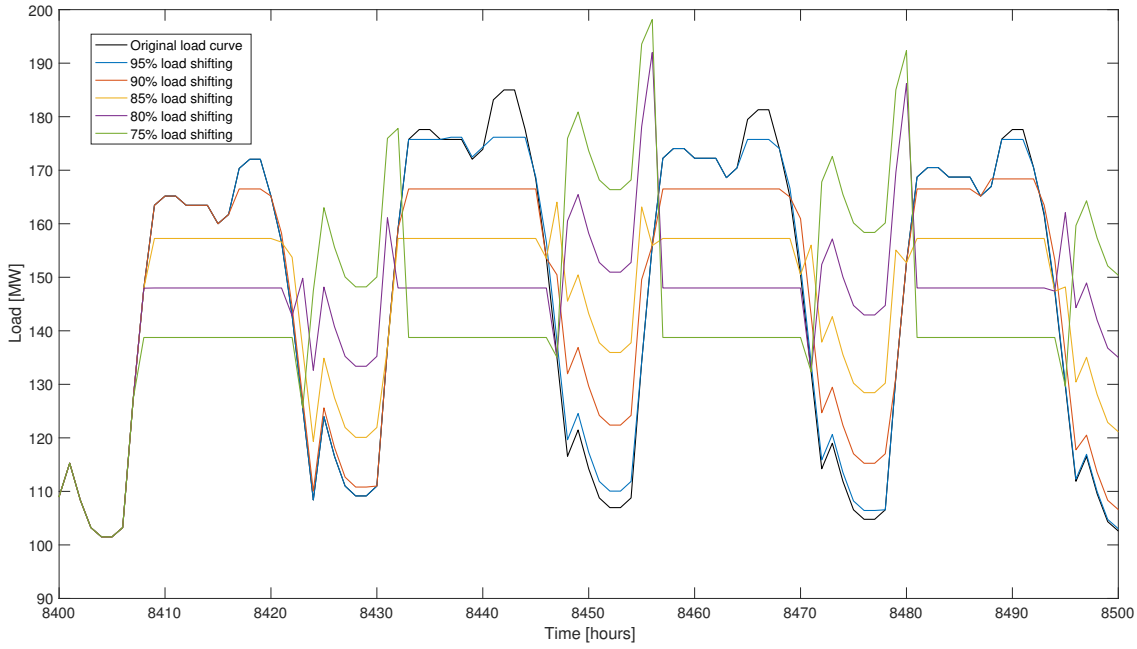

(b) Load shifting levels displayed for a section of the load profile with high load demand.

Figure 6.1: Load shifted curves obtained by applying LSM1.

and especially what are referred to as cold load pick-up characteristics, are issues that can appear when inertial loads like electric boilers and air conditioners are being reconnected after a disconnection period. This occurs as power spikes when the loads are reconnected [59]. Cold load pick-up characteristics are well known issues and optimal control strategies to avoid such problems when

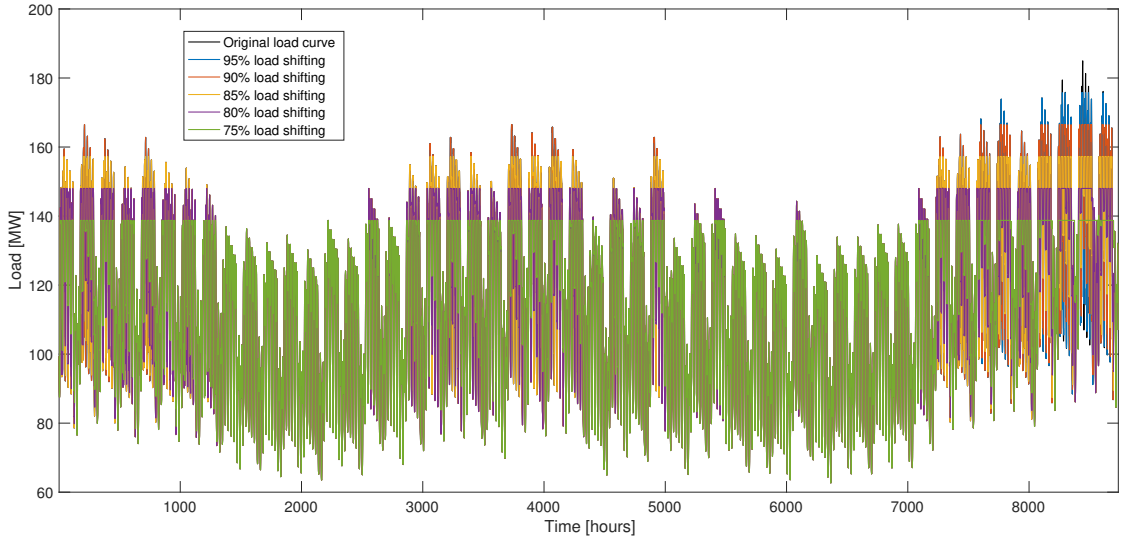

(a) Load shifting levels displayed for the whole load profile.

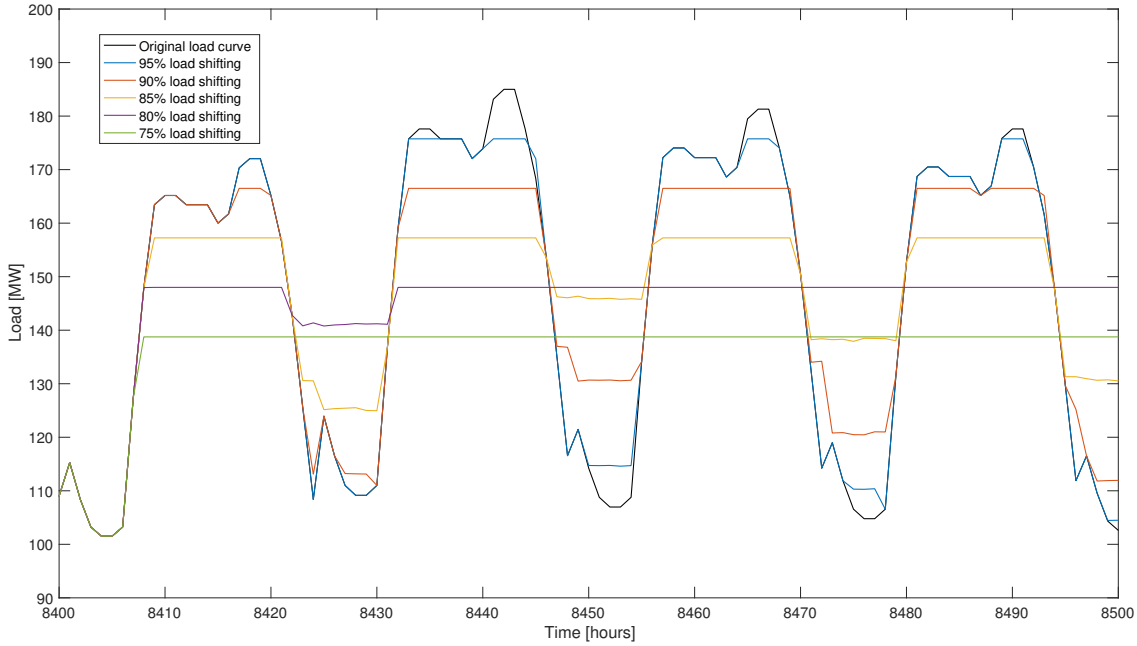

(b) Load shifting levels displayed for a section of the load profile with high load demand.

Figure 6.2: Load shifted curves obtained by applying LSM2.

aggregated loads are shifted in time, is a field of research in itself. Hence, the reader should bear in mind that LSM2 is reflecting an ideal and optimal case. Though not modeled explicitly, LSM1 can illustrate some of the effects that can occur when loads are being shifted in time. The effect of the different valley filling strategies of LSM1 and LSM2 is investigated in the case study.

A reformulated version of LSM2 is utilized in the ELCC calculations. Since the shaving of the peak and the valley filling of LSM2 is performed in an iterative procedure it was found convenient to reformulate this model for the ELCC calculations. In the reformulation, the amount of DSR resources are specified, and the shifted energy from the load shifting procedure will be equal to this amount. The delta applied in the ELCC calculations is 0.00001. The peak shaving stops when the amount reaches the specified DSR resource amount. A main point with this reformulation is that it is possible to keep the available amount of DSR resources constant as the peak load increases in the ELCC calculation procedure. In addition, it will be possible to evaluate the same amount of DSR resources at different buses in the system.

6.3.2 Real-Time Pricing Model

There are two main objectives chosen to investigate in the HLII assessment with the RTP model. These are the following:

1. How do consumers that observe and respond to more hours with higher prices than expected, affect the bus and system adequacy?

2. How do consumers that are more price responsive to the price differences experienced, affect the bus and system adequacy?

The first point is illustrated by considering two outage cases. One that triggers some price differences and price spikes and another case that triggers higher price differences and considerably more price spikes. These outage cases will be explained in detail later in this section. The second point is illustrated by increasing the elasticity coefficients in the PEMs. To begin with, some general specifications for the RTP model are highlighted.

The two load shifting models are implemented to shift load in an equal proportion according to the share of load on the bus, e.g. 90% of the YPL at the bus. For the RTP model, the amount of shifted load varies according to the price difference observed over the 24 hour study period at each node. In the case study, it is chosen to apply nodal prices to investigate if there is an impact of locational marginal prices. An uniform market price common for all load buses could also have been used by for instance setting the price in each hour equal to the highest nodal price observed in each hour. The rescheduling strategy of each bus is equal since the same PEM is used for all buses in the case study. The structure of the PEM is given in Appendix F, and is used for all the simulations.

This is a PEM that reflects an optimizing consumer which shifts load from peak hours to off-peak hours. Off-peak hours are considered to range from hours 1-7 and 23-24. Thus, the valley period consists of 8 hours which resembles the valley period chosen for LSM1 and LSM2. The property given in Equation 4.5.5 is always satisfied. This means that the energy is only shifted in time and not reduced. The equilibrium point chosen in the assessment is initial demand and price in hour 12 each day at the load buses.

The RTP model is only studied with the RTS. The RBTS has only two generating nodes, and an outage case was found to give small changes in loading order since both nodes have to produce in most hours. Recall that all generating units at a bus are represented by one cost function. Consequently, the nodal prices would fluctuate between two price levels. A better illustration of the model is obtained with the RTS which has 10 generating nodes. Prices expected by the consumers are calculated with all units up. For this case the prices at the buses are in the range between 14.21 \$/MWh - 44.80 \$/MWh. The magnitudes of the nodal prices are dependent upon the generator cost functions. Quadratic cost functions are used and the cost coefficients for the generating nodes can be found in Table B.6. The coefficients are similar to examples provided in [56].

Two outage cases are considered to trigger higher prices. These are an outage of generator 25, and generator 30, both placed at bus 23. Generator 25 has a capacity of 155 MW, while generator 30 has a capacity of 350 MW, which is one of the largest units in the system. The cost coefficients of the generating capacity at bus 23 are around the middle compared to the other generating nodes. The highest nodal price obtained when generator 25 is on outage is 47.88 \$/MWh, and the price difference varies from 0 to maximum 11.18 \$/MWh. The highest nodal price obtained when generator 30 is on outage is 51.10 \$/MWh, and the price differences varies from 0 to maximum 15.04 \$/MWh. When the largest generator is on outage, several hours experience higher price differences compared to when the smaller generator is on outage. This is illustrated in Figure 6.3, which shows the nodal prices at three arbitrary buses in the RTS. Figure 6.3a shows the nodal prices at buses 7, 13 and 15 when all components are up, Figure 6.3b shows the nodal prices at the same buses when the generator of 155 MW is on outage and Figure 6.3c shows the nodal prices when the generator of 350 MW is on outage. It can be seen that the last outage case causes more frequent price spikes.

Further, Figure 6.4 illustrates the price difference for the first 100 hours considering the largest generator on outage. Figure 6.4a shows the prices at buses 7, 13 and 15 when all components are up. Figure 6.4b shows the prices for the same buses when the generator is on outage and Figure 6.4c shows the corresponding price difference in each hour at the buses. It can be seen that the

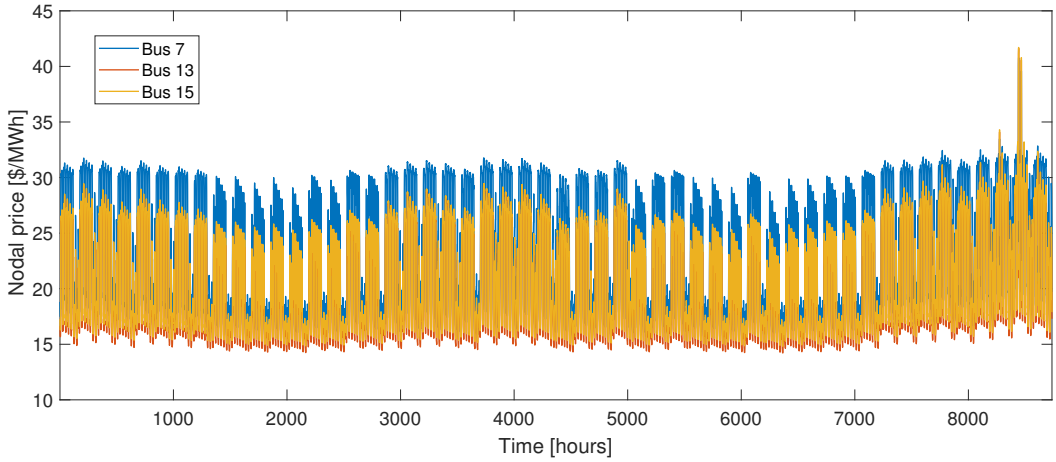

(a) Nodal prices with all components up.

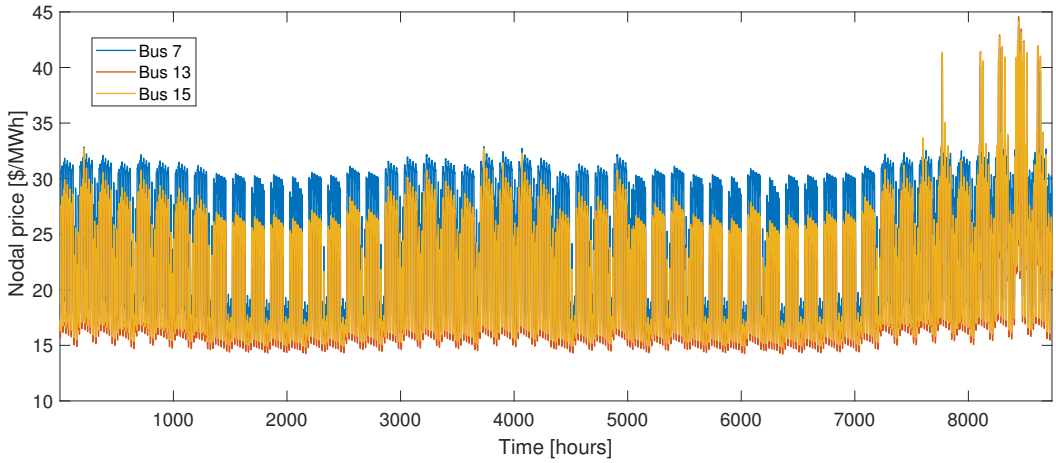

(b) Nodal prices with generator of 155 MW on outage.

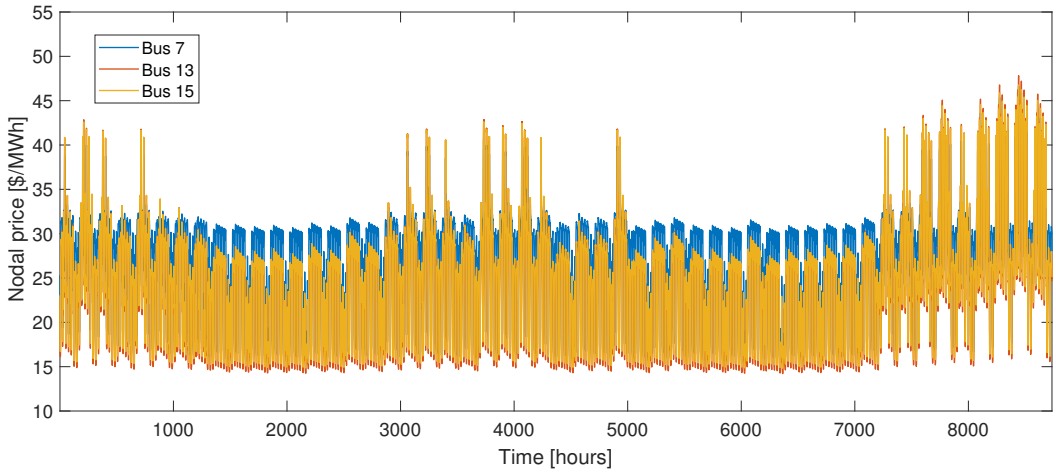

(c) Nodal prices with generator of 350 MW on outage.

Figure 6.3: Nodal prices for bus 7, 13 and 15 in the RTS for the original case and two outage cases.

observed price difference varies between the buses. As noticed, price differences occur in off-peak hours also since an outage is simulated for all hours. Nevertheless, the PEMs that are used reflect consumers that react by reducing load in peak hours and shift load to the off-peak hours with less price differences.

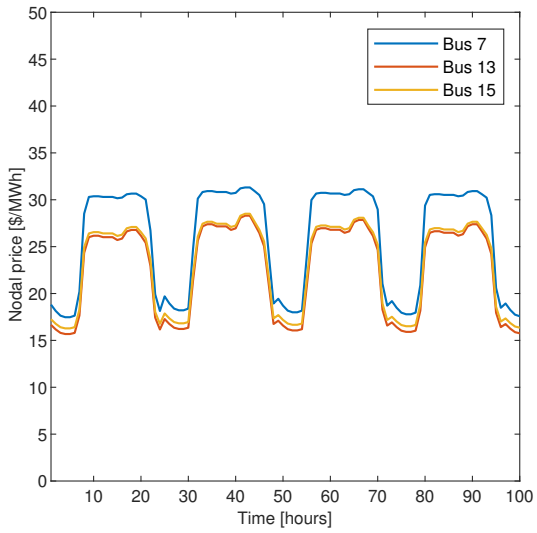

(a) Nodal prices at buses with all components up.

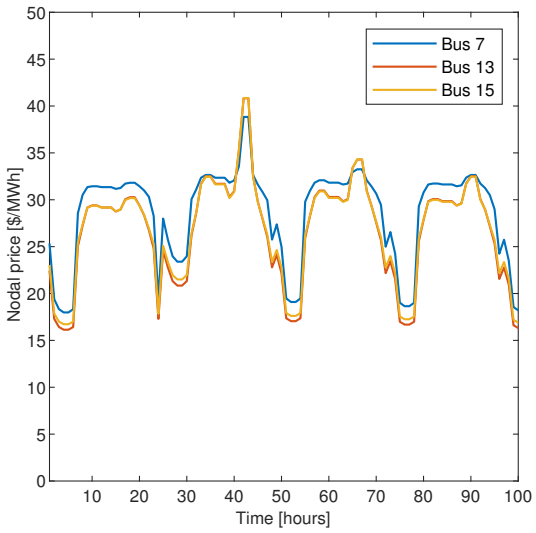

(b) Nodal prices with generator of 350 MW on outage.

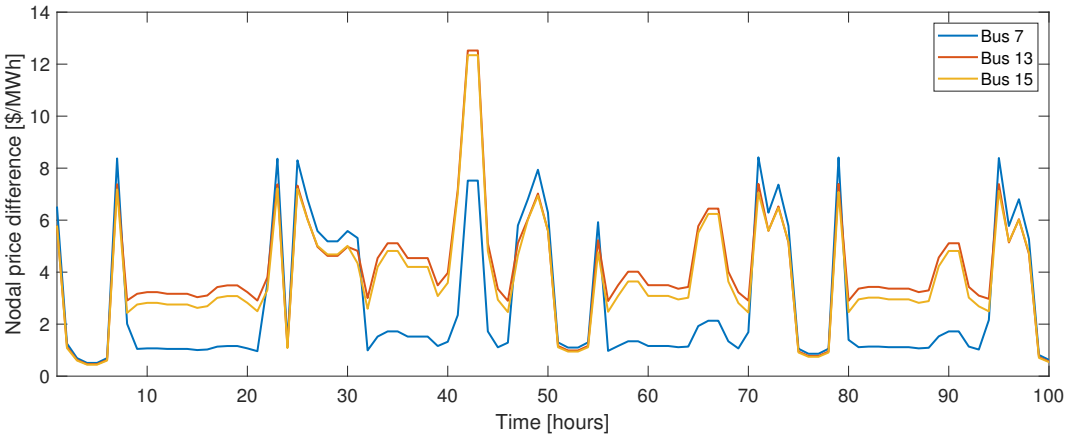

(c) Price difference in nodal prices.

Figure 6.4: Nodal price differences at buses 7, 13 and 15 in the RTS.

The corresponding change in load due to the price difference shown in Figure 6.4c for a section of the load curve is illustrated in Figure 6.5 for buses 7, 13 and 15. Figure 6.5a shows the original load demand and the corresponding price responsive load demand at buses 7, 13 and 15. Self-elasticities of -0.2 and cross-elasticities of 0.025 are used in this example, and is the base case used in the simulations in the case study. As observed, the rescheduling strategy is the same for all buses

yielding an equal response pattern to price differences. Figure 6.5b displays the load change in each hour as a percentage of the original demand for the three buses. Buses with larger price difference have higher relative change in load. This is a contrast to the two load shifting models which are implemented to shift load such that the relative change in load is equal for all buses.

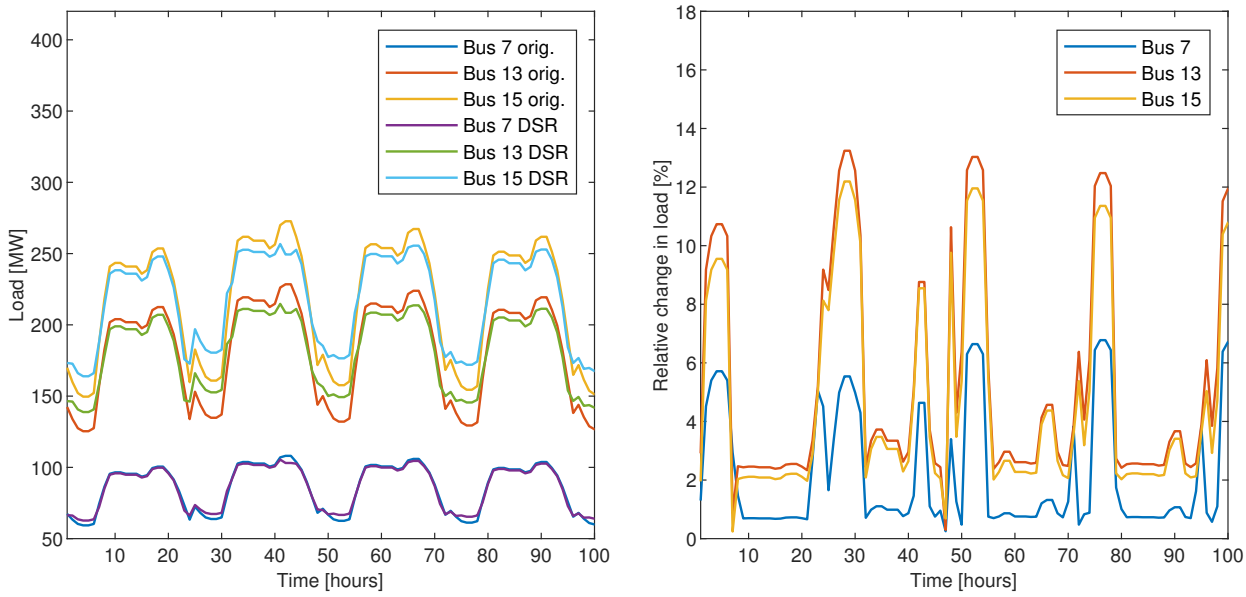

(a) Original and price responsive load demand at buses.

(b) Relative change in load demand at buses.

Figure 6.5: Load response at buses 7, 13 and 15 in the RTS obtained with the RTP model.

Table 6.1 shows the amount of energy shifted at a low demand and high demand period for load response encountered by price differences caused by the largest generator on outage. It can be seen that the amount of energy shifted is differing among buses. Although, the relative energy shifted is not that different for each bus. The relative energy is calculated as the percentage amount of energy shifted in the period with respect to the total energy demand in the time period. 500 hours are considered for both cases. The low demand period is ranging from hours 2000-2500, and the high demand period is ranging from hours 8000-8500. Generally, the values in Table 6.1 can indicate that there is not a large difference in nodal price differences observed at each bus for the case studied. Bus 20 shifts the largest relative amount of energy in both high and low demand periods. At the high demand period, buses 6 and 7 can be noticed to shift a smaller relative amount of energy compared to the rest of the buses.

The relative amount of shifted energy with respect to the total system load is calculated for the low

Table 6.1: Amount of shifted energy at buses in the RTS for a low and high demand period with the RTP model and the largest outage case.

	Low demand period		**High demand period**	
Bus	Energy shifted [MWh]	Amount of demand [%]	Energy shifted [MWh]	Amount of demand [%]
1	840.28	2.84	1808.90	4.63
2	752.63	2.84	1619.30	4.64
3	1340.26	2.73	2967.91	4.59
4	579.07	2.86	1239.99	4.64
5	557.63	2.86	1193.02	4.65
6	1075.37	2.87	2292.77	4.65
7	898.36	2.62	1418.27	3.14
8	1270.28	2.72	2311.42	3.75
9	1368.88	2.88	2916.57	4.66
10	1531.89	2.89	3253.83	4.66
13	2137.09	2.95	4583.04	4.80
14	1482.82	2.80	3244.10	4.64
15	2312.62	2.67	5175.85	4.54
16	744.32	2.73	1658.10	4.61
18	2338.73	2.56	5315.19	4.42
19	1443.84	2.89	3165.02	4.81
20	1066.87	3.04	2307.46	4.99

and high demand periods referred to above for the two outage cases. For the smallest outage case this is 1.42% and 1.67% for the low and high demand period, respectively, and similar 2.79% and 4.52% for the largest outage case. Thus, this shows that the largest outage case leads to greater amount of shifted load in periods of both lower and higher demand because of larger price differences in general. However, it is also noted that the largest outage case shows a greater difference between the amount of shifted load between the two periods due to more price spikes in the high demand period.

6.4 Calculation Methods

This section gives the specifications for the calculation methods used in the case study. Most of the remarks concern the MCS methods.

6.4.1 Analytical Method

The necessary information for the analytical method is covered by the theory and the methodological approach. It can be be noted that the COPT is central in the calculation of the indices and for the discussion of the results obtained with the analytical method. The COPT displayed in Appendix A has 49 capacity outage states and is obtained using a two-state model, i.e. generating units are classified as either up or down. Derated states are not considered in the case study. The software used to calculate the COPT and indices LOLP, LOLE and EENS is developed by [7].

6.4.2 Monte Carlo Simulation

The reader should note some remarks concerning the simulation methods. To begin with, this thesis uses two different simulation approaches, one non-sequential and one sequential approach. There is not much difference between the trustworthiness of the results between these two methods for the case study in this thesis. This is due to the fact that there are no correlation effects between the parameters. E.g., the load is considered to be a constant and it is modified with a DSR model before the simulation starts. If more complex cases are to be evaluated, like the inclusion of correlation effects between renewable production fluctuations, weather dependencies and load demand, or in general other time dependencies, the state transition method is the only method of these two that can capture these features. Since such correlation effects are not considered in this thesis, the state sampling method is also found to be a sufficient simulation method for the cases studied.

Another remark is the number of simulation years used in the simulations. Ideally, the CV should decide the convergence criteria in a MCS. Nevertheless, the simulation framework of [8] uses a fixed number of simulation years. The number of years chosen in [8] is based on reasonable values of CVs, and to some extent also computation time. Since the focus of this thesis has not been to improve the simulation tool, a fixed number of simulation years have been used to obtain the results in this case study as well. The sample sizes are chosen to be equal to the ones found in [8]. 30

000 simulations years are used for all generation system adequacy analysis. This applies to both simulations methods and both test systems. 500 simulations years are used for the state sampling method, while 1000 simulations years in 15 parallels[1], i.e. 15 000 simulations years, are used for the state transition method, in the composite system adequacy analysis. The amount of simulation years are only changed with respect to simulation method for HLII assessment, and not not with respect to test system or OPF model. The amount of simulation years for the sampling method are set lower than the state transition method because the former method yields larger variations between successive system states. Thus, a satisfactory precision of the estimates is obtained with this amount of simulation years. The reader is recommended to see [8] for a consistently discussion of the performance of the simulations methods. Detailed analysis of the method's CVs can also be found in [8].

The most important remarks regarding the CVs for the results in this thesis are given in the following. The CVs of the system indices are in general in the range of 1-2%, which indicates precise estimates. The CVs of bus indices can vary greatly among buses, from e.g. 1-70% in the same simulation, depending on the reliability of the buses. More reliable buses have higher CVs. Thus, as stated in [8], the sample size should be increased if more precise estimates of reliable buses is needed. The CV of the EENS index is in general slightly higher than the CV of the LOLE index which is also stated in [24] to be common. The sample sizes are equal at HLI for the two simulation methods and the CV of the state sampling method is lower for this case. At HLII, sample sizes are chosen such that CVs are closer for the two methods. A main point to highlight is that an increase in CVs is observed as the amount of shifted load increases, since the sample sizes are kept constant and the system becomes more reliable. Thus, the estimates becomes less precise as the frequency and amount of load curtailments decline. Bus indices are more affected by this than the system indices. System indices are observed to be around 2% for greater amount of shifted load. As an example, the CVs for the system LOLE and EENS index for the RST obtained with the state sampling method and AC OPF are 1.06% and 1.54% for no load shifting, respectively, and 1.32% and 1.99% for 80% load shifting. The same CVs for bus 9 which has low curtailment cost and experiences frequent curtailments are 1.29% and 1.53% for no load shifting, and 2.12% and 2.55% for 80% load shifting. As stated before, more reliable buses can obtain high CVs, and this is also observed to be more prominent as the amount of shifted load increases. Thus, using a fixed amount of simulation years should be noted as a shortcoming with respect to precision of estimates,

[1]Parallel processing is used to reduce the computation time. Loops are processed in parallel by different workers in the software.

especially bus indices, as the amount of shifted load increases.

Lastly, the reader can note that the DC model has lower computation time than the AC model, especially for the largest test system. Also, due to the increased amount of simulation years for the state transition method in the HLII assessment, this method has substantially longer computation time. Thus, the state transition method with AC OPF for the RTS is not conducted in the case study. Computation time for the state sampling method with RTS and AC OPF is approximately 5 hours which is the longest computation time for the assessment in the case study. The other simulations conducted with DC OPF have in general 5-35 minutes computation time. The simulations are performed on a computer with 28 cores and 384 GB memory.

6.5 HLI Assessment: Impact on System Indices

This section gives the results for the impact of load shifting on adequacy indices for a HLI assessment of the RBTS. LSM1 and LSM2 are the DSR models used in this assessment. The results obtained with the analytical method are displayed first, after comes the results obtained with MCS.

The main objectives of the HLI assessment are the following:

1. Investigate how increasing load shifting percentages of LSM1 and LSM2 change system adequacy indices, and highlight potential differences between the two methods with respect to valley filling.

2. Compare the the results of the analytical method and MCS.

3. For MCS, compare results obtained with the state sampling method and the state transition method.

6.5.1 Indices Obtained With the Analytical Method

Table 6.2 and Table 6.3 show how LOLE and EENS change for increasing amount of shaved energy by utilizing LSM1 and LSM2 for load shifting, respectively. In addition, Table 6.4 shows how LOLE and EENS change for increasing amount of clipped energy. For this case the shaved energy are not recovered. The first column of the tables refers to the percentage of load shifting or peak clipping applied on the original load profile. The total amount of shaved energy for each level is also given

in the tables.

Table 6.2: System indices at HLI for the RBTS obtained by LSM1. Indices are calculated by an analytical method.

Load Shifting [%]	Peak value [MW]	Shaved Energy [MWh]	LOLE [hours/year]	EENS [MWh/year]
100	185.00	0.00	1.0915	9.8603
95	175.75	60.33	1.0623	9.6351
90	166.50	585.64	1.0546	8.4711
85	157.25	2903.76	0.4510	5.2978
80	148.00	9695.59	0.4437	4.3541
75	138.75	23088.01	0.3598	4.1545

Table 6.3: System indices at HLI for the RBTS obtained by LSM2. Indices are calculated by an analytical method.

Load Shifting [%]	Peak value [MW]	Shaved Energy [MWh]	LOLE [hours/year]	EENS [MWh/year]
100	185.00	0.00	1.0915	9.8603
95	175.75	60.33	1.0624	9.6256
90	166.50	585.64	1.0540	8.4317
85	157.25	2903.76	0.4407	5.1890
80	148.00	9695.59	0.3942	3.7614
75	138.75	23088.01	0.1157	1.6078

Table 6.4: System indices at HLI for the RBTS obtained by peak clipping. Indices are calculated by an analytical method.

Load Shifting [%]	Peak value [MW]	Shaved Energy [MWh]	LOLE [hours/year]	EENS [MWh/year]
100	185.00	0.00	1.0915	9.8603
95	175.75	60.33	1.0623	9.6169
90	166.50	585.64	1.0516	8.3921
85	157.25	2903.76	0.4367	5.1437
80	148.00	9695.59	0.3764	3.6079
75	138.75	23088.01	0.1025	1.4140

It can be seen from Tables 6.2-6.3 that the load shifting contributes to a clear improvement of the indices. For example, with a load shifting level of 85%, the LOLE value is reduced by 58.68% compared to the original value for LSM1. At the same load shifting level, the EENS index is reduced by 46.27% compared to the original value for LSM1. By comparing the LOLE and EENS values in Table 6.2 and Table 6.3 the difference can generally be observed to be small. However, for 80% and especially 75% load shifting, LSM2 gives noticeable lower LOLE and EENS values. For these load shifting percentages, the valley filling procedure in LSM1 gives several hours exceeding the pre-specified peak level. This effect is also illustrated in Figure 6.1. Therefore, it is reasonable to obtain a larger difference between the indices for the two methods at higher load shifting levels.

Comparing the index values in Table 6.4 to the ones in Table 6.2 and Table 6.3, it can be observed that the values for LOLE and EENS do not differ much. This indicates that the load shifted to valley hours do not significantly contribute to lower the system adequacy. Similar observations was found in [36] where the RTS was used as test system. It can also be observed that the values for LOLE and EENS for 75% peak clipping are closer to the values obtained with LSM2 than with LSM1. This supports the observation that for large amounts of shaved energy the valley filling of LSM1 has a decreasing positive effect since more valley hours get higher load values.

Further, it can also be observed from Tables 6.2-6.4 that the LOLE values are significantly decreased from 90% to 85% load shifting/peak clipping. For example, in Table 6.2 from 1.0546 hours/year to 0.4510 hours/year. This can be explained in connection to the states in the COPT for the RBTS given in Table A.2. At 90% load shifting, the new system peak value is 166.5 MW, hence an outage capacity greater than the total installed capacity of 240 MW less 166.5 MW, that is 73.5 MW, is

at least needed to cause a loss of load situation. In Table A.2 this corresponds to state 16, where the cumulative probability to have an outage capacity greater or equal to 75 MW is 0.00227587. At 85% load shifting, the new system peak value is 157.25 MW, which gives a minimum of 82.75 MW outage capacity needed to cause a loss of load situation. In Table A.2 this corresponds to state 18, where the cumulative probability to have an outage capacity greater or equal to 85 MW is 0.00027199, which is a reduction of 88% compared to the cumulative probability in state 16. This observation supports the significant decrease in the LOLE index for these two load shifting levels as the main contributions from the LOLP values come from the cumulative probability of state 16 and 18, respectively. Recall Equation 3.5.3 for the calculation of the LOLE index.

Again, by referring to Table 6.2, it can be observed that the values of EENS are reduced more uniformly and do not reflect the same significant decrease as observed for the LOLE values. One explanation to this can be that when calculating EENS, individual probabilities are used and not cumulative probabilities as for the LOLE index, see Equation 3.5.6. These individual probabilities are displayed in the third column in Table A.2. As observed, the individual probabilities can both increase and decrease as the outage capacity increases. Moreover, the same grouping of values for neighbouring states can not be observed for the individual probabilities as for the cumulative probabilities. Furthermore, when utilizing a load shifted curve, more of the peak hours, which are the hours that contributes most to LOLE and EENS, occur with equal values due to the peak shaving procedure of LSM1 and LSM2. This effect in the load profile together with the mentioned difference between the individual and cumulative probabilities can indicate why the LOLE index has more polarizing results compared to the EENS index for the RBTS.

6.5.2 Indices Obtained With Monte Carlo Simulation

Table 6.5 and Table 6.6 show the reliability indices for the RBTS when LSM1 is utilized for load shifting. Similarly, Table 6.7 and Table 6.8 show the results for the indices when LSM2 is used. Standard deviations of the LOL and the energy not supplied (ENS) from the samples are included in the tables to give a measure of the sample variance. In addition, the re-engineered version of the LOLP index described in the theory is also provided in the tables.

Table 6.5: LOLE indices at HLI for the RBTS obtained by MCS and LSM1.

Simulation method	Load shifting [%]	LOLE [hours/year]	LOL SD [hours/year]	$LOLP^{MCS}$
State sampling	100	1.0891	1.0448	0.000125
	95	1.0681	1.0338	0.000122
	90	1.0523	1.0187	0.000120
	85	0.4482	0.6709	0.000051
	80	0.4484	0.6629	0.000051
	75	0.3611	0.5991	0.000041
State transition	100	1.0885	4.2371	0.000125
	95	1.0628	4.1811	0.000122
	90	1.0172	4.1681	0.000116
	85	0.4208	2.7075	0.000048
	80	0.4254	2.7166	0.000049
	75	0.3562	1.9214	0.000041

Table 6.6: EENS indices at HLI for the RBTS obtained by MCS and LSM1.

Simulation method	Load shifting [%]	EENS [MWh/year]	ENS SD [MWh/year]
State sampling	100	9.8005	13.0390
	95	9.7286	12.8438
	90	8.5235	11.7602
	85	5.3232	10.1115
	80	4.4257	8.4945
	75	4.0839	8.9624
State transition	100	10.1187	56.9411
	95	9.7732	57.8280
	90	8.1153	48.4173
	85	5.0773	45.0322
	80	4.2215	35.5049
	75	4.0706	30.8620

Table 6.7: LOLE indices at HLI for the RBTS obtained by MCS and LSM2.

Simulation method	Load shifting [%]	LOLE [hours/year]	LOL SD [hours/year]	$LOLP^{MCS}$
State sampling	100	1.0891	1.0448	0.000125
	95	1.0659	1.0310	0.000122
	90	1.0473	1.0210	0.000120
	85	0.4419	0.6668	0.000051
	80	0.3946	0.6263	0.000045
	75	0.1152	0.3405	0.000013
State transition	100	1.0885	4.2371	0.000125
	95	1.0549	4.2731	0.000121
	90	1.0236	4.2021	0.000117
	85	0.4353	2.7031	0.000050
	80	0.3686	2.5464	0.000042
	75	0.1139	1.5085	0.000013

Table 6.8: EENS at HLI for the RBTS obtained by MCS and LSM2.

Simulation method	Load shifting [%]	EENS [MWh/year]	ENS SD [MWh/year]
State sampling	100	9.8005	13.0390
	95	9.7103	12.9420
	90	8.3973	11.6902
	85	5.1659	9.8510
	80	3.7782	7.7427
	75	1.5805	5.4812
State transition	100	10.1187	56.9411
	95	9.5261	57.2645
	90	8.4010	53.4955
	85	5.1577	41.9294
	80	3.3735	30.4161
	75	1.6010	25.1314

From the results shown in Tables 6.5-6.8, it can generally be observed that the results resemble

the results obtained with the analytical approach. The simulation results for the LOLE and the LOLP^{MCS} index also do a leap from 90% to 85% load shifting, whereas the values of the EENS index are more uniformly reduced. This tendency is also illustrated in Figure 6.6 where the state transition method is used to obtain the LOLE distribution for load shifting levels 90% and 85%. By comparing Figure 6.6a and Figure 6.6b it can be seen that the highest bars between 1-15 hours/year are reduced and that the bar representing 0 hours/year is increased with load shifting level 85%.

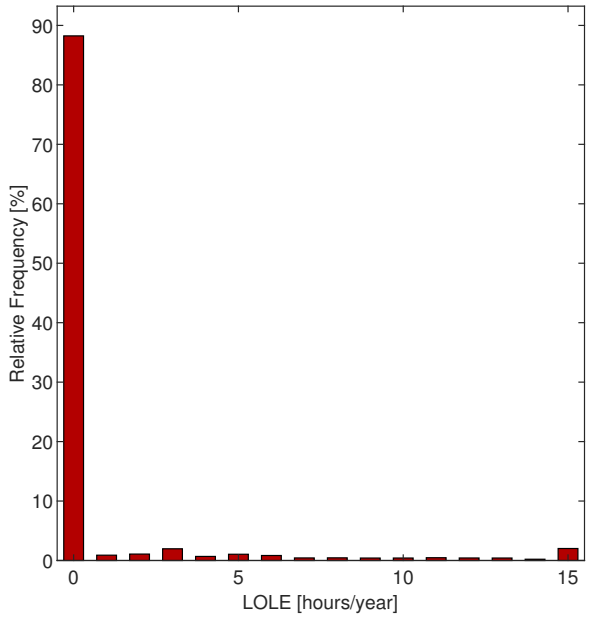

(a) The LOLE distribution at 90% load shifting.

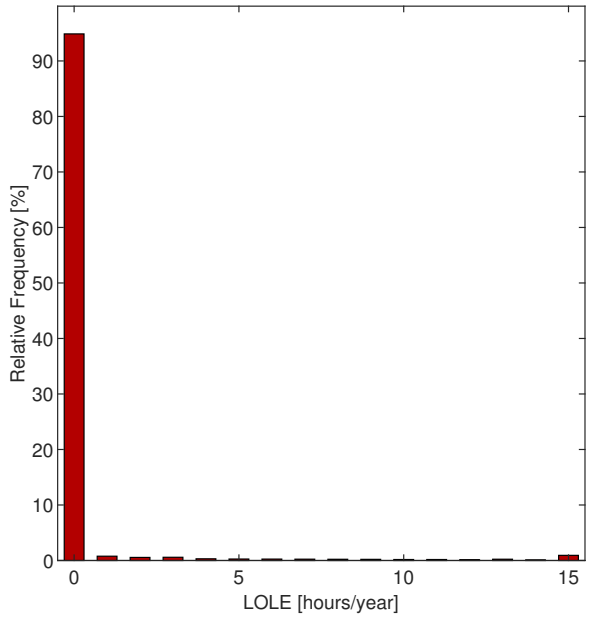

(b) The LOLE distribution at 85% load shifting.

Figure 6.6: Comparison of the LOLE distributions obtained at 90% and 85% load shifting with LSM1 and the state transition method.

From the tables it can also be observed that the state sampling and the state transition method yield similar results. However, as mentioned in Section 6.4.2 it can be noticed that the state transition method has higher standard deviations for the indices, which indicates a poorer precision of the estimates. Recall that an equal sample size is used for both simulation methods in the HLI assessment.

Lastly, Figure 6.7 shows the LOLE distribution for load shifting level 75% obtained with LSM1 and LSM2, respectively. The state transition method is used to obtain the distributions. These graphs illustrates the observed difference between the load shifting methods at higher load shifting percentages. It can be seen from Figure 6.7a that the bars corresponding to 1-3 hours/year are increased, especially 1 hours/year. This is due to the high load spikes that occur with LSM1 at

this load shifting percentage. Figure 6.7b shows that the bar representing 0 hours/year is almost accounting for 100% of the evaluated states in the simulation when LSM2 is used at the same load shifting level.

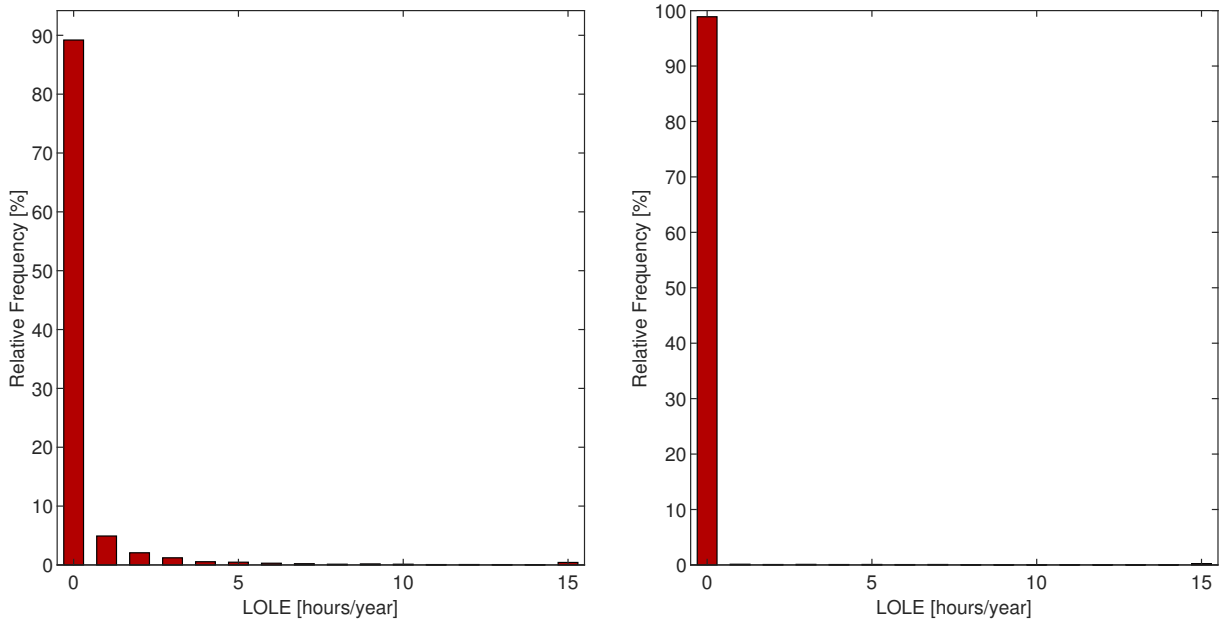

(a) The LOLE distribution at 75% load shifting obtained with LSM1.

(b) The LOLE distribution at 75% load shifting obtained with LSM2.

Figure 6.7: Comparison of the LOLE distributions obtained at 75% load shifting with LSM1 and LSM2.

6.6 HLII Assessment: Impact on System and Bus Indices

This section provides the results for the impact of load shifting models, and the RTP model on system and bus indices in a HLII assessment[2]. The results for LSM1 and LSM2 are displayed first, then the results obtained with the RTP model are given. The results obtained with a DC OPF model are always provided first and second comes the results obtained with an AC OPF model. Only the LOLE and EENS indices are given for the analysis in this and the next sections.

The main objectives with the HLII assessment are the following:

[2]System indices are calculated as the average of the sum of bus index estimates in each simulation year, and not as the sum of the final estimates. Hence, it can be observed that the system indices can be slightly different from the sum of the bus indices obtained in the tables.

1. Compare system indices with the ones obtained in the HLI assessment for the RBTS for increasing load shifting percentage.

2. Explore how curtailment philosophy and system topology affect the bus indices of the two systems, and investigate how increased load shifting affects the bus indices.

3. Investigate the difference in indices obtained with a DC OPF model and an AC OPF model for increasing load shifting percentage.

4. Reveal if there are any distinct differences between the indices obtained with the state sampling and the state transition method.

5. The objectives for the RTP-model are as stated in Section 6.3.2.

6.6.1 Indices Obtained With Load Shifting Models

The results for the RBTS are displayed and discussed first, after comes the results for the RTS. Subscripts *'LSM1'* and *'LSM2'* refer to indices obtained with a load curve modified by LSM1 and LSM2, respectively.

6.6.1.1 RBTS and DC OPF Model

Table 6.9 shows the indices obtained by the state sampling method. Similarly, Table 6.10 shows the indices obtained by the state transition method. Bus 1 has no load connected to it and is left out of the tables.

Table 6.9: System and bus indices for the RBTS obtained by the state sampling method, DC OPF, LSM1 and LSM2.

Load shifting [%]	Bus	$LOLE_{LSM1}$ [hours/year]	$EENS_{LSM1}$ [MWh/year]	$LOLE_{LSM2}$ [hours/year]	$EENS_{LSM2}$ [MWh/year]
100	2	0.0000	0.0000	0.0000	0.0000
	3	1.1300	10.1667	1.1300	10.1667
	4	0.0000	0.0000	0.0000	0.0000
	5	0.0160	0.1743	0.0160	0.1743
	6	10.0480	123.0853	10.0480	123.0853
	System	11.1780	133.4263	11.1780	133.4263
90	2	0.0060	0.0686	0.0000	0.0000
	3	0.9960	8.5536	1.0460	7.7765
	4	0.0000	0.0000	0.0000	0.0000
	5	0.0100	0.1258	0.0060	0.0733
	6	10.1180	124.5861	10.2500	125.6739
	System	11.1180	133.3340	11.2960	133.5236
80	2	0.0000	0.0000	0.0000	0.0000
	3	0.4780	5.3909	0.4100	4.0036
	4	0.0000	0.0000	0.0000	0.0000
	5	0.0020	0.0204	0.0100	0.1123
	6	9.8940	120.8769	9.8080	120.3019
	System	10.3720	126.2882	10.2180	124.4179

Table 6.10: System and bus indices for the RBTS obtained by the state transition method, DC OPF, LSM1 and LSM2.

Load shifting [%]	Bus	$LOLE_{LSM1}$ [hours/year]	$EENS_{LSM1}$ [MWh/year]	$LOLE_{LSM2}$ [hours/year]	$EENS_{LSM2}$ [MWh/year]
100	2	0.0005	0.0081	0.0005	0.0081
	3	1.1250	9.9184	1.1250	9.9184
	4	0.0000	0.0000	0.0000	0.0000
	5	0.0106	0.1352	0.0106	0.1352
	6	9.8877	121.5674	9.8877	121.5674
	System	11.0127	131.6291	11.0127	131.6291
90	2	0.0014	0.0179	0.0005	0.0081
	3	1.0847	8.9670	1.0869	8.2816
	4	0.0002	0.0045	0.0000	0.0000
	5	0.0161	0.1977	0.0106	0.1354
	6	9.9290	121.7463	9.8877	121.5672
	System	11.0145	130.9334	10.9746	129.9923
80	2	0.0022	0.0234	0.0005	0.0079
	3	0.4455	4.4315	0.3683	3.4783
	4	0.0000	0.0000	0.0000	0.0000
	5	0.0084	0.1037	0.0106	0.1362
	6	9.8253	120.3436	9.8877	121.5567
	System	10.2727	124.9022	10.2560	125.1790

Some observations can be made from the results in Table 6.9 and Table 6.10. First, by comparing the system values of LOLE and EENS to the results from the HLI analysis, it is observed that the LOLE and EENS indices are approximately 10 and 13 times larger, respectively, for the HLII analysis. It is reasonable that an inclusion of the transmission grid will lower the reliability, as a capacity deficit can also be due to losses of lines and not only losses of generating units. Furthermore, it can be observed that two buses have higher values for the indices than the others, namely bus 3 and bus 6. The reader should bear in mind that the load curtailment philosophy of the buses are dependent on the load curtailment costs. Bus 3 has the lowest load curtailment cost, and hence it is intuitive that the LOLE and EENS indices are higher for this bus. It can be observed that bus 6 contributes almost solely to the system unreliability. This can be explained due to the fact that this is the only

radial connection in the RBTS network.

In relation to the above-mentioned point, it is noticed that for the HLI analysis it is observed that load shifting has a positive effect on the adequacy indices, i.e. the indices are decreasing as the amount of load shifting is increasing. The same tendency is not that evident for the HLII results. This however, seems to be a result of the radial connection to bus 6 and the fact that the RBTS is a small network. The impact of the radial connection is explored in Table 6.11, where the FOR of the line between bus 5 and 6 is set to 0, indicating that the line is 100% reliable. The LOLE and EENS values obtained at bus 6 are now only due to load curtailments because of capacity deficits or violations of power flow limits on lines, and not due to outage of the line between bus 5 and 6. It can be observed that the bus indices at bus 6 and the system indices are strongly reduced compared to the values obtained in Table 6.9 and Table 6.10. This observation supports the argument that the radial connection to bus 6 is the element contributing most to the system unreliability. The system indices in Table 6.11 are more equal to the ones obtained for the HLI analysis of the RBTS, and the load shifting is improving the indices. Similarly, as found for the HLI analysis, LSM2 is advantageous for higher load shifting percentages, i.e. 80%. At 90%, the system indices of LSM2 are in fact slightly higher than the ones obtained with LSM1.

It can also be noted from Table 6.11 that the indices for buses 5 and 6 are observed to be equal for all load shifting percentages. The reader can note that this last observation is dependent upon the share of load and curtailment costs at these buses. Buses 5 and 6 have equal share of load, and a curtailment cost of 8.6323 \$/kWh and 5.5132 \$/kWh, respectively. Some simple sensitivity analysis is performed to investigate this dependency. If the share of load is kept constant it is found that the buses obtain different index values when the cost of load curtailment is changed at one of the two buses to be equal or lower than the lowest curtailment cost of all buses. Further, if the curtailment cost is kept equal, and the share of load is doubled at one of the buses, this yields different EENS index values at the two buses. When the share of load is in the ratio 1:2, the LOLE values is the same at the two buses, but the bus with greatest share of load has about doubled the value of the EENS index.

Table 6.11: System and bus indices obtained for the RBTS with a 100% reliable connection between bus 5 and 6 using the state sampling method, LSM1 and LSM2.

Load shifting [%]	Bus	$LOLE_{LSM1}$ [hours/year]	$EENS_{LSM1}$ [MWh/year]	$LOLE_{LSM2}$ [hours/year]	$EENS_{LSM2}$ [MWh/year]
100	2	0.0000	0.0000	0.0000	0.0000
	3	1.0620	9.8851	1.0620	9.8851
	4	0.0000	0.0000	0.0000	0.0000
	5	0.0100	0.1252	0.0100	0.1252
	6	0.0100	0.1252	0.0100	0.1252
	System	1.0720	10.1355	1.0720	10.1355
90	2	0.0000	0.0000	0.0000	0.0000
	3	0.9960	7.8165	1.0460	8.1731
	4	0.0000	0.0000	0.0000	0.0000
	5	0.0100	0.1059	0.0060	0.0663
	6	0.0100	0.1059	0.0060	0.0663
	System	1.0060	8.0283	1.0520	8.3057
80	2	0.0020	0.0249	0.0000	0.0000
	3	0.5080	4.7894	0.3720	3.2789
	4	0.0000	0.0000	0.0000	0.0000
	5	0.0100	0.1032	0.0140	0.1657
	6	0.0100	0.1032	0.0140	0.1657
	System	0.5200	5.0207	0.3860	3.6102

6.6.1.2 RTS and DC OPF Model

Table 6.12 and Tables 6.13-6.14 shows the results for increasing load shifting by the state sampling and state transition method, respectively. Only buses with index values different from zero are included in the tables. It can be noted that of the 24 buses in the RTS, buses with loads connected are buses 1-10, 13-16, and 18-20.

Table 6.12: System and bus indices for the RTS obtained by the state sampling method, DC OPF, LSM1 and LSM2.

Load shifting [%]	Bus	$LOLE_{LSM1}$ [hours/year]	$EENS_{LSM1}$ [MWh/year]	$LOLE_{LSM2}$ [hours/year]	$EENS_{LSM2}$ [MWh/year]
100	5	0.0040	0.1741	0.0040	0.1741
	6	0.0100	0.8153	0.0100	0.8153
	7	3.0360	235.5335	3.0360	235.5335
	8	0.0040	0.4370	0.0040	0.4370
	9	9.4000	856.5188	9.4000	856.5188
	10	0.1020	8.1650	0.1020	8.1650
	14	2.9080	261.4774	2.9080	261.4774
	18	0.0200	1.1070	0.0200	1.1070
	19	0.5980	46.6423	0.5980	46.6423
	System	12.4420	1410.8706	12.4420	1410.8706
90	4	0.0020	0.1166	0.0000	0.0000
	5	0.0000	0.0000	0.0040	0.1894
	6	0.0080	0.6620	0.0100	0.8139
	7	2.9420	224.2591	2.9940	231.9646
	8	0.0060	0.5333	0.0000	0.0000
	9	7.5600	662.9593	3.7940	282.9740
	10	0.0780	5.2969	0.0360	2.5349
	14	2.2040	190.0633	0.9940	84.0516
	18	0.0100	0.7935	0.0040	0.3817
	19	0.4340	35.0770	0.1940	13.8493
	System	10.5080	1119.7611	10.6980	1156.0195
80	4	0.0000	0.0000	0.0020	0.1166
	5	0.0040	0.1894	0.0000	0.0000
	6	0.0100	0.8139	0.0080	0.6620
	7	2.9940	231.9646	2.9680	226.8185
	8	0.0000	0.0000	0.0060	0.5333
	9	3.7940	282.9740	2.9460	214.3431
	10	0.0360	2.5349	0.0240	1.1921
	14	0.9940	84.0516	0.7700	59.9875
	18	0.0040	0.3817	0.0020	0.1578
	19	0.1940	13.8493	0.1420	10.1973
	System	6.7960	616.7595	5.9200	514.0083

Table 6.13: System and bus indices for the RTS obtained by the state transition method, DC OPF, LSM1 and LSM2.

Load shifting [%]	Bus	$LOLE_{LSM1}$ [hours/year]	$EENS_{LSM1}$ [MWh/year]	$LOLE_{LSM2}$ [hours/year]	$EENS_{LSM2}$ [MWh/year]
100	4	0.0022	0.0856	0.0022	0.0856
	5	0.0007	0.0376	0.0007	0.0376
	6	0.0083	0.7042	0.0083	0.7042
	7	3.0872	238.3393	3.0872	238.3393
	8	0.0027	0.2775	0.0027	0.2775
	9	9.4267	862.3322	9.4267	862.3322
	10	0.1330	10.1552	0.1330	10.1552
	14	2.9158	263.5841	2.9158	263.5841
	18	0.0194	1.3706	0.0194	1.3706
	19	0.6580	54.4431	0.6580	54.4431
	20	0.0003	0.0071	0.0003	0.0071
	System	12.5170	1431.3366	12.5170	1431.3366
90	4	0.0002	0.0114	0.0015	0.0616
	5	0.0005	0.0218	0.0020	0.0761
	6	0.0069	0.5473	0.0046	0.3977
	7	2.8873	222.0633	2.9016	223.6743
	8	0.0017	0.1654	0.0025	0.2517
	9	7.7483	687.6367	7.5596	660.3800
	10	0.0867	5.7165	0.0903	5.9790
	14	2.3388	202.0538	2.1989	186.3025
	18	0.0086	0.3682	0.0123	0.8895
	19	0.4634	36.4290	0.4500	37.0282
	System	10.6382	1155.0134	10.4617	1115.0405

Table 6.14: System and bus indices for the RTS obtained by the state transition method, DC OPF, LSM1 and LSM2, continued.

Load shifting [%]	Bus	$LOLE_{LSM1}$ [hours/year]	$EENS_{LSM1}$ [MWh/year]	$LOLE_{LSM2}$ [hours/year]	$EENS_{LSM2}$ [MWh/year]
80	4	0.0009	0.0346	0.0015	0.0614
	5	0.0007	0.0298	0.0020	0.0771
	6	0.0072	0.5785	0.0046	0.4035
	7	2.9219	225.1461	2.9016	223.7855
	8	0.0046	0.5019	0.0025	0.2529
	9	3.8251	292.9177	3.0434	222.4201
	10	0.0282	2.2977	0.0227	1.6685
	14	1.0149	82.9505	0.7832	58.9840
	18	0.0034	0.2615	0.0023	0.1871
	19	0.1795	14.0176	0.1269	9.0404
	System	6.7553	618.7360	5.9508	516.8805

From the tables, there is not much difference observed between the indices obtained by the two simulation approaches. To begin with, bus 7 is the only radial connection in the RTS network. The index values at bus 7 is observed not to be improved with increasing load shifting. As reviewed, the radial connection in the RBTS is the main influencing factor for the system reliability. The radial connection to bus 7 is not dominating the system reliability in the same way since the RTS is a larger system. However, since increased load shifting does not noticeably improve the indices at bus 7, this indicates that most of the curtailments are due to loss of the transmission line that connects the bus to the rest of the network. Similarly, it is also found for the RTS that buses with lower priority, i.e. lower curtailment cost, have higher values of LOLE and EENS. Buses 9, 14 and 19 are the three buses with lowest priority in the given order. It can be observed that these buses obtain the greatest change in index values as the load shifting increases. This is intuitive since these buses are the first priority when load needs to be shed, and this need will be less frequent when the peak demand is reduced. The tendency can be more variable for buses that obtain lower index values, i.e. reliable buses like bus 4 and 8. This may be because CVs of reliable buses are found to be high with the sample size used in the simulations. Load buses that never experience load curtailments based on the results in the tables are buses 1-3, 13, 15-16 and 20. Explanations to this can be that buses 1, 2 and 16 have fairly high curtailment costs. Buses 1, 2 and 15 have several generators

situated at the node and buses 3, 16 and 20 are well connected buses with 3-4 transmission lines to other buses.

6.6.1.3 RBTS and AC OPF Model

The results obtain with an AC OPF model using state sampling and state transition for the RBTS are shown in Table 6.15 and Table 6.16, respectively.

Table 6.15: System and bus indices for the RBTS obtained by the state sampling method, AC OPF, LSM1 and LSM2.

Load shifting [%]	Bus	$LOLE_{LSM1}$ [hours/year]	$EENS_{LSM1}$ [MWh/year]	$LOLE_{LSM2}$ [hours/year]	$EENS_{LSM2}$ [MWh/year]
100	2	0.0020	0.0210	0.0020	0.0210
	3	1.8240	15.9998	1.8240	15.9998
	4	0.0020	0.0419	0.0020	0.0419
	5	0.0160	0.1666	0.0160	0.1666
	6	11.3920	126.5521	11.3920	126.5521
	System	12.4560	142.7814	12.4560	142.7814
90	2	0.0000	0.0000	0.0000	0.0000
	3	1.7500	13.9498	1.7440	14.9068
	4	0.0000	0.0000	0.0000	0.0000
	5	0.0100	0.1299	0.0140	0.1556
	6	11.0980	122.6745	10.9420	121.4635
	System	12.2520	136.7542	12.0500	136.5259
80	2	0.0040	0.0361	0.0000	0.0000
	3	0.6980	7.3860	0.5820	5.5522
	4	0.0000	0.0000	0.0000	0.0000
	5	0.0120	0.1642	0.0180	0.2120
	6	10.4240	125.6809	10.4200	126.4070
	System	10.9020	133.2672	10.8320	132.1712

Table 6.16: System and bus indices obtained by the state transition method, AC OPF, LSM1 and LSM2.

Load shifting [%]	Bus	$LOLE_{LSM1}$ [hours/year]	$EENS_{LSM1}$ [MWh/year]	$LOLE_{LSM2}$ [hours/year]	$EENS_{LSM2}$ [MWh/year]
100	2	0.0005	0.0081	0.0005	0.0081
	3	1.8699	15.6613	1.8699	15.6613
	4	0.0001	0.0000	0.0001	0.0000
	5	0.0107	0.1359	0.0107	0.1359
	6	11.2877	125.0065	11.2877	125.0065
	System	12.3945	140.8118	12.3945	140.8118
90	2	0.0005	0.0081	0.0005	0.0081
	3	1.6917	13.7682	1.6820	13.6938
	4	0.0001	0.0000	0.0001	0.0000
	5	0.0107	0.1359	0.0107	0.1360
	6	11.1569	123.7856	11.1655	123.7484
	System	12.2171	137.6979	12.2158	137.5863
80	2	0.0005	0.0079	0.0005	0.0079
	3	0.6525	6.1597	0.5601	5.2545
	4	0.0001	0.0000	0.0001	0.0000
	5	0.0107	0.1369	0.0107	0.1368
	6	10.2355	123.0341	10.1537	122.8006
	System	10.6711	129.3386	10.5507	128.1998

Based on the indices in the tables, the same observations with respect to the radial connection and curtailment costs are also evident for the AC model. What should be noted in addition is that the bus and system indices are increased compared to the results of the DC model. This is mostly because of two features with the AC model. Firstly, transmission losses are included yielding that more generating capacity is needed to serve the same load compared to the DC model. Another element that can increase the indices is that voltage limits are introduced at all buses in the AC model. Thus, some load curtailments can be necessary to carry out to satisfy voltage constraints in

the system.

6.6.1.4 RTS and AC OPF Model

Tables 6.17-6.18 shows the results for the RTS using the state sampling approach. The state transition approach is not included here due to limits in computational time. Again, only buses with index values different from zero are displayed in the tables.

Table 6.17: System and bus indices for the RTS obtained by the state sampling method, AC OPF, LSM1 and LSM2.

Load shifting [%]	Bus	$LOLE_{LSM1}$ [hours/year]	$EENS_{LSM1}$ [MWh/year]	$LOLE_{LSM2}$ [hours/year]	$EENS_{LSM2}$ [MWh/year]
100	3	0.1700	0.7270	0.1700	0.7270
	5	0.0020	0.0969	0.0020	0.0969
	6	3.3940	45.9138	3.3940	45.9138
	7	3.4200	249.6544	3.4200	249.6544
	8	0.0120	0.4631	0.0120	0.4631
	9	11.5180	1043.3636	11.5180	1043.3636
	10	3.5660	9.4202	3.5660	9.4202
	14	11.5020	317.6220	11.5020	317.6220
	15	0.1340	0.0138	0.1340	0.0138
	18	0.6440	0.6992	0.6440	0.6992
	19	11.4320	63.7084	11.4320	63.7084
	20	0.1340	0.0160	0.1340	0.0160
	System	18.3320	1731.6984	18.3320	1731.6984
90	3	0.1200	0.6772	0.1220	0.6774
	5	0.0020	0.0969	0.0020	0.0969
	6	3.3920	45.2229	3.4060	45.2664
	7	3.4240	249.8835	3.4120	248.8947
	8	0.0120	0.4631	0.0120	0.4631
	9	9.5220	828.6080	9.4040	826.6160
	10	2.8980	6.1936	2.8840	6.1240
	14	9.5160	248.2950	9.3980	247.3376
	15	0.0960	0.0096	0.0980	0.0098
	18	0.5660	0.2114	0.5700	0.1698
	19	9.4420	45.3558	9.3360	44.9024
	20	0.0960	0.0114	0.0980	0.0116
	System	16.3280	1425.0283	16.2120	1420.5696

Table 6.18: System and bus indices for the RTS obtained by the state sampling method, AC OPF, LSM1 and LSM2, continued.

Load shifting [%]	Bus	$LOLE_{LSM1}$ [hours/year]	$EENS_{LSM1}$ [MWh/year]	$LOLE_{LSM2}$ [hours/year]	$EENS_{LSM2}$ [MWh/year]
80	3	0.0540	0.6034	0.0320	0.5438
	5	0.0020	0.0969	0.0020	0.0969
	6	3.5560	37.5630	3.5100	36.2734
	7	3.4260	249.7563	3.4380	250.3774
	8	0.0100	0.4359	0.0080	0.4345
	9	4.6720	360.3474	3.8920	286.3094
	10	1.1360	1.3710	0.9200	0.3160
	14	4.6660	95.0208	3.8880	70.9084
	15	0.0260	0.0026	0.0120	0.0012
	18	0.1680	0.0174	0.1280	0.0130
	19	4.6140	17.2276	3.8400	10.6246
	20	0.0260	0.0026	0.0120	0.0012
	System	11.6640	762.4449	10.8460	655.8997

Firstly, it can also be noted for the RTS that the bus and system indices are increased compared to the results from the DC model. It appears that the LOLE index is most sensitive to the DC assumptions. For instance, the percentage increase for the system LOLE and EENS indices obtained with LSM1 in Table 6.12 compared to the values in Tables 6.17-6.18, is 47% (LOLE) and 23% (EENS) for 100% load shifting, 55% and 27% for 90% load shifting and 72% and 24% for 80% load shifting. This indicates that the LOLE index is more sensitive to the DC assumptions and that this sensitivity increases as the load shifting percentage increases. The EENS index shows a more stable increase in system index values for increasing load shifting percentage. Secondly, it can be observed that more buses have index values different from zero compared to the results obtained with the DC model. Buses 6 and 10 can be observed to be particularly affected when an AC model is used, compared to the DC results. These buses are close in location and have medium curtailment costs. It can be noted that the indices at bus 6 do not improve with increasing load shifting, whereas some improvement can be seen at bus 10. It can appear that these buses, and especially bus 6, have higher values of LOLE and EENS when the AC model is used because of voltage constraints that

need to be fulfilled.

Next, some comparison and discussion concerning the HLII assessment for the RTS conducted in this thesis with respect to literature will be given. To begin with, the author in [8] conducted a comparison with benchmark literature for the MCS software used in this thesis. As stated by [8], the estimates obtained in the HLII assessment compared to the HLI assessment are more influenced by the choices made to evaluate the system states. This can be choices related to the contingency solvers such as constraints in the OPF that decide feasible system states or how system states with isolated buses are dealt with[3]. References found in literature that utilize models similar to LSM1 in a HLII assessment of the RTS are [36] and [43]. Few details concerning the calculation procedure are given in these papers, hence it should be noted that it can be hard to compare the estimates, but some similarities and differences will be highlighted. First of all, [36] and [43] divide the load among different load sectors which gives a more realistic case. Seven different load sectors are considered, i.e. agricultural, large users, office, industrial, commercial and residential. The assessment in this thesis uses the same load profile for all buses resulting in a system peak load of 2850 MW. When load buses are divided into the seven sectors with dissimilar load profiles, it results in a system peak load of 2754.35 MW since the peak loads at each bus do not occur at the same time. The fact that this thesis uses the same load profile at all buses should be noted as a shortcoming when evaluating the impact of DSR on system and bus indices. This gives aggregated effects, both when shaving the peak loads and adding loads to the valleys.

Having this in mind, it can however be noted that the obtained system indices for the base case, i.e. no load shifting, are higher for the two papers [36, 43] than the indices obtained with both the DC and AC model of this thesis. The system indices obtained with state sampling and the AC OPF model in this thesis are 18.33 hours/year for the LOLE index (LSM1) and 1731.70 MWh/year for the EENS index (LSM1). In the mentioned papers the same indices are around 36 hours/year for the LOLE index and around 4500 MWh/year for the EENS index. It can also be noted that the system indices obtained with load shifting in the papers achieve a greater improvement than the indices obtained with increasing load shifting in this thesis for the RTS. For example, at 80% load shifting the system indices in the papers are in fact reduced to lower values than in this thesis, both for LSM1 and LSM2. Nevertheless, as mentioned there can be several differences in the choices made in the HLII assessment of the studies compared to those in this thesis. For instance, in [36]

[3]The contingency solvers for the software used in this thesis are implemented such that generators on islanded nodes are not able to fulfill their load requirements. In addition, if the slack bus is islanded from the system, all loads are shed expect the load on the slack bus [8].

a load curtailment philosophy with shedding of loads closest to the component on outage is used, while individual curtailment costs are used in this thesis. Further, the results obtained with the AC model for the RTS are from a non-sequential simulation method in this thesis, while as given in [43], sequential MCS is used. The standard deviations are provided for the LOLE system index in [43] and are given to be 32.11, 23.36 and 8.41 hours/year for 100%, 90% and 80% load shifting, respectively. In this thesis the standard deviations for the LOLE system index obtained with state sampling, AC OPF and LSM1 are 4.35, 4.13 and 3.33 hours/year for 100%, 90% and 80% load shifting, respectively.

6.6.2 Indices Obtained With Real-Time Pricing Model

As mentioned in Section 6.3.2, only the RTS is used as test system for the RTP model. Due to negligible differences in index values for the state sampling and state transition method, only the results using the state sampling method are displayed. Self-elasticity coefficients equal to -0.2 and cross-elasticity coefficients equal to 0.025 are used for the results obtained in Tables 6.19-6.20. The former table shows the results for an outage of the smallest generator, i.e. less price differences observed at the buses. The latter table shows the results for an outage of the largest generator, i.e. larger price differences observed at the buses. The indices in the tables are obtained with DC OPF and AC OPF.

Table 6.19: System and bus indices for the RTS obtained by the RTP model with outage of a generator of 155 MW.

Bus	**DC OPF**		**AC OPF**	
	LOLE [hours/year]	*EENS* [MWh/year]	*LOLE* [hours/year]	*EENS* [MWh/year]
3	0.0000	0.0000	0.1100	0.6258
5	0.0040	0.1732	0.0020	0.0955
6	0.0100	0.8235	3.2660	41.7980
7	3.0100	232.9514	3.4440	248.3953
8	0.0040	0.4347	0.0100	0.4362
9	6.7560	582.2459	8.0700	715.3998
10	0.0700	5.4130	2.4660	4.9012
14	2.0420	173.3662	8.0520	211.7542
15	0.0000	0.0000	0.0820	0.0082
18	0.0100	0.5207	0.4160	0.1164
19	0.4080	29.3284	8.0020	38.5898
20	0.0000	0.0000	0.0820	0.0092
System	9.7740	1025.2571	14.7860	1262.1296

Table 6.20: System and bus indices for the RTS obtained by the RTP model with outage of a generator of 350 MW.

Bus	**DC OPF**		**AC OPF**	
	LOLE [hours/year]	*EENS* [MWh/year]	*LOLE* [hours/year]	*EENS* [MWh/year]
3	0.0000	0.0000	0.0380	0.7026
4	0.0020	0.1138	0.0000	0.0000
5	0.0000	0.0000	0.0020	0.0734
6	0.0080	0.6399	3.1100	30.1410
7	2.9700	227.6404	3.4240	246.2499
8	0.0060	0.5523	0.0060	0.4687
9	3.1580	254.2810	4.0280	321.1656
10	0.0220	1.3006	1.0660	1.1458
14	0.9060	68.4759	4.0200	83.9816
15	0.0000	0.0000	0.1400	0.0142
18	0.0020	0.2694	0.1400	0.0142
19	0.1640	12.6959	3.9700	11.8378
20	0.0000	0.0000	0.0160	0.0016
System	6.1360	565.9693	10.5720	695.7836

Some main observations can be made from the two tables above. Firstly, it can be seen that larger price differences yield lower indices since more load is shifted. For instance, compared to the results obtained with no load shifting, the LOLE and EENS indices are reduced with 19% and 27% for AC OPF and the smallest outage case, respectively, and 42% and 60% for AC OPF and the largest outage case. The system indices obtained with smaller price differences are in the range between 80%-90% load shifting, while the system indices obtained with larger price differences are closer to 80% load shifting. It can be noted that the total amount of shifted energy in the yearly system load profile for the case with smaller price differences is 190 910 MWh, while the total amount of energy shifted in the case of larger price differences is 454 221 MWh. In comparison, the amount of energy shifted at load shifting levels 90% and 80% are 929 MWh and 9022 MWh, respectively. The RTP model shifts load in most hours due to the fact that there is a price difference in most hours. LSM1 and LSM2 are more effective in the sense that they target only the peak hours that contribute most to the system unreliability. When an outage case is simulated for all hours, also periods with lower demand get affected and these hours are not the critical ones if the objective is

to reduce peak demand and improve the reliability. In relation to this, price spikes which especially occur in high demand periods and give larger price differences for the largest outage case studied, can be particular beneficial for the reliability. This effect can be similar to CPP which can be used during contingencies or other events leading to high wholesale prices [4].

Moreover, the buses with highest index values are similar to the ones obtained with the load shifting models. Bus 7 with the radial connection, and buses 9, 14 and 19 with lowest curtailment costs are the buses that have the most observable impact. As before, the AC conditions increase the indices at buses and for the system. Buses 6 and 10 are again the most noticeably affected buses when constraints in the AC OPF are accounted for. Thus, applying nodal prices for the two cases studied does not appear to affect the trend for the bus indices compared to the indices obtained with LSM1 and LSM2. This can be intuitive since the buses with lowest curtailment costs will still account for much of the curtailments, and radial and less connected buses are still vulnerable. In addition, these potential differences can be hard to capture since the curtailment philosophy is a dominating factor for the bus indices. If there had been a curtailment philosophy of shedding load closest to the fault location, this could have revealed other results. Evaluating another outage case could also have given other results, e.g. including outages of transmission lines that would affect some buses extra hard. Also, it must be emphasized that all buses have the same load profiles and the same PEM structure and elasticity coefficients, leading to equal rescheduling strategy. If different load profiles and PEMs had been used this could possibly have changed the results as well.

The self- and cross-elasticities are changed in order to investigate how more or less price responsive consumers affect the reliability indices. Self-elasticity coefficients are increased and cross-elasticity coefficients are increased correspondingly such that Equation 4.5.5 always is fulfilled. The sensitivity analysis is performed using the state sampling method and an AC model for the case with largest price differences. Table 6.21 shows how selected bus indices and system indices change when the self- and cross-elastcities increase. The buses displayed are bus 6 and bus 7 which are buses with less connections to the rest of the network, and buses 9 and 14 which are the two buses with the lowest curtailment costs. Indices of all buses are provided in Appendix G. The structure of the PEM is the same as referred to before. To illustrate the effect of increasing elasticity coefficients, Figure 6.8 shows how a section of the load demand changes for increasing elasticity at bus 1. The effect is found to be similar at the other buses in the system. The cross-elasticities are the same as found in Table 6.21.

Table 6.21: Selected bus indices for the RTS with changing price elasticity.

Elasticity coefficients	Bus	LOLE [hours/year]	EENS [MWh/year]
ε_{ii} = -0.1, ε_{ij} = 0.0125	6	3.2620	38.9188
	7	3.4420	249.6365
	9	6.3420	560.6240
	14	6.3340	156.5738
	System	13.0520	1038.9279
ε_{ii} = -0.2, ε_{ij} = 0.025	6	3.1100	30.1410
	7	3.4240	246.2499
	9	4.0280	321.1656
	14	4.0200	83.9816
	System	10.5720	695.7836
ε_{ii} = -0.3, ε_{ij} = 0.0375	6	3.1980	27.6406
	7	3.4520	247.9779
	9	3.2120	251.7026
	14	3.2080	64.6992
	System	9.8700	604.8545
ε_{ii} = -0.4, ε_{ij} = 0.0500	6	3.1460	22.9342
	7	3.4820	249.8561
	9	4.1380	390.4580
	14	4.1280	128.4958
	System	10.7860	823.1154

It can be observed for the first three cases of increasing elasticity coefficients in Table 6.21 that the system indices decrease as the absolute value of the elasticities increases. Contrarily, the last case in Table 6.21 shows that the system LOLE and EENS have increased. This increase occurs because of load spikes that are introduced when a great amount of load is shifted from the peak period to the valley period (8 hours). Some of the valley loads are exceeding the original peak load. As observed from Figure 6.8, a spike reaching higher than the original peak is introduced at around hour 200 when e_{ii} = -0.4. This becomes more frequent as the load demand increases and the price differences increase during the yearly profile. It should be noted that this effect can be reduced if the price

calculation is performed in the iterative procedure mentioned in the theory and shown in Figure 4.8. These load spikes would result in high prices that can be reduced if there is a dynamic interaction between price and demand. Figure 6.9 shows the nodal prices obtained for bus 1 with the load curve of e_{ii} = -0.4. As can be seen, the high load in hour 200, which also will occur at other buses due to similar load pattern, causes a price spike. A more sophisticated implementation of the RTP model should account for such effects by applying an iterative framework. These observations also highlight that price sensitive consumers can potentially lead to increased volatility. As stated in [60] where the effect of RTP on power system volatility was investigated, absence of a controlled feedback loop between price and demand can increase the uncertainty between demand and generation and thereby create a more volatile system. Thus, control of smart loads at the consumer side by aggregation services might be necessary if DSR resources shall participate in the electricity market without increasing the uncertainty.

Further, the bus indices given in Table 6.21 show that the indices at buses with fewer connections to the rest of the network are less affected by increased price responsiveness. The buses with lowest load curtailment costs show the same tendency as the system indices for increasing elasticity coefficients since those buses are the first choice when loads need to be curtailed during capacity shortages.

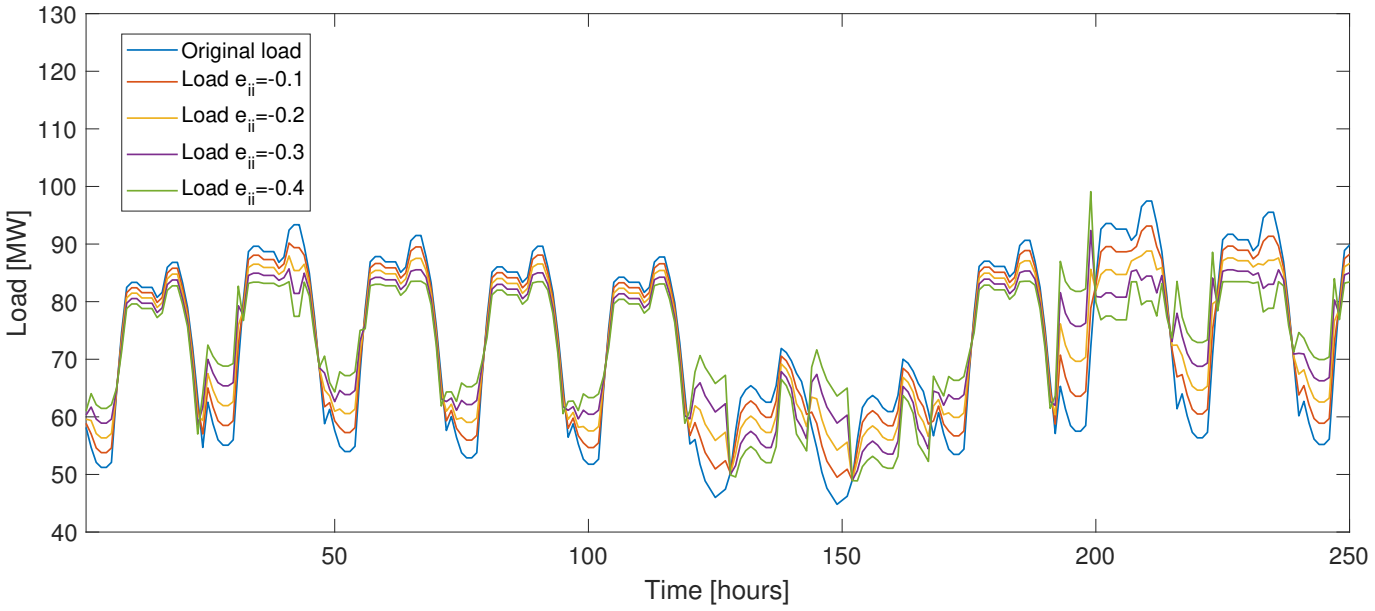

Figure 6.8: Load curves for changing price elasticity at bus 1 in the RTS.

Some remarks regarding the PEM and the elasticity coefficients should be highlighted. In the theory chapter about DSR it was discussed that smart meters and real-time monitoring could

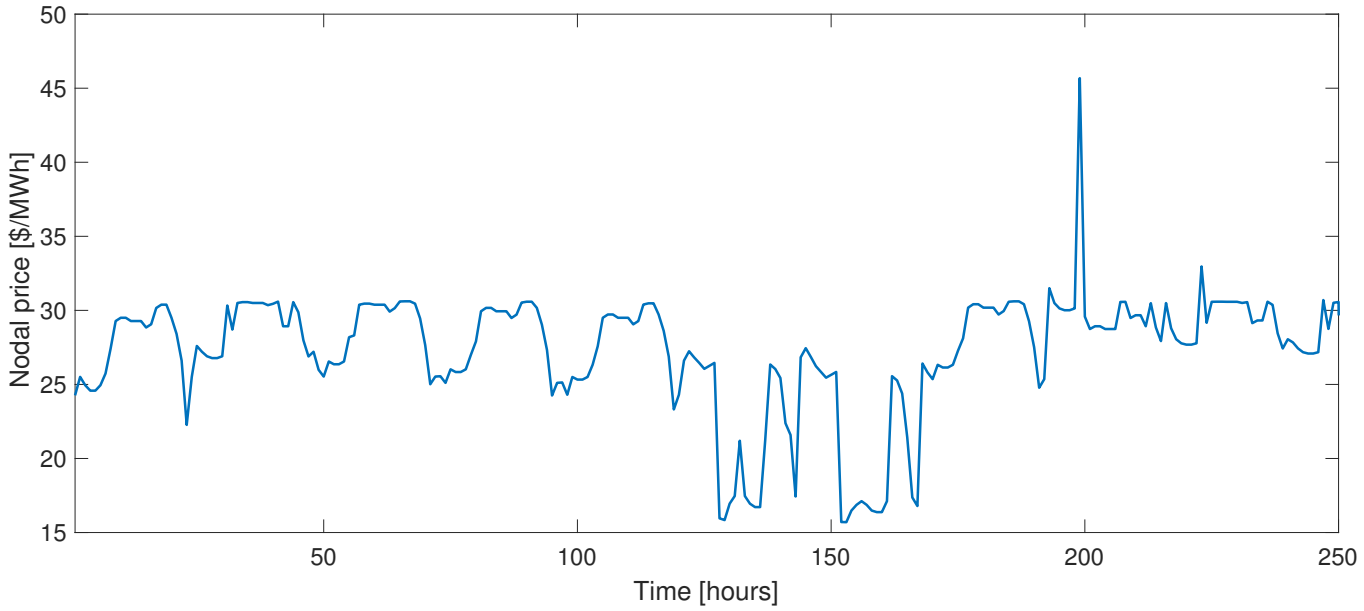

Figure 6.9: Nodal price at bus 1 in the RST for load curve obtained with e_{ii} = -0.4.

increase the price elasticity of electric demand. In addition, ICT and aggregation services could increase the price elasticity even more. Nevertheless, there is still uncertainty regarding the degree of price responsiveness of the future consumer. This will be much dependent upon the future market solutions and the possible earnings for the consumers to participate with flexible demand. Further, estimating trustworthy elasticity coefficients is a research field in its own, and would require a large volume of price and demand data for yearly profiles. With the installation of smart meters this can be easier to obtain.

This thesis has not focused on utilizing real-world elasticities, but rather on illustrating the effect of a price responsive consumer. More realistic PEM structures and coefficients are used in [52]. The authors of this paper put forward that using constant values of self- and cross-elasticities is not reflective of a real-world scenario. Taking self elasticity as an example, it is more realistic that a price difference during peak hours, i.e. the hours with highest spot prices, would encourage a greater load reduction than if the same price difference was observed during early or late hours of the day. Hence, the study in [52] uses varying self-elasticities to reflect that it would be most attractive to reduce load during these hours with respect to price levels. For the case studied in this thesis it was found that setting the self-elasticity coefficients of off-peak hours lower than the coefficients in peak hours, did not change the load shifting pattern and amounts considerably compared to constant values. This is most likely because a price difference is encountered in most hours and because the energy that is reduced has to be recovered during the 24 hour study period. The outage cases in this

thesis account for all hours in the yearly profile. The effect of using PEMs with varying elasticity coefficients, both self- and cross-elasticities, in a more realistic case study where outage incidents have different duration should be more visible.

It can also be mentioned that, as stated in [53], with the future smart grid, elasticity coefficients can be set by consumer load control algorithms. It can be agreed between the consumer and the aggregator/utility about the loads that can be controlled within certain restrictions, such as duration and time of the day, and these agreements can be reflected in the PEM structure and the elasticity coefficients used by the load control algorithms.

Lastly, some points for improvement are worth highlighting with respect to the RTP model and the assessment conducted. It is important to recognize that load changes are performed before the simulations are carried out in the case study. A more realistic implementation of the RTP model would be that the price responsiveness of the consumers occurs in relation to the outage cases in the simulations. The fact that the load is changed in advance and only accounting for one outage case weakens the foundation to say much about how locational marginal prices can be beneficial for the reliability of the system. The results obtained in this assessment do not reflect the potential benefit that can arise if the nodal prices are related to the actual system state in the simulations. To achieve this the nodal prices should be updated every study period, e.g. every 24 hours, to reflect the current system state[4]. A sequential simulation approach like the state transition method is necessary to use to capture the correlation effect between duration of contingencies, nodal prices and load response.

As shown in Figure 6.4 and Figure 6.5, the load response can differ among buses due to dissimilar observed price differences. If the RTP model is implemented as just described, these price differences among buses would change as contingencies occur different places in the system. To illustrate this, two additional example cases of nodal prices and nodal price differences are provided in Appendix H. These examples include transmission line outages and illustrate that line outages can affect some buses extra hard. At the same time, it is reasonable that consumers can be price responsive also when no contingencies are present, similar to the effect shown in the case study when the load is changed in advance and not related to the current system state. A fully realistic RTP model would account for both possibilities. This would be the possibility for the consumer to shift load from peak to off-peak hours during the day, and the possibility to react to prices during contingencies

[4]The length of the study period can depend upon which market the DSR resources participate in. The study period will be shorter if DSR resources can participate in the intra-day market.

and stressed system states.

6.7 ELCC Calculations

The results for the ELCC calculations are displayed in this section. System indices are used in all the evaluations. The reliability level for the original load profile is used for all cases as reference level, i.e. the LOLE or EENS value at a YPL equal to 185 MW for the RBTS and at a YPL equal to 2850 MW for the RTS.

The main objectives of the ELCC calculations are the following:

1. Investigate how LOLE and EENS perform as adequacy indices in the calculations for the two test systems.

2. Investigate and compare the development in ELCC for increasing amount of DSR resources available for load shifting at HLI and HLII for both test systems.

3. Evaluate the ELCC for a fixed amount of DSR resources on each bus in the RTS to reveal possible differences among buses in this network.

6.7.1 Performance of LOLE and EENS in the Calculations

The performance of LOLE and EENS in the ELCC calculations is investigated first. Example plots are shown for each test system with system indices calculated at HLI and HLII. ELCC values from indices obtained with the analytical method for increasing peak load at HLI for the RBTS are also included.

6.7.1.1 RBTS

Figure 6.10 shows the performance of LOLE and EENS at HLI for an example case of 6000 MWh available DSR resources where indices are calculated with the analytical method. Figure 6.11 displays the same case for system indices calculated with MCS at HLI. Lastly, Figure 6.12 shows the performance of the system indices at HLII calculated with MCS.

It should be noted that the increase of system peak load for the analytical method is 1 MW, while

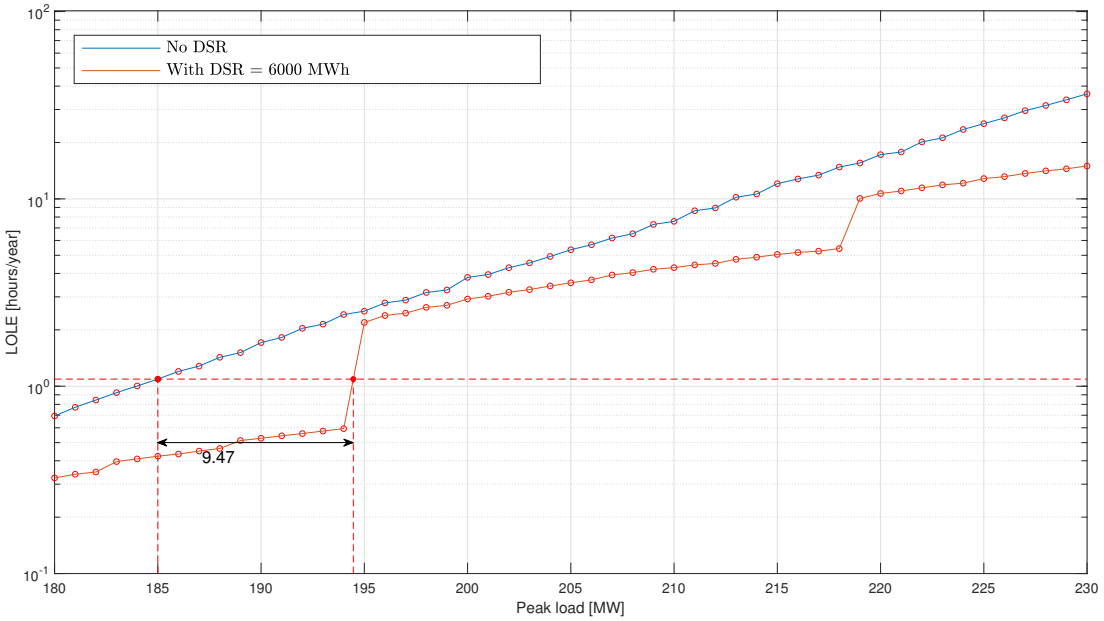

(a) ELCC with LOLE as the reliability index for 6000 MWh available DSR.

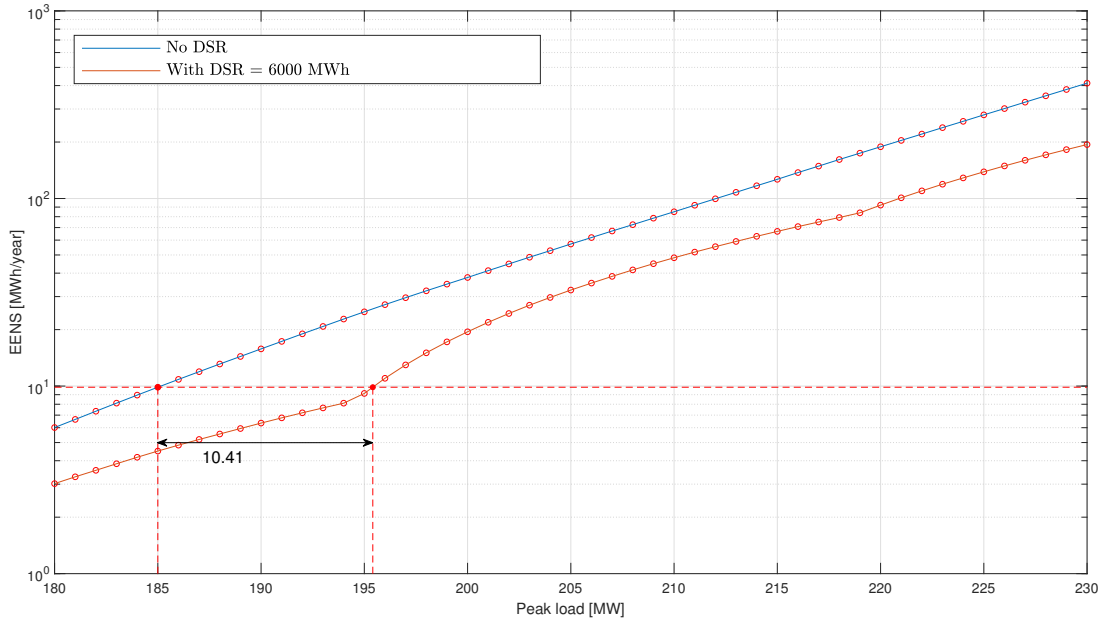

(b) ELCC with EENS as the reliability index for 6000 MWh available DSR.

Figure 6.10: Performance of LOLE and EENS in ELCC evaluation calculated with an analytical method for the RBTS at HLI.

for the MCS it is 5 MW due to computation time. A first remark for all figures is that the curves obtained using EENS as reliability index occur to be smooth, while the curves obtained using LOLE

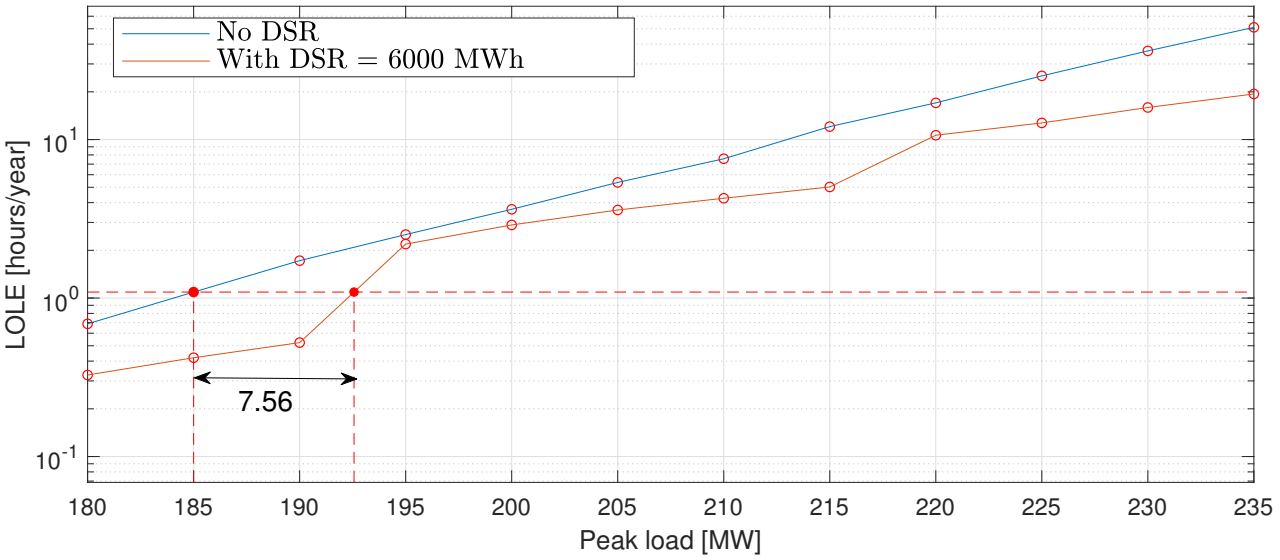

(a) ELCC with LOLE as the reliability index for 6000 MWh available DSR.

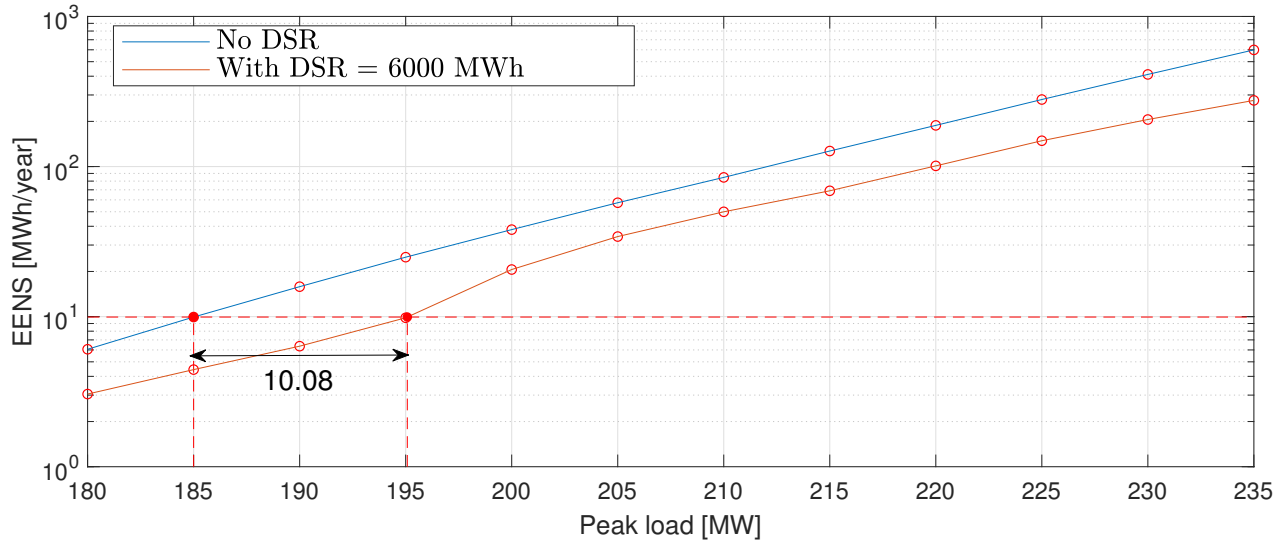

(b) ELCC with EENS as the reliability index for 6000 MWh available DSR.

Figure 6.11: Performance of LOLE and EENS in ELCC evaluation calculated with MCS for the RBTS at HLI.

as reliability index appear to be step-wise or less smooth for the system with DSR resources. It can be difficult to state a unique answer for this step-wise behaviour. Nevertheless, a possible explanation is given in the following. Based on results from Section 6.5.1, this step-wise behavior can be indicated to appear both as a result of the flattening of the load curve when utilizing load shifting and the fact that RBTS is not a very large system, resulting in a moderate amount of states in the COPT. When the load curve is flattened out, more hours occur with the same load

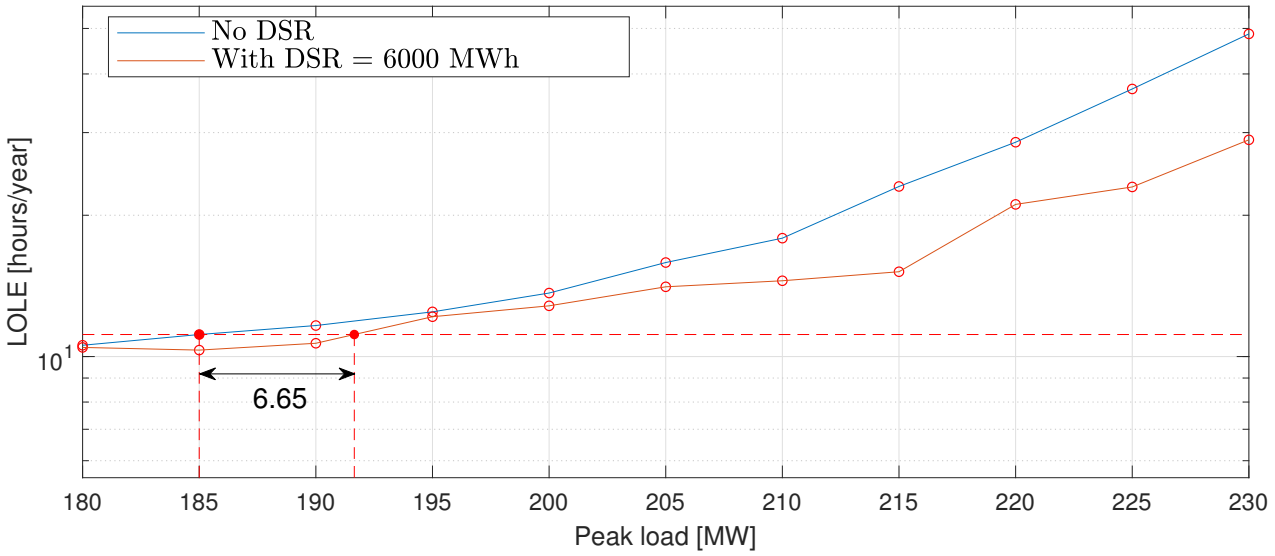

(a) ELCC with LOLE as the reliability index for 6000 MWh available DSR.

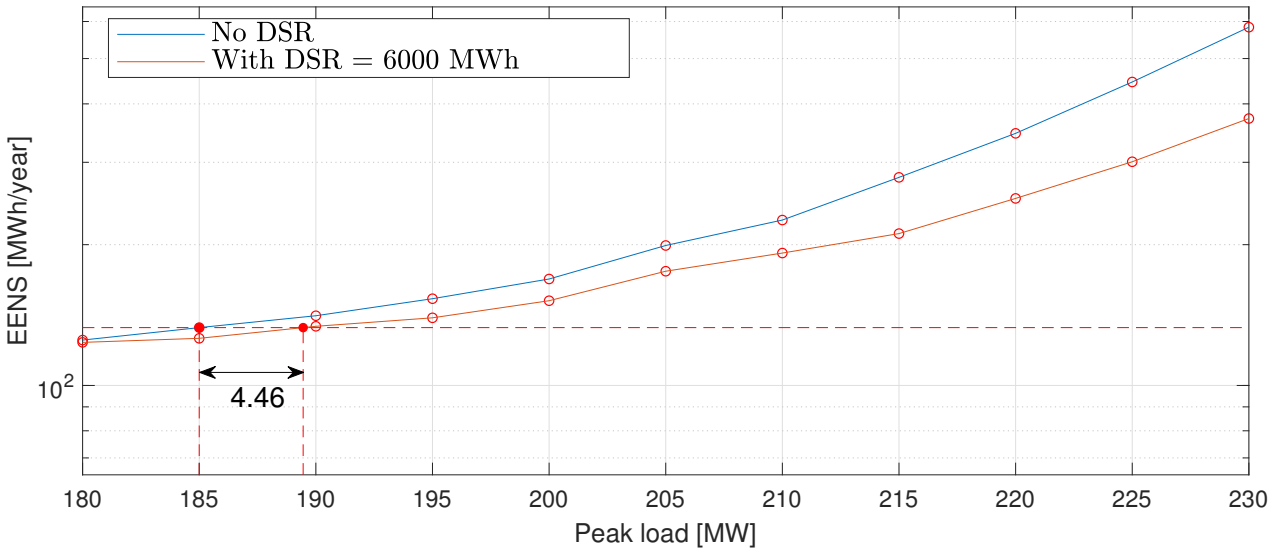

(b) ELCC with EENS as the reliability index for 6000 MWh available DSR.

Figure 6.12: Performance of LOLE and EENS in ELCC evaluation calculated with MCS for the RBTS at HLII.

value and the number of LOLE values becomes limited. The cumulative probabilities in the COPT used to obtain the LOLE index show a grouping tendency for the RBTS. Thus, it can appear that at a certain point when increasing the load, the main contribution to the LOLE index changes to another group of cumulative probabilities. Also, from the results obtained in Section 6.5.2 it was found that the LOLE index had the same leaping tendency when MCS was used, and Figure 6.11a also indicates a step-wise curve for increasing peak load.

From Figure 6.12, which shows the ELCC at HLII, it can be seen that the curves representing the system with and without DSR resources are closer for lower peak loads compared to the curves obtained at HLI. It can be observed that the step-wise tendency for the LOLE index is also present at HLII. Including the transmission grid yields several additional combinations of outage states. Hence, the same arguments as used for the curves at HLI might not be valid. Nevertheless, it is noted that since the same tendency is evident at HLII for the RBTS, this can be due to the small system size and simple system configuration. In addition, as a main point worth highlighting, it should be recognized that a step-wise curve will give an ELCC that varies greatly depending upon the reliability reference level used. Stated another way, this means that a discontinuous curve can yield great changes in ELCC values for small changes in reliability reference level. This leads to less trustworthy results, and can be an argument for using the EENS index for this particular system when calculating the ELCC values.

6.7.1.2 RTS

Figure 6.13 and Figure 6.14 display the performance of LOLE and EENS as reliability index in ELCC calculations for the RTS at HLI and HLII, respectively. The examples use 75000 MWh DSR resources available for load shifting. A load increment of 20 MW is used when increasing the system peak load.

From these plots it can be seen that both indices result in smooth curves at HLI and HLII. As mentioned, the RTS is a much larger system compared to the RBTS. There are more generating units and transmission lines in this system, yielding more possible combinations of outage states and thus more possible LOLE values. There are not drawn any certain conclusions since the procedure is only tested on two systems. Nevertheless, it can be noted that there are implications that the system size, including a larger variety of outage states, is decisive for the performance of the LOLE index in the ELCC procedure with the DSR model, LSM2, used in this thesis.

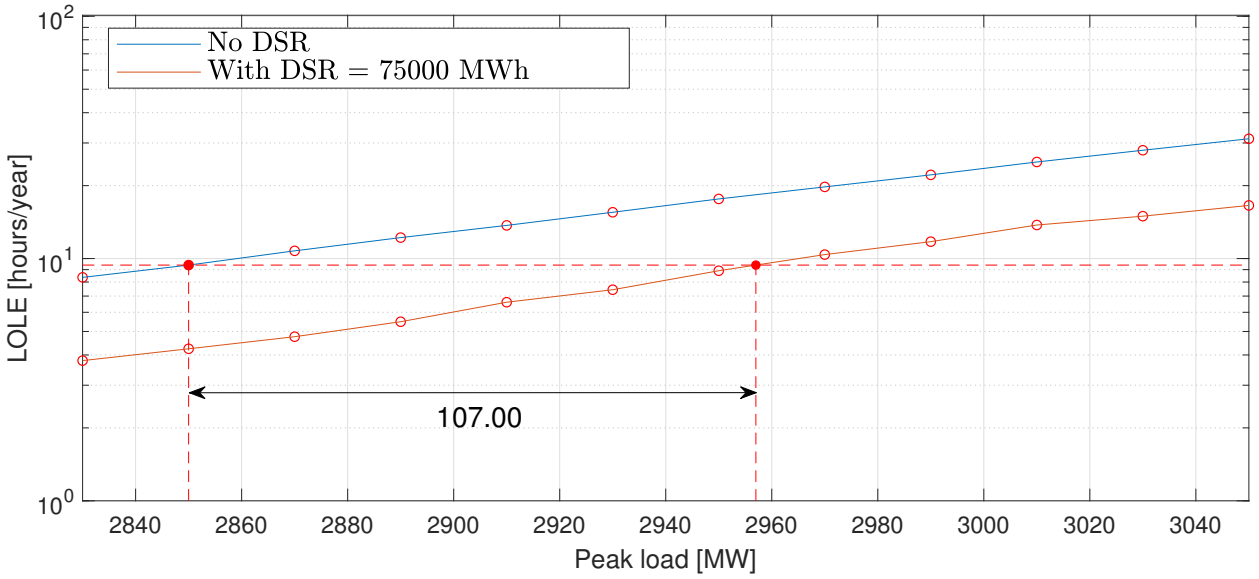

(a) ELCC with LOLE as the reliability index for 75000 MWh available DSR.

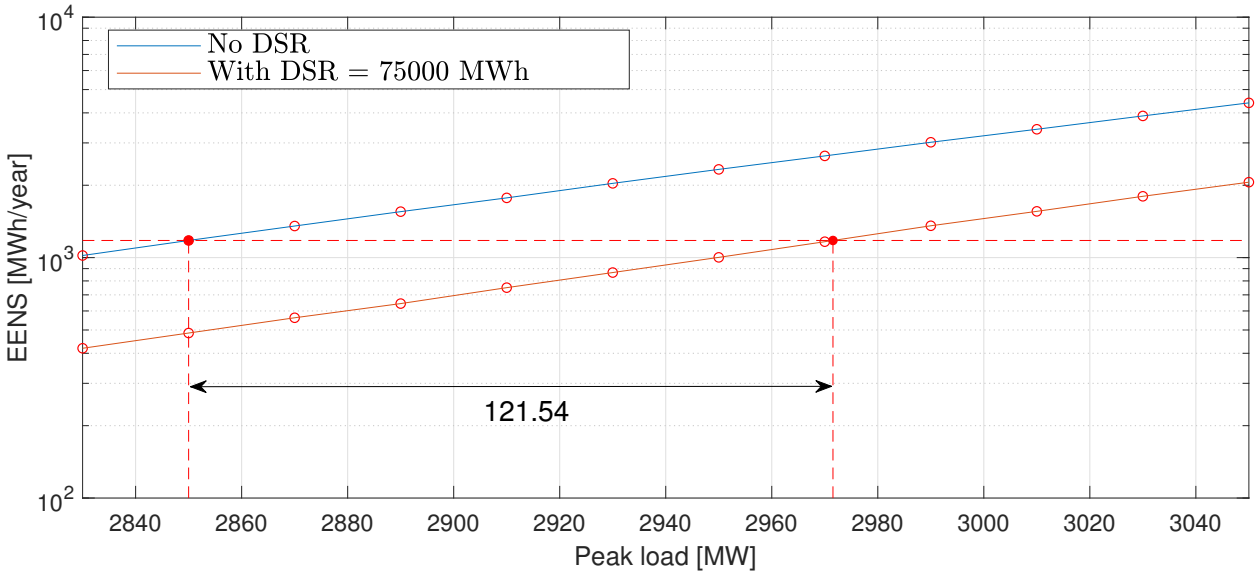

(b) ELCC with EENS as the reliability index for 75000 MWh available DSR.

Figure 6.13: Performance of LOLE and EENS in ELCC evaluation calculated with MCS for the RTS at HLI.

6.7.2 ELCC for Changing Amount of Demand Side Resources

ELCC values are calculated for increasing amount of available DSR resources for load shifting. The specified amount of MWh DSR resource applies for all buses together. The modifications are performed on the system load profile, and bus loads are obtained as a given share of the system

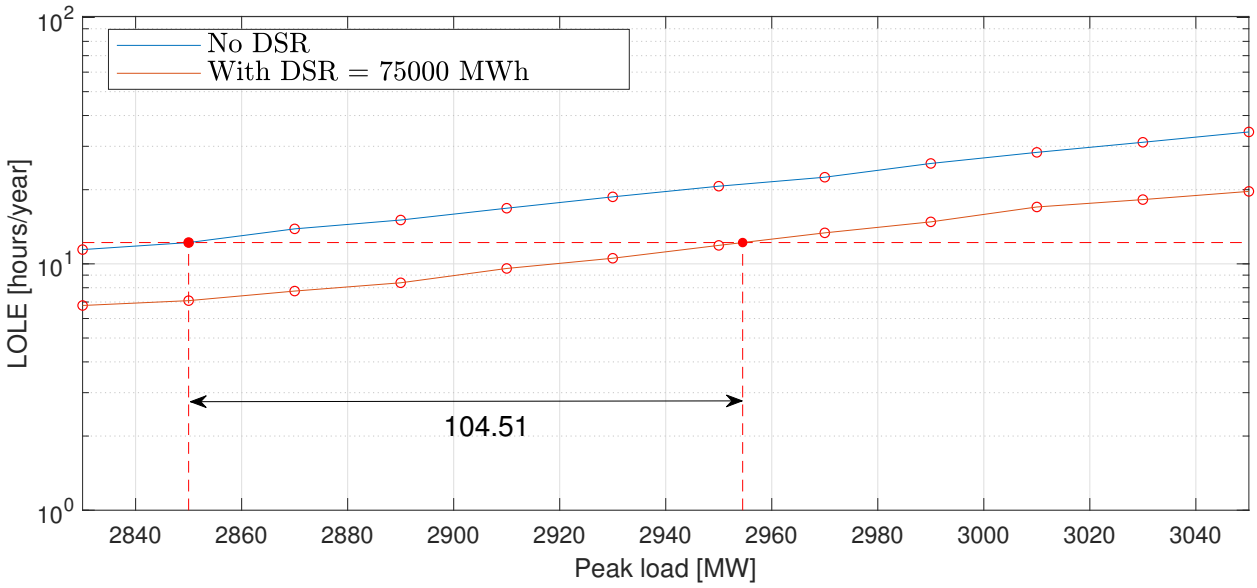

(a) ELCC with LOLE as the reliability index for 75000 MWh available DSR.

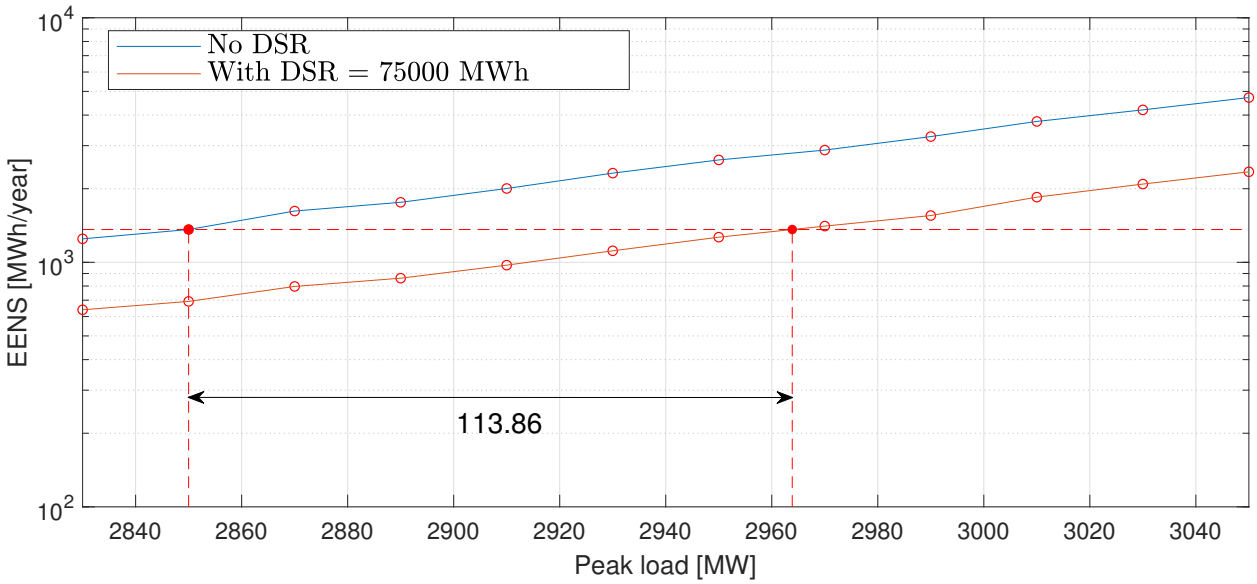

(b) ELCC with EENS as the reliability index for 75000 MWh available DSR.

Figure 6.14: Performance of LOLE and EENS in ELCC evaluation calculated with MCS for the RTS at HLII.

load as before. Figure 6.15 shows the results for the RBTS. EENS is used as reliability index in these ELCC calculations since the LOLE index is found to have a step-wise curve. Similarly, Figure 6.17 shows the results for the RTS. The amount of DSR resources is increased until a flat profile is obtained for the highest peak load, i.e. the peak and valley are at the same level for these high demand days. This corresponds to about 75% load shifting.

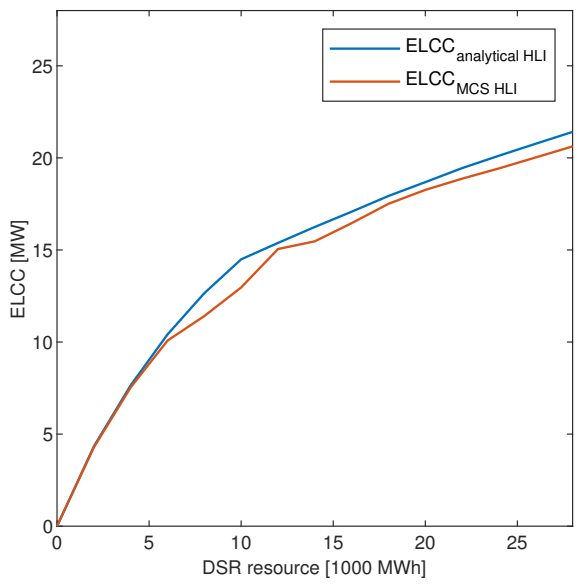

(a) ELCC at HLI calculated with analytical method and MCS.

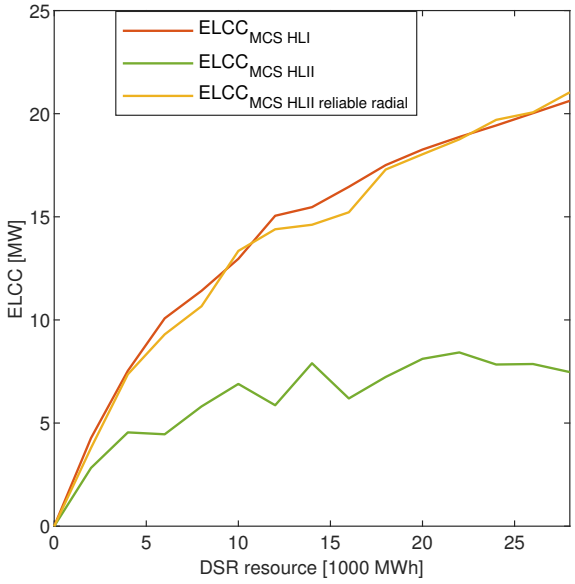

(b) ELCC at HLI and HLII calculated with MCS.

Figure 6.15: ELCC for the RBTS with increasing amount of demand side resources.

It can be observed from Figure 6.15a that the ELCC values for increasing amount of DSR resources calculated by an analytical method and MCS are almost identical up to around 7000 MWh DSR resources. The analytical method estimates higher ELCC values as the amount of DSR resources increases. The reader should recall that the CV of system indices obtained with MCS is observed to increase slightly as the load shifting increases. In addition, the load increment is larger in the MCS than in the analytical method which can affect the accuracy of the results. Further, it can be observed from Figure 6.15a that the value of the ELCC is increasing more rapidly in the beginning. The slope of the curve decreases after around 10 000 MWh, meaning that having more available DSR resources than this do not contribute as much as the first 10 000 MWh in meeting additional load while maintaining the reliability level. This is due to the fact that most of the EENS occurs within a few hours of the year. Targeting these hours with load shifting will have the greatest impact on the adequacy of the system when an increase in peak load is evaluated. Thus, as the amount of DSR resources increase, the value of having this flexibility reduces because the hours that contribute most to the EENS index have already been covered. This decreasing returns to scale in capacity value for DSR resources was also found by the authors in [54]. By referring to Figure 6.16, this observation is further illustrated by showing the hours with highest EENS at HLI obtained with the analytical method for the RBTS. The plot shows both the original load curve and

load shifted curves. The effect of 90% and 80% load shifting are given to exemplify that shaving more of the peak energy reduces the contribution from the hours which constitute the highest EENS values. As an example, the top 300 hours contribute with about 60% of the total EENS value for the original system load in the RBTS. The rest of the hours throughout the year account for the remaining 40%, i.e. using extra resources to target these hours will not reduce the EENS value as much as for the top 300 hours.

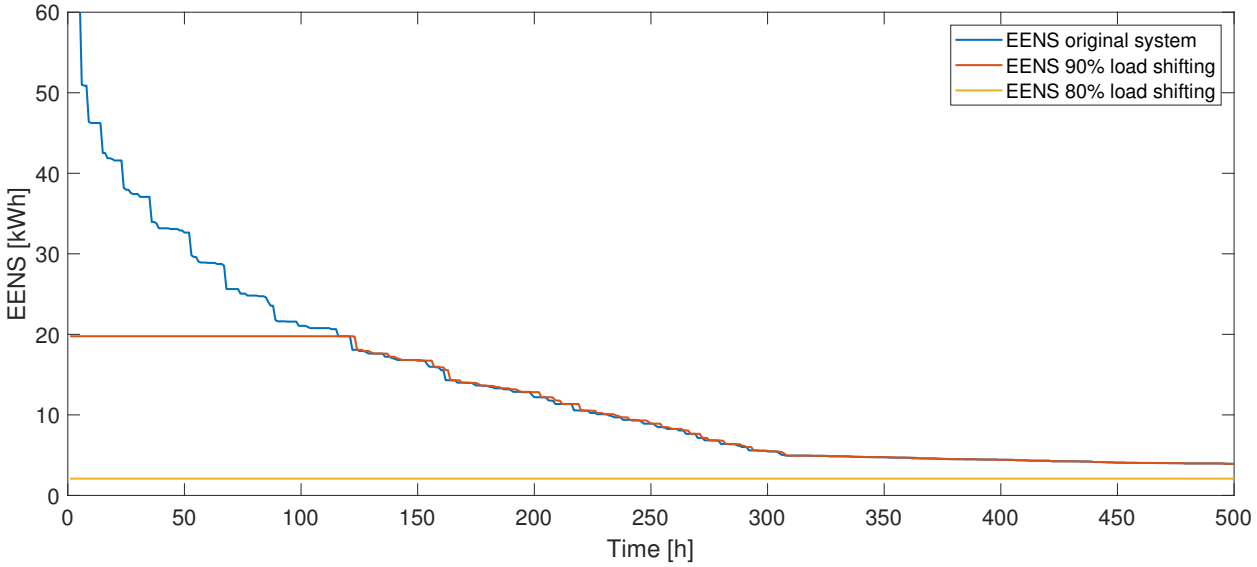

Figure 6.16: The effect of increased load shifting on the amount of EENS in each hour.

Figure 6.15b shows the ELCC for increasing amount of DSR resources at HLI and HLII for the RBTS, both calculated with MCS. As observed, the ELCC at HLII is fluctuating for the normal system. The ELCC is also calculated with a 100% reliable radial between bus 5 and bus 6 which is closer to the curve obtained for HLI. Recall from the results obtained in Section 6.6.1.1 that the radial connection between bus 5 and bus 6 is the main contribution to the system unreliability. The results from this section show that load shifting has little impact on the improvement of the system indices. Hence, this is pointed out as the main reason as to why the ELCC fluctuates for increasing amount of DSR resources at HLII for the original RBTS system.

The results for the ELCC values obtained with indices EENS and LOLE at HLI and HLII for the RTS are displayed and compared in Figure 6.17. Some observations are made from these four plots, as follows. Figure 6.17a shows that the ELCC calculated with EENS as the reliability index is higher than for the LOLE index at HLI. Figure 6.17b shows that there is less difference between the ELCC values of EENS and LOLE at HLII. Further, Figure 6.17c compares the ELCC at HLI

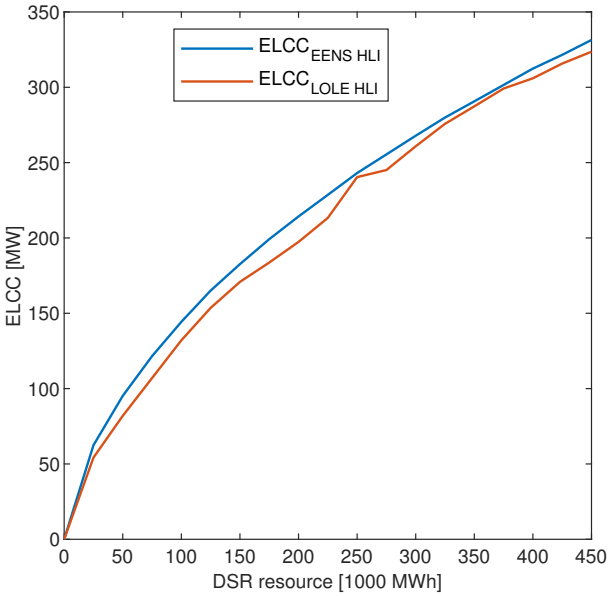

(a) ELCC at HLI with indices EENS and LOLE.

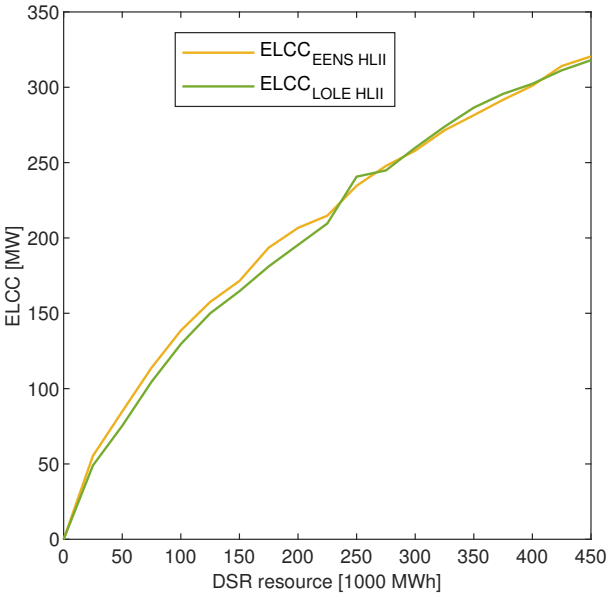

(b) ELCC at HLII with indices EENS and LOLE.

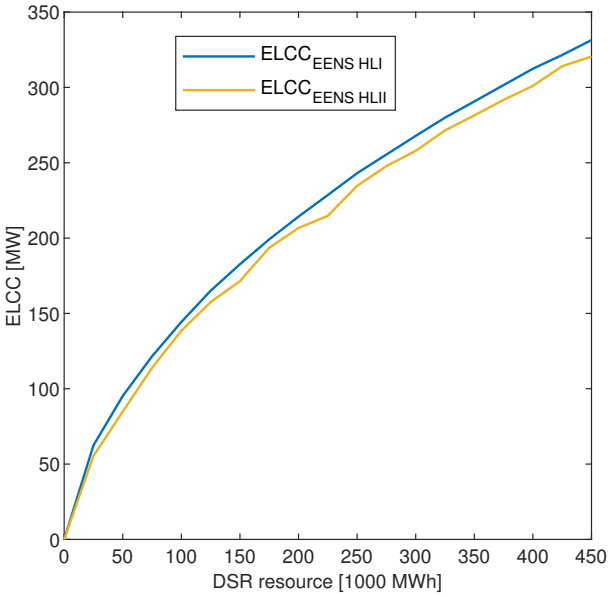

(c) ELCC at HLI and HLII with index EENS.

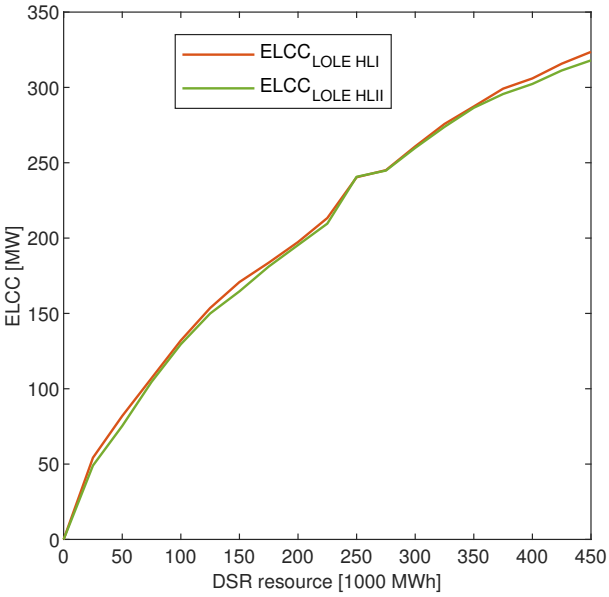

(d) ELCC at HLI and HLII with index LOLE.

Figure 6.17: ELCC for the RTS with increasing amount of demand side resources.

and HLII with EENS as reliability index, and Figure 6.17d displays the same, but with LOLE as reliability index. The two latter plots indicate that the ELCC at HLI is larger than the ELCC at HLII. This is intuitive since the transmission network is included in the HLII assessment and thus

there are more contingencies to account for. Nevertheless, the small difference between the ELCC at HLI and HLII obtained with the EENS index and especially the LOLE index support the fact that the network of the RTS is a reliable grid, and that generation outages are the cause of most load curtailments. This tendency was also found in [43]. The study in [43] calculated the ELCC for the RTS at HLII and the authors also found that the EENS index gave higher ELCC values than the ELCC when LOLE was used as reliability index. Moreover, the study in [43] calculated the ELCC for various load shifting levels, similar to the ones obtained by LSM1, including results with three different reference reliability levels. As pointed out by the authors, the reference level chosen in the ELCC procedure affects the results. However, large differences between the ELCC values calculated with EENS and LOLE at a given load shifting level were not found in the study, but it was highlighted that larger differences could occur at other reference levels. Thus, the reader should bear in mind that the results obtained in Figure 6.15 and Figure 6.17 are only valid for the particular reference level chosen. Lastly, compared to the curves obtained for the RBTS, the same decreasing returns to scale is not that evident for the amounts evaluated in Figure 6.17. The calculations are stopped when the load profile reaches a flat profile for the highest peak loads. This is also done for the results obtained in Figure 6.15 for the RBTS. The results indicate that the RTS reaches a decreasing effect in ELCC later than the RBTS when the reference reliability level is obtained at the original YPL for the system.

This section ends with a short notice of the simplifications and limitations that need to be put forward. It should be highlighted again that LSM2 for load shifting is utilized in all the ELCC calculations, and as discussed earlier this is a model that provides optimistic estimates. In addition, the results at HLII are obtained with a DC model. Hence, transmission losses and voltage constraints are not accounted for. As reviewed in the HLII assessment, these additional constraints would increase the index values. Thus, using an AC OPF would most likely give a greater difference between the ELCC obtained at HLII compared to HLI. The reader can also bear in mind that the HLII assessment showed that the EENS index is less sensitive to the DC assumptions for increased load shifting compared to the LOLE index. Thus, EENS can be a better choice as the reliability index in the ELCC procedure when a DC model is used.

6.7.3 ELCC for Demand Side Response Applied at Different Buses

The ELCC for DSR applied at the load buses in the RTS is investigated. Load shifting is carried out at one bus while the other buses have their normal load profile. The results are displayed in

Table 6.22. An amount of 8900 MWh energy available for load shifting is applied at the bus. System indices are calculated and the corresponding ELCCs are found. Only system indices are evaluated because the precision of the estimates of bus indices is lower. In addition, the load curtailment philosophy is a dominating factor for the values of the bus indices, and load shifting is shown to lead to most visible improvement of the buses with lowest curtailment costs. Carrying out load shifting on a particular bus might not improve the indices at that bus, but at other buses in the system. Hence, it is found convenient to analyze the potential improvement on the system reliability. It can be noted that an amount of 8900 MWh corresponds to about 75% load shifting at the smallest bus load in the system which is 2.5% of the system load, and between 85-80% load shifting at the largest bus loads which are about 10% of the system load. The results in Table 6.22 are given in ascending order with respect to the share of system load.

Table 6.22: ELCC for an amount of 8900 MWh DSR available for load shifting at different buses in the RTS.

Bus	Share of system load	$ELCC_{LOLE}$ [MW]	$ELCC_{EENS}$ [MW]
5	0.025	9.3264	6.7993
4	0.026	2.7438	6.1528
2	0.034	2.9312	5.4686
16	0.035	1.3661	5.7025
1	0.038	6.6864	8.7943
7	0.044	9.9072	9.9453
20	0.045	6.7489	6.8696
6	0.048	9.8440	6.0927
8	0.06	8.9808	8.3736
9	0.061	10.1700	8.8045
3	0.063	9.2988	9.0170
19	0.064	7.1304	5.0544
10	0.068	7.6956	9.8265
14	0.068	11.3710	13.5681
13	0.093	11.9298	14.7321
15	0.111	14.8579	17.2399
18	0.117	14.6240	15.2810

It can be observed from Table 6.22 that the ELCC values are differing for buses with similar share

of load. For example, buses 10 and 14, which are both 6.8% of the system load have different ELCC values. The $ELCC_{LOLE}$ is fluctuating more as the share of load increases, while the $ELCC_{EENS}$ is showing a tendency towards increasing value as the share of load increases. However, this is not consistent for all cases. For instance, bus 7 has an $ELCC_{EENS}$ higher than bus 19 although it has 30% lower share of the system load. Buses with largest share of load in the system, buses 13, 15, and 18, have the highest ELCC values. This is intuitive since the amount of energy shifted at these buses contributes to lower the system peak more than if the same amount is applied at a bus with smaller share of load. For example, when 8900 MWh is shifted at bus 18 it yields a system peak load of 2793 MW, while if the same amount is applied at bus 5, it only reduces the system peak load to 2832 MW.

The variations of ELCC values among the buses can be due to several reasons. This can be network topology, transmission constraints, load curtailment philosophy, etc. It can be hard to observe any distinct trends. However, buses that have fewer connections to the rest of the network appear to get higher ELCC values despite lower share of load. For example, bus 7 is the only radial connection, and buses 5 and 6 have only two connections to other buses. Reasons for this can be that with increasing peak load demand, the transmission lines to/from these buses will be more heavily loaded. An outage of one of the lines connected to bus 5 and bus 6 can be critical. Hence, shifting load at the bus can relieve some transfer capacity. Further, the results obtained in the HLII assessment reveal that the bus indices at bus 7 do not change much with increasing load shifting. However, bus 7 has three generating units connected to the bus and can produce 300 MW. More of the produced energy at this bus can be transferred to the rest of the system when the peak load at the bus is reduced. Again, it should be noted that the observations made from Table 6.22 can change for another reliability reference level or another amount of DSR resources.

Despite the various reasons for the different ELCC values, the results in Table 6.22 show that the same amount of shifted energy in a yearly load profile can have dissimilar value in terms of ELCC at different locations in a network. Thus, the ELCC approach given in this thesis can be extended to a more sophisticated optimization problem, where the goal can be to allocate DSR resources at a combination of buses that would be most beneficial for maintaining the adequacy in a system with increasing load demand.

Chapter 7

Conclusions and Future Work

7.1 Conclusions

The aim of this thesis is to incorporate DSR in power system adequacy assessment. This is found interesting due to several reasons. Firstly, increased amount of intermittent renewable resources, phase-out of flexible coal and gas power plants, in addition to a changing energy demand at the consumer side with increased use of power demanding appliances, challenge the adequacy of supply and point towards a power system that can experience a rising scarcity of flexibility. Secondly, new technology such as smart meters, smart house technology and upcoming market solutions can enable consumers to offer DSR resources that can improve the adequacy of the system.

Two methods for load shifting are implemented in this thesis, referred to as LSM1 and LSM2. LSM1 is based on a model found in literature which has a load recovery procedure that can create spikes in the load profile for greater amount of shifted load. Such spikes can illustrate rebound effects that can appear when inertial or storable loads are being reconnected after a disconnection period. Thus, a modified version of LSM1, named LSM2 is created. In LSM2, a uniformly distributed load level in the valleys is proposed. The main objective by implementing LSM2 in addition to LSM1 is to investigate how the different valley filling procedures of the two methods affect the adequacy. LSM1 and LSM2 are effective from a centralized authority's point of view. However, in a deregulated power system, DSR can be achieved with active participation of consumers responding to price signals. A RTP model is implemented based on literature of consumer modelling through price elasticity matrices and nodal price calculation by OPF. Further, a method to calculate the ELCC of DSR

resources at HLI and HLII is presented. Few sources in literature deal with this concept for DSR resources that are used for load shifting. Existing software that calculates the ELCC at HLI for other types of resources like additional generating units or interconnector capacity is extended to handle DSR resources available for load shifting for both HLI and HLII evaluations. Changes are made to LSM2 which allows the user of the software to specify the available amount of MWh of energy that can be used for load shifting at system or bus loads in the ELCC calculations. The HLI and HLII assessment, and ELCC calculations are performed on two standard test systems, the RBTS and the RTS.

The results for the HLI assessment performed on the RBTS show that load shifting, accomplished by peak clipping and valley filling, have a positive influence on the adequacy indices. As the load shifting percentage increases, the LOLE and EENS values decrease. It is found that shaving the peak hours increases the adequacy of the system, while valley filling does not significantly contribute to lower the system adequacy. The results obtained with LSM1 and LSM2 do in general not differ much. However, at higher load shifting percentages it is observed that LSM2 gives recognizably lower values than LSM1. This is a result of the different valley filling procedures of the two methods. It is highlighted that LSM2 represents an ideal and optimal case, while LSM1 can give effects similar to rebound or cold load pick-up characteristics that can occur when loads are reconnected after a disconnection period. The results indicate that such power spikes are negative for the adequacy when the load is aggregated. The results obtained with MCS are similar to the indices obtained with the analytical method, and this indicates that the simulation methods perform satisfactorily at HLI. The results obtained with the state sampling and the state transition method prove to be similar since there are no time dependencies included in the analysis.

The results for the HLII assessment reveal that including the transmission grid in the analysis increases the system indices of both test systems. Further, the radial connection of the smaller RBTS network is dominating the unreliability of the system. Performing load shifting does not improve the bus or system indices noticeably. This is changed when the radial connection is made 100% reliable. The results obtained for the larger RTS network are not affected much by the reliability of the radial connection in this network, but bus indices of radial connections and less connected buses do not improve noticeably with increased load shifting percentage. Moreover, for both systems it is noted that buses with lower curtailment costs appear with higher values of LOLE and EENS since such buses are the first choice when load needs to be curtailed. For the RTS, load shifting is observed to improve the system indices, and especially the indices of buses with lower

curtailment costs. Further, the indices obtained with a DC OPF are lower than the indices obtained with an AC OPF. This is because the AC OPF formulation accounts for transmission losses and voltage constraints. It is also found that the LOLE index is more sensitive to the DC assumptions compared to the EENS index, and this sensitivity becomes more noticeable for increased load shifting percentages. Furthermore, for the RTS it is noted that buses that are particularly affected by the AC OPF constraints observe none or less improvement with increased load shifting. This can be due to load curtailments to fulfill voltage constraints.

The RTP model is used for the RTS with two different outage cases to trigger higher nodal prices. The first case is a generator of 155 MW on outage on bus 23 and the second is an outage of a generator of 350 MW on the same bus. The latter introduces larger price differences and more price spikes in high demand periods. The results reveal that the latter case leads to lower indices. Furthermore, the same buses with higher index values for LSM1 and LSM2 are also found to have higher index values for the RTP model. It is observed that varying nodal prices are not changing the buses that account for most of the curtailed load for the two cases evaluated in the assessment. This could have changed with another curtailment philosophy, e.g. shed the loads that are closest to the fault location. Evaluating another outage case could also have given other results, e.g. including outages of transmission lines that would affect some buses extra hard. Further, the effect of changing elasticity coefficients is investigated for the largest outage case. It is found that increasing elasticity coefficients lowers the system and bus indices to a certain point. At a self-elasticity coefficient equal to -0.4, load spikes are introduced, and the indices increases compared to the results obtained with a self-elasticity coefficient equal to -0.3. It is pointed out that these spikes can be reduced if there is a dynamic interaction between price and demand. Moreover, it is highlighted that a more realistic implementation of the RTP model can be to update nodal prices every study period such that the prices reflect the current system state. In addition, a main shortcoming with the load model used in this thesis is that all load profiles are equal. Equal PEM structures and elasticity coefficients give aggregated effects because of identical rescheduling strategy and load response pattern for all buses.

The results for the ELCC calculations show that the LOLE index give a step-wise curve, while the EENS index give a smoother curve for the RBTS. This behavior is not found for the larger RTS network. The step-wise cuve of the LOLE index can be due to the smaller system size and simpler system configuration of the RBTS. Indications for this are found from the analytical method due to a grouping of states for the cumulative probabilities used to calculate the LOLE index for

the RBTS at HLI. Nevertheless, any unique answer to this observation cannot be authoritatively stated. Only the EENS index is used in the further analysis for the RBTS. The results reveal a decreasing returns to scale for the RBTS in case of increasing amount of DSR resources at HLI. The established explanation for this is that as the amount of DSR resources increases the value of this flexibility becomes reduced because the hours that contribute most to the EENS index are already covered. At HLII, the ELCC is found to fluctuate for increasing amounts of DSR resources for the RBTS. The fluctuating effect is not present if the radial line between bus 5 and bus 6 is made 100% reliable. This is consistent with the results obtained in the HLII assessment which show that this radial connection is dominating the system unreliability. Moreover, it is found that there is little difference in the development of the ELCC at HLI and HLII for the RTS. This supports the fact that the RTS has a reliable grid, and that most contingencies are generator outages. Also, only DC OPF is used in the ELCC calculations. Using an AC OPF model could increase the difference. Further, it is found that when EENS is used as reliability index this yields higher ELCC values than when LOLE is used. This difference is not large and decreases at HLII compared to HLI. It is highlighted that all the ELCC results and observed tendencies can change with another reference reliability level than the original level used in the case study.

Lastly, the ELCC for a fixed amount of DSR on each bus in the RTS is evaluated. The results show that the ELCC is varying among the buses. The three buses with largest share of load have higher ELCC values. For the other buses there are not observed any particular trends, although it appears that less connected buses obtain higher ELCC values compared to buses with similar or higher share of load that are better connected. This can be because the transmission lines to/from these buses are more heavily loaded when the load demand increases. Despite the various possible reasons for the different ELCC values, a main point worth observing is that the values are unequal, indicating that the same amount of shifted energy in a yearly load profile can have dissimilar value in terms of ELCC at different locations in a network.

7.2 Future Work

There are several recommendations for future work based on the methodological approach and the case study presented in this thesis. One of the main shortcomings with the case study is that equal load profiles are used for all loads, in addition to equal PEMs for the RTP model. This gives aggregated effects which do not corresponds to a real-life scenario. Dividing the load among different

load sectors will give a more realistic case study. The PEMs should also reflect the consumer, e.g. there are differences in the ability of the residential, commercial and industry sectors to shift load. Utilizing real load data and spot prices can also be an option. A flaw with the nodal prices used in the case study is that the outage simulated for all hours causes a price difference in most hours in the yearly profile. Using real spot prices can give a more realistic distribution of price differences. Another aspect that is not considered in this thesis is load forecast uncertainty, which is an important consideration in long term planning. Including how load forecast uncertainty will affect the results obtained with DSR models can be a relevant extension to the analysis.

Little attention is paid to the technical issues with load shifting in this thesis. Not all loads are suited to be shifted. In relation to this, availability, response time and duration constraints of shiftable loads can be interesting to include. Detailed modelling of rebound effects and cold load pick-up characteristics can be valuable to investigate further. Moreover, battery storage can be seen as a useful and perhaps necessary complement to realize load shifting. Thus, investigating DSR with battery storage facilities can be a relevant topic for further research.

Changing load curtailment philosophy in the contingency solvers can also be worth highlighting. The current models use individual curtailment costs which lead to some buses having higher index values in all the cases. It can be interesting to explore different philosophies. As mentioned, one relevant curtailment philosophy can be to shed load closest to the fault location. Bus indices will in this way better reflect which buses that are more or less reliable based on component FORs and system topology, and the effect of DSR can become more evident at these buses.

The RTP model can be made more realistic by letting nodal prices be updated in every study period to reflect the current system state. The RTP model can also be extended to a market model including demand side bidding with modeling of consumer benefit. The price calculation should then be conducted in an iterative procedure. Furthermore, the possible impact of a peak demand tariff can be interesting to investigate. This can capture both the increased incentives to reduce peak demand, but also possible negative economic consequences of rebound effects.

The ELCC procedure only utilizes LSM2 which is an optimistic model. Extending the ELCC procedure to include the RTP model can be a natural next step. The ELCC procedure can also benefit from being utilized with sector load curves or real load data. Moreover, using ELCC as a measure for finding the optimal allocation of DSR resources in a network can be another interesting topic. Moreover, this thesis focus on one capacity credit measure. The ELCC measures the amount

of load increase allowed in the presence of DSR resources while maintaining the original reliability level. Investigating and comparing other capacity credits for the evaluation of DSR in a long-term planning perspective can be useful.

Lastly, it can be put forward that improving the efficiency and the precision of the MCS tools can be valuable. The CV should be used as a convergence criteria to obtain estimates with equal precision in the simulations since it is observed that the CVs increase when the load shifting percentage increases. Development of variance reduction techniques to improve the efficiency can also be established in relation to this. Especially the ELCC procedure can benefit from shorter computation time to obtain estimates. Only the DC OPF model is used in the case study since a lot of simulations are needed to obtain an ELCC value. The AC OPF model has a too long computation time for larger systems at the current state to be used in the ELCC procedure.

Bibliography

[1] Roy Billinton and Ronald N. Allan. *Reliability Evaluation of Power Systems, 2nd Edition*. Boston, MA: Springer US, 1996.

[2] Statnett et al. *Generation Adequacy – market measures to secure it and methodology for assessment*. Tech. rep. Statnett, FINGRID, Svenska Kräftnett and Energinet, 2016. URL: http://www.statnett.no/Global/Dokumenter/Nyheter%5C%20-%5C%20vedlegg/Nyheter%5C%202017/Generation_%20Adequacy_market%5C%20measures%5C%20to%5C%20secure%5C%20it%5C%20and%5C%20methodology%5C%20for%5C%2020assessment.pdf.

[3] Anders Kringstad et al. *Fleksibilitet i det nordiske kraftmarkedet, 2018-2040*. Tech. rep. Statnett, January 2018. URL: https://www.statnett.no/globalassets/for-aktorer-i-kraftsystemet/planer-og-analyser/2018-Fleksibilitet-i-det-nordiske-kraftmarkedet-2018-2040.

[4] Goran Strbac. "Demand side management: Benefits and challenges". In: *Energy Policy* 36.12 (December 2008), pp. 4419–4426.

[5] Haakon Vennemo et al. *Flexible demand for electricity and power: Barriers and opportunities*. Tech. rep. Nordic Council of Ministers, 2017. URL: https://books.google.no/books?id=KJVGDwAAQBAJ&printsec=frontcover&hl=no&source=gbs_ge_summary_r&cad=0#v=onepage&q&f=false.

[6] Sheila Nolan et al. "A Methodology for Estimating the Capacity Value of Demand Response". In: *2014 IEEE PES General Meeting: Conference & Exposition* (July 2014). DOI: 10.1109/PESGM.2014.6939174.

[7] Kjetil Koldingsnes. "Reliability-based Derating Approach for Interconnectors". Master thesis. NTNU, June 2017.

[8] Øystein Stake Laengen. "Application of Monte Carlo Simulation to Power System Adequacy Assessment". Master thesis. NTNU, June 2018.

[9] Marta Poncela Blanco et al. *Generation Adequacy Methodologies Review*. Tech. rep. Joint Research Center, September 2016. URL: http://publications.jrc.ec.europa.eu/repository/bitstream/JRC101590/jrc101590_online_rev1_19sept2016.pdf.

[10] Marko Čepin. *Assessment of Power System Reliability, 1st Edition*. Germany: Springer Verlag, 2011.

[11] International Electrotechnical Commision. *IEC/IEV 617-01-01, electropedia*. URL: http://www.electropedia.org/iev/iev.nsf/display?openform&ievref=617-01-01.

[12] Gerd Kjølle. *State of the art on reliability assessment in power systems*. Tech. rep. SINTEF, 2014. URL: https://www.sintef.no/globalassets/project/garpur/deliverables/garpur-d1.1-state-of-the-art-on-reliability-assessment-in-power-systems.pdf.

[13] Prabha Kundur et al. "Definition and Classification of Power System Stability". In: *IEEE Transactions on Power Systems* 19.3 (August 2004), pp. 1387–1401. DOI: 10.1109/TPWRS.2004.825981.

[14] David Elmakias. *New Computational Methods in Power System Reliability*. Springer Berlin Heidelberg, 2008.

[15] ENTSOE. *ENTSO-E business glossary*. URL: https://docstore.entsoe.eu/data/data-portal/glossary/Pages/home.aspx.

[16] Jan Machowski et al. *Power System Dynamics: Stability and Control, Second Edition*. United Kingdom: John Wiley & Sons Ltd, 2012.

[17] Roy Billinton and Ronald N. Allan. "Basic Power System Reliability Concepts". In: *Reliability Engineering and System Safety* 27.3 (1990), pp. 365–384. DOI: 10.1016/0951-8320(90)90007-A.

[18] Roy Billinton and Peng Wang. "Teaching Distribution System Reliability Evaluation Using Monte Carlo Simulation". In: *IEEE Transactions on Power Systems* 14.2 (May 1999), pp. 397–403. DOI: 10.1109/59.761856.

[19] Ove Wolfgang et al. *Magasindisponering før og etter energiloven*. Tech. rep. SINTEF Energy, October 2007. URL: https://evalueringsportalen.no/evaluering/magasindisponering-for-og-etter-energiloven/magasindisponering%5C%20f%C3%B8r%5C%20og%5C%20etter%5C%20energiloven.pdf/@@inline.

[20] Mauro Augusto da Rosa. "Agent-based Technology Applied to Power Systems Reliability". PhD thesis. Faculty of Enegineering of the University of Porto, July 2009.

[21] Marvin Rausand and Arnljot Høyland. *System Reliability Theory: Models, Statistical Methods, and Applications*. Hoboken, New Jersey: Wiley-Interscience, 2004.

[22] North American Electric Reliability Corporation. *Probabilistic Adequacy and Measures*. Tech. rep. NERC, April 2018. URL: https://www.nerc.com/comm/PC/Documents/2.d_Probabilistic_Adequacy_and_Measures_Report_Final.pdf.

[23] Harry G. Stoll. *Least-Cost Electric Utility Planning*. New York: John Wiley & Sons, 1989.

[24] Roy Billinton and Wenyuan Li. *Reliability Assessments of Power Systems Using Monte Carlo Methods*. New York: Springer Science, 1994.

[25] Ronald E. Walpole et al. *Probability and Statistics for Engineers & Scientists, 9th ed.* Essex, Harlow: Pearson Education, 2016.

[26] William L. Dunn and J. Kenneth Shultis. *Exploring Monte Carlo Methods*. Amsterdam: Elsevier, 2012.

[27] Roy Billinton et al. "A Reliability Test System for Educational Purposes - Basic Data". In: *IEEE Transactions on Power Systems* 4.3 (August 1989), pp. 1238–1244. DOI: 10.1109/59.32623.

[28] P. F. Chairman et al. "IEEE Reliability Test System". In: *IEEE Transactions on Power Apparatus and Systems* PAS-98.6 (November 1979), pp. 2047–2054. DOI: 10.1109/TPAS.1979.319398.

[29] Hussein Jumma Jabir et al. "Impacts of Demand-Side Management on Electrical Power Systems: A Review". In: *Energies* 11.5 (May 2018). DOI: 10.3390/en11051050.

[30] Daniel S. Kirschen. "Demand-Side View of Electricity Markets". In: *IEEE Transactions on Power Systems* 18.2 (May 2003), pp. 520–527. DOI: 10.1109/TPWRS.2003.810692.

[31] TemaNord. *Demand side flexibility in the Nordic electricity market: From a Distribution System Operator Perspective*. Tech. rep. Nordic Council of Ministers, December 2017. URL: https://books.google.no/books?id=fv9CDwAAQBAJ&printsec=frontcover&hl=no&source=gbs_ge_summary_r&cad=0#v=onepage&q&f=false.

[32] Eric Hirst. "Reliability Benefits of Price-Responsive Demand". In: *IEEE Power Engineering Review* 22.11 (December 2002), pp. 16–21. DOI: 10.1109/MPER.2002.1045564.

[33] Eilert Bjerkan et al. *Fleksibilitet – Fremtidig organisering av monopol og marked*. Tech. rep. Enfo Consulting, May 2016. URL: https://www.energinorge.no/contentassets/e393a68f81e74426a3c510b93d942e3d/fleksibilitet--fremtidig-organisering-av-monopol-og-marked.pdf.

[34] ENTSO-E. *Market design for demand side response*. Tech. rep. ENTSO-E, November 2015. URL: https://www.entsoe.eu/2015/11/27/policy_paper_on_market_design_for_demand_side_response/.

[35] NODES. *White paper: A fully integrated marketplace for flexibility.* Tech. rep. NODES, November 2018. URL: https://nodesmarket.com/2018/11/07/document-test/.

[36] Dange Huang et al. "Effects of Demand Side Management on Bulk System Adequacy Evaluation". In: *2010 IEEE 11th International Conference on Probabilistic Methods Applied to Power Systems* (June 2010), pp. 593–598. DOI: 10.1109/PMAPS.2010.5529011.

[37] M.H Albadi and E.F. El-Saadany. "A summary of demand response in electricity markets". In: *Electric Power Systems Research* 78.11 (May 2008), pp. 1989–1996. DOI: 10.1016/j.epsr.2008.04.002.

[38] Hussein Jumma Jabir et al. "Impact of Demand-Side Management on the Reliability of Generation Systems". In: *Energies* 11.8 (August 2018). DOI: 10.3390/en11082155.

[39] Jiashen Teh et al. "Composite Reliability Evaluation of Load Demand Side Management and Dynamic Thermal Rating Systems". In: *Energies* 11.2 (February 2018), pp. 466–481. DOI: 10.3390/en11020466.

[40] Dange Huang and Roy Billinton. "Effects of Load Sector Demand Side Management Applications in Generating Capacity Adequacy Assessment". In: *IEEE Transactions on Power Systems* 27.1 (February 2012), pp. 335–343. DOI: 10.1109/TPWRS.2011.2164425.

[41] Ming Zhou et al. "Impact of Demand Side Management on Composite Generation and Transmission System Reliability". In: *2006 IEEE PES Power Systems Conference and Exposition* (November 2006), pp. 819–824. DOI: 10.1109/PSCE.2006.296421.

[42] E. M. Saied et al. "Impact of Demand-Side Management on Power System Reliability". In: *i-Manager's Journal on Electrical Engineering* 8.4 (April 2015), pp. 26–33.

[43] Dange Huang and Roy Billinton. "Impacts of Demand Side Management on Bulk System Reliability Evaluation Considering Load Forecast Uncertainty". In: *2011 IEEE Electrical Power and Energy Conference* (October 2011), pp. 272–277. DOI: 10.1109/EPEC.2011.6070210.

[44] R. Billinton and D. Lakhanpal. "Impacts of demand-side management on reliability cost/reliability worth analysis". In: *IEE Proceedings-Generation Transmission And Distribution* 143.3 (May 1996), pp. 225–231.

[45] S. Rahman and R. Rinaldy. "An Efficient Load Model for Analyzing Demand Side Management Impacts". In: *IEEE Transactions on Power Systems* 8.3 (August 1993), pp. 1219–1226. DOI: 10.1109/59.260874.

[46] A. R. Osareh et al. "An efficient approach to identify and integrate demand-side management on electric utility generation planning". In: *Electric Power Systems Research* 36.1 (August 1996), pp. 3–11. DOI: 10.1016/0378-7796(95)01010-6.

[47] A. K. David and Y. C Lee. "Dynamic Tariffs: Theory of utility-consumer interaction". In: *IEEE Transactions on Power Systems* 4.3 (August 1989), pp. 904–911. DOI: 10.1109/59.32578.

[48] A. K. David and Y. Z Li. "Effect of inter-temporal factors on the real time pricing of electricity". In: *IEEE Transactions on Power Systems* 8.1 (February 1993), pp. 44–52. DOI: 10.1109/59.221247.

[49] Daniel S. Kirchen et al. "Factoring the Elasticity of Demand in Electricity Prices". In: *IEEE Transactions on Power Systems* 15.2 (May 2000), pp. 612–617. DOI: 10.1109/59.867149.

[50] L. Goel et al. "Reliability Enhancement of A Deregulated Power System Considering Demand Response". In: *2006 IEEE Power Engineering Society General Meeting* (June 2006). DOI: 10.1109/PES.2006.1708965.

[51] L. Goel et al. "Nodal price volatility and reliability enhancement of restructured power systems considering demand-price elasticity". In: *Electric Power Systems Research* 78.10 (February 2008), pp. 1655–1663. DOI: 10.1016/j.epsr.2008.02.012.

[52] Naveen Venkatesan et al. "Market Optimization for Microgrid with Demand Response Model". In: *2011 North American Power Symposium* (August 2011). DOI: 10.1109/NAPS.2011.6025176.

[53] J. Wang et al. "A New Wholsesale Bidding Mechanism for Enhanced Demand Response In Smart Grids". In: *2010 Innovative Smart Grid Technologies (ISGT)* (January 2010). DOI: 10.1109/ISGT.2010.5434766.

[54] Robert Earle et al. "Measuring the capacity impacts of demand response". In: *Electricity Journal* 22.6 (July 2009), pp. 47–58. DOI: 10.1016/J.TEJ.2009.05.014.

[55] Simon Tindemans et al. *Resilience performance of smart distribution networks*. Tech. rep. Imperial College London, December 2014. URL: https://innovation.ukpowernetworks.co.uk/innovation/en/Projects/tier-2-projects/Low-Carbon-London-(LCL)/Project-Documents/LCL%5C%20Learning%5C%20Report%5C%20-%5C%20D4%5C%20-%5C%20Resilience%5C%20performance%5C%20of%5C%20smart%5C%20distribution%5C%20networks.pdf.

[56] Ivar Wangensteen. *Power System Economics - the Nordic Electricity Market, 2nd edition*. Norway: Fagbokforlaget, 2012.

[57] Ray D. Zimmerman et al. *MATPOWER - Free, open-source Electric Power System Simulation and Optimization Tools for MATLAB and Octave*. 2019. URL: https://www.pserc.cornell.edu/matpower/.

[58] MathWorks. *fmincon*. 2019. URL: https://se.mathworks.com/help/optim/ug/fmincon.html#busp5fq-6.

[59] N. Saker et al. "Demand Side Management of Electrical Water Heaters and Evaluation of the Cold Load Pick-Up Characteristics (CLPU)". In: *2011 IEEE Trondheim PowerTech* (June 2011), pp. 1–8. DOI: 10.1109/PTC.2011.6019312.

[60] Mardavij Roozbehani et al. "Volatility of Power Grids Under Real-Time Pricing". In: *IEEE Transactions on Power Systems* 27.4 (May 2012), pp. 1926–1940. DOI: 10.1109/TPWRS.2012.2195037.

[61] CWE MC Project. *CWE Questions & Answers*. Tech. rep. EPEX SPOT, December 2011. URL: https://www.apxgroup.com/wp-content/uploads/FAQ_-_update_121211.pdf.

[62] Hadi Saadat. *Power System Analysis, Third Edition*. USA: PSA Publishing, 2010.

Appendix A

Data for the RBTS

The RBTS is a smaller test system with 6 buses and a total number of 11 generating units. The total installed capacity is equal to 240 MW and the YPL of this system is 185 MW. As stated in [27] the main objective of the RBTS is: *"to make it sufficiently small to permit the conduct of a large number of reliability studies with reasonable solution time but sufficiently detailed to reflect the actual complexities involved in a practical reliability analysis."* Table A.1 shows the generation data for the RBTS. The associated COPT for the system is given in Table A.2. Line outage data and line parameters are provided in Table A.3 and Table A.4, respectively. The bus specifications of the system are shown in Table A.5. The information provided in the tables can also be found in [27]. Lastly, Figure A.1 displays the RBTS network configuration.

Table A.1: Generation data for the RBTS.

Unit size [MW]	Bus	Min reactive [MVAr]	Max reactive [MVAr]	FOR	Failure rate [1/year]	Repair rate [1/year]
10	1	0	7	0.020	4.0	196.0
20	1	-7	12	0.025	5.0	195.0
40	1	-15	17	0.030	6.0	194.0
40	1	-15	17	0.030	6.0	194.0
5	2	0	5	0.010	2.0	198.0
5	2	0	5	0.010	2.0	198.0
20	2	-7	12	0.015	2.4	157.6
20	2	-7	12	0.015	2.4	157.6
20	2	-7	12	0.015	2.4	157.6
20	2	-7	12	0.015	2.4	157.6
40	2	-15	17	0.020	3.0	147.0

Table A.2: COPT for the RBTS.

State j	Capacity outage x_j [MW]	Individual prob. $p(X = x_j)$	Cumulative prob. $P(X \geq x_j)$
1	0	0.81285961	1.00000000
2	5	0.01642141	0.18714039
3	10	0.01667191	0.17071898
4	15	0.00033513	0.15404707
5	20	0.07035854	0.15371194
6	25	0.00142135	0.08335340
7	30	0.00144303	0.08193205
8	35	0.00002901	0.08048902
9	40	0.06926973	0.08046001
10	45	0.00139939	0.01119028
11	50	0.00142073	0.00979090
12	55	0.00002856	0.00837017
13	60	0.00582845	0.00834161
14	65	0.00011774	0.00251316
15	70	0.00011954	0.00239541
16	75	0.00000240	0.00227587
17	80	0.00200148	0.00227347
18	85	0.00004043	0.00027199
19	90	0.00004105	0.00023155
20	95	0.00000083	0.00019050
21	100	0.00015945	0.00018968
22	105	0.00000322	0.00003023
23	110	0.00000327	0.00002701
24	115	0.00000007	0.00002374
25	120	0.00002122	0.00002367
26	125	0.00000043	0.00000245
27	130	0.00000044	0.00000202
28	135	0.00000000	0.00000158
29	140	0.00000146	0.00000157
.	.	.	.
.	.	.	.
.	.	.	.
47	230	4.48791E-16	4.57857E-16
48	235	9.02138E-18	9.06693E-18
49	240	4.55625E-20	4.55625E-20

Table A.3: Line outage data for the RBTS.

Line	From	To	Failure rate [1/year]	MTTR [hours]	FOR
1	1	3	1.5	10	0.00171
2	2	4	5.0	10	0.00568
3	1	2	4.0	10	0.00455
4	3	4	1.0	10	0.00114
5	3	5	1.0	10	0.00114
6	1	3	1.5	10	0.00171
7	2	4	5.0	10	0.00568
8	4	5	1.0	10	0.00114
9	5	6	1.0	10	0.00114

Table A.4: Line parameters for the RBTS.

Line	From	To	Resistance [pu]	Reactance [pu]	Susceptance/2 [pu]	Current rating [pu]
1	1	3	0.0342	0.18	0.0106	0.85
2	2	4	0.1140	0.60	0.0352	0.71
3	1	2	0.0912	0.48	0.0282	0.71
4	3	4	0.0228	0.12	0.0071	0.71
5	3	5	0.0228	0.12	0.0071	0.71
6	1	3	0.0342	0.18	0.0106	0.85
7	2	4	0.1140	0.60	0.0352	0.71
8	4	5	0.0228	0.12	0.0071	0.71
9	5	6	0.0228	0.12	0.0071	0.71

Table A.5: Bus specifications for the RBTS.

Bus	Share of system load	Min voltage [pu]	Max voltage [pu]	Curtailment cost [$/kWh]
1	0	0.97	1.05	0
2	0.1081	0.97	1.05	9.6325
3	0.4595	0.97	1.05	4.3769
4	0.2162	0.97	1.05	8.0267
5	0.1081	0.97	1.05	8.6323
6	0.1081	0.97	1.05	5.5132

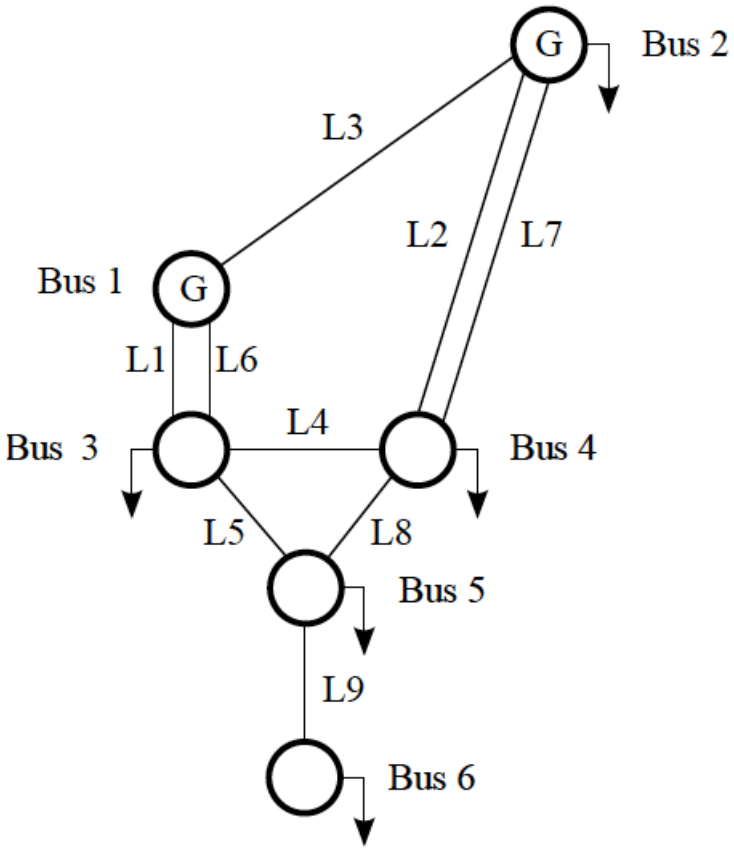

Figure A.1: The RBTS network, taken from [8].

Appendix B

Data for the RTS

The RTS is the most frequently used test system for reliability assessment. It consists of 24 buses, 32 generators, has a total installed capacity of 3405 MW and a YPL of 2850 MW [28]. Table B.1 shows the generation data for the RTS. Line outage data is provided in Table B.2 and Table B.3. Line parameters are given in Table B.4 and Table B.5. The bus specifications of the system are shown in Table B.6. The column named 'Number' in this table provides the new numbering order when bus 13 is made as slack bus. Furthermore, Figure B.1 displays the network configuration for the RTS. The information provided in this appendix can also be found in [28]. The production cost coefficients of generating buses shown in Table B.6 are not found in [28], but are chosen similar to coefficients provided in [56]. These coefficients are only used for calculation of nodal prices.

Table B.1: Generation data for the RTS.

Unit size [MW]	Bus	Min reactive [MVAr]	Max reactive [MVAr]	FOR	MTTF [hours]	MTTR [hours]
12	15	0	6	0.02	2940	60
12	15	0	6	0.02	2940	60
12	15	0	6	0.02	2940	60
12	15	0	6	0.02	2940	60
12	15	0	6	0.02	2940	60
20	1	0	10	0.10	450	50
20	1	0	10	0.10	450	50
20	2	0	10	0.10	450	50
20	2	0	10	0.10	450	50
50	22	-10	16	0.01	1980	20
50	22	-10	16	0.01	1980	20
50	22	-10	16	0.01	1980	20
50	22	-10	16	0.01	1980	20
50	22	-10	16	0.01	1980	20
50	22	-10	16	0.01	1980	20
76	1	-25	30	0.02	1960	40
76	1	-25	30	0.02	1960	40
76	2	-25	30	0.02	1960	40
76	2	-25	30	0.02	1960	40
100	7	0	60	0.04	1200	50
100	7	0	60	0.04	1200	50
100	7	0	60	0.04	1200	50
155	15	-50	80	0.04	960	40
155	16	-50	80	0.04	960	40
155	23	-50	80	0.04	960	40
155	23	-50	80	0.04	960	40
197	13	0	80	0.05	950	50
197	13	0	80	0.05	950	50
197	13	0	80	0.05	950	50
350	23	-25	150	0.08	1150	100
400	18	-50	200	0.12	1100	150
400	21	-50	200	0.12	1100	150
0	14	-50	200	0	-	-
0	6	-100	0	0	-	-

Table B.2: Line outage data for the RTS (line 1-18).

Line	From	To	FOR	Failure rate [1/year]	MTTR [hours]
1	1	2	0.000438164	0.24	16
2	1	3	0.000581853	0.51	10
3	1	5	0.000376570	0.33	10
4	2	4	0.000445007	0.39	10
5	2	6	0.000547645	0.48	10
6	3	9	0.000433602	0.38	10
7	3	24	0.001750356	0.02	768
8	4	9	0.000410790	0.36	10
9	5	10	0.000387977	0.34	10
10	6	10	0.001316757	0.33	35
11	7	8	0.000342349	0.30	10
12	8	9	0.000502031	0.44	10
13	8	10	0.000502031	0.44	10
14	9	11	0.001750356	0.02	768
15	9	12	0.001750356	0.02	768
16	10	11	0.001750356	0.02	768
17	10	12	0.001750356	0.02	768
18	11	13	0.000502031	0.40	11

Table B.3: Line outage data for the RTS (line 19-38).

Line	From	To	FOR	Failure rate [1/year]	MTTR [hours]
19	11	14	0.000489486	0.39	11
20	12	13	0.000502031	0.40	11
21	12	23	0.000652542	0.52	11
22	13	23	0.000614918	0.49	11
23	14	16	0.000476941	0.38	11
24	15	16	0.000414212	0.33	11
25	15	21	0.000514575	0.41	11
26	15	21	0.000514575	0.41	11
27	15	24	0.000514575	0.41	11
28	16	17	0.000439305	0.35	11
29	16	19	0.000426758	0.34	11
30	17	18	0.000401665	0.32	11
31	17	22	0.000677623	0.54	11
32	18	21	0.000439305	0.35	11
33	18	21	0.000439305	0.35	11
34	19	20	0.000476941	0.38	11
35	19	20	0.000476941	0.38	11
36	20	23	0.000426758	0.34	11
37	20	23	0.000426758	0.34	11
38	21	22	0.000564749	0.45	11

Table B.4: Line parameters for the RTS (line 1-18).

Line	From	To	Resistance [pu]	Reactance [pu]	Susceptance/2 [pu]	Current rating [pu]
1	1	2	0.0026	0.0139	0.23055	1.93
2	1	3	0.0546	0.2112	0.0286	2.08
3	1	5	0.0218	0.0845	0.01145	2.08
4	2	4	0.0328	0.1267	0.01715	2.08
5	2	6	0.0497	0.1920	0.0260	2.08
6	3	9	0.0308	0.1190	0.0161	2.08
7	3	24	0.0023	0.0839	0	5.1
8	4	9	0.0268	0.1037	0.01405	2.08
9	5	10	0.0228	0.0883	0.01195	2.08
10	6	10	0.0139	0.0605	1.2295	1.93
11	7	8	0.0159	0.0614	0.0083	2.08
12	8	9	0.0427	0.1651	0.02235	2.08
13	8	10	0.0427	0.1651	0.02235	2.08
14	9	11	0.0023	0.0839	0	5.1
15	9	12	0.0023	0.0839	0	5.1
16	10	11	0.0023	0.0839	0	5.1
17	10	12	0.0023	0.0839	0	5.1
18	11	13	0.0061	0.0476	0.04995	6

Table B.5: Line parameters for the RTS (line19-38).

Line	From	To	Resistance [pu]	Reactance [pu]	Susceptance/2 [pu]	Current rating [pu]
19	11	14	0.0054	0.0418	0.04395	6
20	12	13	0.0061	0.0476	0.04995	6
21	12	23	0.0124	0.0966	0.1015	6
22	13	23	0.0111	0.0865	0.0909	6
23	14	16	0.0050	0.0389	0.0409	6
24	15	16	0.0022	0.0173	0.0182	6
25	15	21	0.0063	0.0490	0.0515	6
26	15	21	0.0063	0.0490	0.0515	6
27	15	24	0.0067	0.0519	0.05455	6
28	16	17	0.0033	0.0259	0.02725	6
29	16	19	0.0030	0.0231	0.02425	6
30	17	18	0.0018	0.0144	0.01515	6
31	17	22	0.0135	0.1053	0.1106	6
32	18	21	0.0033	0.0259	0.02725	6
33	18	21	0.0033	0.0259	0.02725	6
34	19	20	0.0051	0.0396	0.04165	6
35	19	20	0.0051	0.0396	0.04165	6
36	20	23	0.0028	0.0216	0.02275	6
37	20	23	0.0028	0.0216	0.02275	6
38	21	22	0.0087	0.0678	0.0712	6

Table B.6: Bus specifications for the RTS.

Bus	Share of system load	Min voltage [pu]	Max voltage [pu]	Curtailment cost [$/kWh]	b-coefficient [$/MWh]	c-coefficient [$/MWh^2]	Number
1	0.038	0.95	1.05	8.9815	12	0.5	13
2	0.034	0.95	1.05	7.3606	50	0.8	12
3	0.063	0.95	1.05	5.8990	0	0	11
4	0.026	0.95	1.05	9.5992	0	0	10
5	0.025	0.95	1.05	9.2323	0	0	9
6	0.048	0.95	1.05	6.5238	0	0	8
7	0.044	0.95	1.05	7.0291	30	0.6	7
8	0.06	0.95	1.05	7.7742	0	0	6
9	0.061	0.95	1.05	3.6623	0	0	5
10	0.068	0.95	1.05	5.1940	0	0	4
11	0	0.95	1.05	0	0	0	3
12	0	0.95	1.05	0	0	0	2
13	0.093	0.95	1.05	7.2813	10	0.4	1
14	0.068	0.95	1.05	4.3717	0	0	20
15	0.111	0.95	1.05	5.9744	14	0.5	18
16	0.035	0.95	1.05	7.2305	16	0.6	17
17	0	0.95	1.05	0	0	0	21
18	0.117	0.95	1.05	5.6149	25	0.6	22
19	0.064	0.95	1.05	4.5430	0	0	16
20	0.045	0.95	1.05	5.6836	0	0	15
21	0	0.95	1.05	0	40	0.7	23
22	0	0.95	1.05	0	21.5	0.8	24
23	0	0.95	1.05	0	13	0.4	14
24	0	0.95	1.05	0	0	0	19

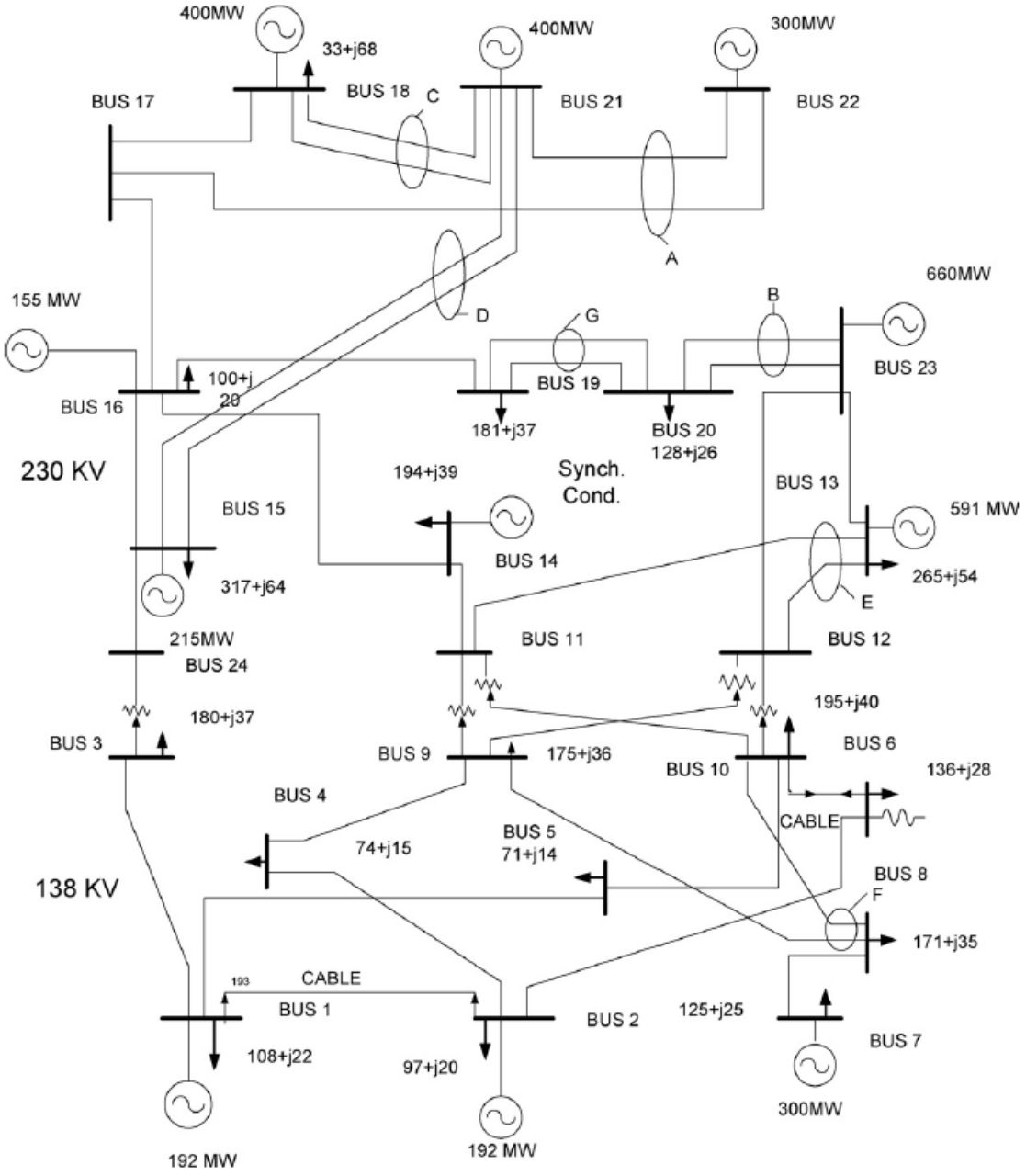

Figure B.1: The RTS network, taken from [51].

Appendix C

Load Data for the Test Systems

Table C.1: Weekly load data.

Week w	WPL [% of YPL]	Week w	WPL [% of YPL]	Week w	WPL [% of YPL]	Week w	WPL [% of YPL]
1	86.2	14	75.0	27	75.5	40	72.4
2	90.0	15	72.1	28	81.6	41	74.3
3	87.8	16	80.0	29	80.1	42	74.4
4	83.4	17	75.4	30	88.0	43	80.0
5	88.0	18	83.7	31	72.2	44	88.1
6	84.1	19	87.0	32	77.6	45	88.5
7	83.2	20	88.0	33	80.0	46	90.9
8	80.6	21	85.6	34	72.9	47	94.0
9	74.0	22	81.1	35	72.6	48	89.0
10	73.7	23	90.0	36	70.5	49	94.2
11	71.5	24	88.7	37	78.0	50	97.0
12	72.7	25	89.6	38	69.5	51	100.0
13	70.4	26	86.1	39	72.4	52	95.2

Table C.2: Daily load data.

Day d	DPL [% of WPL]
1	93
2	100
3	98
4	96
5	94
6	77
7	75

Table C.3: Hourly load data.

	Winter weeks 1-8 & 44-52		Summer weeks 18-30		Spring/fall weeks 9-17 & 31-43	
Hour h	Weekday [% of DPL]	Weekend [% of DPL]	Weekday [% of DPL]	Weekend [% of DPL]	Weekday [% of DPL]	Weekend [% of DPL]
1	67	78	64	74	63	75
2	63	72	60	70	62	73
3	60	68	58	66	60	69
4	59	66	56	65	58	66
5	59	64	56	64	59	65
6	60	65	58	62	65	65
7	74	66	64	62	72	68
8	86	70	76	66	83	74
9	95	80	87	81	95	83
10	96	88	95	86	99	89
11	96	90	99	91	100	92
12	95	91	100	93	99	94
13	95	90	99	93	93	91
14	95	88	100	92	92	90
15	93	87	100	91	90	90
16	94	87	97	91	88	86
17	99	91	96	92	90	85
18	100	100	96	94	92	88
19	100	99	93	95	96	92
20	96	97	92	95	98	100
21	91	94	92	100	96	97
22	83	92	93	93	90	95
23	73	87	87	88	80	90
24	63	81	72	80	70	85

Appendix D

DC Optimal Power Flow Model

A DC power flow formulation only considers the active power flow. With respect to an OPF formulation, the main advantage is that the power flow equations simplifies to a linear description. Four assumptions are made for the DC model [8]:

1. Active power losses are relatively low, which implies that line reactances are much larger than line resistances: $x_{ij} >> r_{ij}$. Thus, the admittance of a line is only represented by its susceptance: $y_{ij} = \frac{1}{jx_{ij}} = -b_{ij}$.

2. Magnitude of the bus voltages is set to a flat voltage profile, i.e. $|V_i| = 1.0$ pu.

3. Voltage angle differences between buses are expected to be small, yielding that the sine and cosine terms in the active power flow equation simplifies to $sin\delta_{ij} \approx \delta_{ij}$ and $cos\delta_{ij} \approx 1$.

4. Susceptances to earth are neglected for all lines.

Taking these assumptions into account, the active power flow equations can be simplified to the formula shown in Equation D.0.1.

$$P_i = P_{Gi} - P_{Di} = \sum_{j=1}^{k} B_{ij}\delta_{ij} \tag{D.0.1}$$

where P_i is the net injection of active power at bus i, δ_{ij} is the voltage angle difference between two buses $(\delta_i - \delta_j)$ and B_{ij} is the imaginary part of Y_{ij}. B_{ij} is the element in row i and column j in the

admittance matrix, Y_{Bus}, of the network. The voltage angles must be expressed in radians.

The active power flow on the line between bus i and bus j can be described by the difference in bus voltage angles divided by the reactance of the line, X_{ij}, as given in Equation D.0.2.

$$P_{ij} = \frac{\delta_i - \delta_j}{X_{ij}} \tag{D.0.2}$$

With these power flow equations given, the DC OPF formulation can be formulated as shown in Equations D.0.3-D.0.7.

$$\text{Min f} = [W] \cdot [X] \tag{D.0.3}$$

$$[K] \cdot [X] = \sum_{i=1}^{k} P_{load,i} \tag{D.0.4}$$

$$|[A] \cdot [P]| \leq [T_{lim}] \tag{D.0.5}$$

$$0 \leq P_{gi} \leq P_{cap,i} \tag{D.0.6}$$

$$0 \leq C_i \leq P_{load,i} \tag{D.0.7}$$

An explanation of the model is given below:

1. Equation D.0.3 is the objective function stating that the goal is to minimize the cost of corrective actions. [W] is the vector containing the cost of the possible post-contingency actions. If the system consists of k buses, the amount of possible actions will be 2k. The first k elements are the cost of rescheduling generation at each bus and the next k elements are the cost of load curtailment at each bus. Thus $[W] = [w_1\ w_2\ ...\ w_{2k}]$. Since the cost of rescheduling is set to zero, the objective is indeed to minimize the cost of load curtailments. The [X] vector is the vector of decision variables and it is ordered with the first k elements giving the generation at the buses, and the next k elements representing the load curtailments at the buses, $[X] = [P_{gi}\ ...\ P_{gk}\ C_1\ ...\ C_k]^T$.

2. Equation D.0.4 gives the power balance requirement. [K] is a row vector with 2k elements, which all are ones. $[K] \cdot [X]$ expresses the sum of all generation and load curtailments. Thus, Equation D.0.4 indicates that the sum of generation and load curtailment must equal the load requirement, i.e. there must be a power balance in the system at all times.

3. Equation D.0.5 is the constraint giving the power flow limit of the lines, where $[T_{lim}]$ is a vector containing the power flow limits of all lines. [A] is a matrix referred to as a sensitivity matrix or a matrix of power transfer distribution factors (PTDF)[1]. [P] is a vector of net injected active power at each bus. The formulation in Equation D.0.5 is derived using the equations for the DC power flow and the active power flow on a line.

4. Equation D.0.6 says that the generation at a bus, P_{gi}, can not exceed the generating capacity of that bus, $P_{cap,i}$, neither can the generation at a bus be negative.

5. Equation D.0.7 is the constraint describing that the load curtailment, C_i, at a bus can not exceed the load requirement at that bus, $P_{load,i}$. Also, the load curtailment at a bus can not be negative.

[1] A PTDF represents the change in flow on a line for changed node injection at a specific bus [61]. This indicates that the power flow on a certain line can be expressed by the sum of net power injections multiplied by the corresponding PTDFs.

Appendix E

AC Optimal Power Flow Model

The AC model presented in [8] is a bus injection model, using bus voltage phasors and bus current injections to calculate the active and reactive power injections at each bus. The transmission lines are represented by their π-equivalent. Furthermore, the admittance matrix of the network, Y_{Bus}, is separated into its real and imaginary parts, yielding a conductance matrix, G_{Bus}, and a susceptance matrix, B_{Bus}. The power flow equations for active and reactive power can then be formulated as in Equation E.0.1 and Equation E.0.2, respectively. In these formulations, voltage phasors are expressed in polar coordinates and the bus admittance matrix elements are given in rectangular coordinates. The derivation of the power flow equations can be found in textbooks for power system analysis, e.g. [62].

$$P_i(V,\delta) = V_i \cdot \sum_{j=1}^{k} V_j \cdot [G_{ij} \cdot cos(\delta_i - \delta_j) + B_{ij} \cdot sin(\delta_i - \delta_j)] \tag{E.0.1}$$

$$Q_i(V,\delta) = V_i \cdot \sum_{j=1}^{k} V_j \cdot [G_{ij} \cdot sin(\delta_i - \delta_j) - B_{ij} \cdot cos(\delta_i - \delta_j)] \tag{E.0.2}$$

The OPF formulation for the AC model is formulated as given in Equation E.0.3-E.0.13. The reader should note that all quantities must be given in per unit, and angles must be specified in radians in this formulation. It should also be clarified that some of the constraints in the model are rewritten in a format that suits better for the non-linear solver used in the software. The reader is referred

to see [8] for more details. Nevertheless, the constraints express the same as the ones displayed in the AC model below.

$$\text{Min f} = [X] \cdot [W] \tag{E.0.3}$$

$$P_{gi} + C_{Pi} - P_{load,i} - P_i(V, \delta) = 0 \tag{E.0.4}$$

$$Q_{gi} + C_{Qi} - Q_{load,i} - Q_i(V, \delta) = 0 \tag{E.0.5}$$

$$I_{mn} \leq I_{mn}^{max} \tag{E.0.6}$$

$$H_{load,i} \cdot C_{Pi} - C_{Qi} = 0 \tag{E.0.7}$$

$$0 \leq P_{gi} \leq P_{gi}^{max} \tag{E.0.8}$$

$$Q_{gi}^{min} \leq Q_{gi} \leq Q_{gi}^{max} \tag{E.0.9}$$

$$0 \leq C_{Pi} \leq P_{load,i} \tag{E.0.10}$$

$$0 \leq C_{Qi} \leq Q_{load,i} \tag{E.0.11}$$

$$V_i^{min} \leq V_i \leq V_i^{max} \tag{E.0.12}$$

$$-\pi \leq \delta_i \leq \pi \tag{E.0.13}$$

An explanation of the model is given below:

1. Same as for the DC model, Equation E.0.3 displays the objective function where the goal is to minimize the cost of load curtailments because the cost of rescheduling is set to zero. The vector of decision variables, [X], is divided into independent variables that are controllable (control variables): active and reactive power generation and load curtailments, and dependent variables (state variables): voltage magnitudes and voltage angles, yielding $[X] = [P_{g1}\ ...\ Q_{g1}\ ...\ C_P\ ...\ C_Q\ ...\ V_1\ ...\ \delta_1\ ...]$. Thus, [X] consists of 6k elements. The cost vector, [W], will have to have the same amount of elements. These will reflect the cost of active and reactive generator rescheduling and active and reactive load curtailments, $[W] = [w_1\ w_2\ ...\ w_{6k}]^T$.

2. Equation E.0.4 gives the active power balance requirement where P_{gi} is active power generation at bus i, C_{Pi} is the active load curtailment at bus i, $P_{load,i}$ is the active load requirement at bus i and $P_i(V, \delta)$ is the active power injection at bus i calculated by Equation E.0.1.

3. Equation E.0.5 gives the reactive power balance requirement. The notation is similar to that described for Equation E.0.4 except that all terms consider reactive power and the reactive power injection, $Q_i(V, \delta)$ is calculated by Equation E.0.2.

4. Equation E.0.6 says that the current flowing in a line, I_{mn}, is limited by the maximum current rating of the line, I_{mn}^{max}. The current flowing though a line $m - n$ is calculated by the voltage drop over the given line multiplied by its series admittance.

5. Equation E.0.7 is necessary to include because of the requirement of fixed power factors for the loads in case of load curtailments. $H_{load,i}$ is a value expressing the relationship between active and reactive power demand at each bus. The power factor will be constant if this relation is kept constant.

6. Equation E.0.8 says that the active power generation at bus i, P_{gi}, cannot exceed the maximum generating capacity of that bus, neither can it be negative.

7. Equation E.0.9 displays the reactive power generation limits of bus i, set by a minimum and a maximum value.

8. Equation E.0.10 says that the load curtailment of active power at a bus, C_{Pi}, cannot exceed the load requirement of that bus. Also, the load curtailment of active power cannot be negative.

9. Equation E.0.11 displays the same as Equation E.0.10 for load curtailment of reactive power

at a bus.

10. Equation E.0.12 gives the voltage requirements at each bus. More specific, the voltage magnitude, V_i, at each bus must be within a specified minimum and maximum value.

11. Equation E.0.13 defines the range for the voltage angles. It can be noted that the slack bus of the system will have a fixed angle of zero radians.

Appendix F

PEM Structure of Optimizing Consumer (24x24)

$$\begin{bmatrix}
\varepsilon_{ii} & \varepsilon_{ij} & \varepsilon_{ij} & \varepsilon_{ij} & \varepsilon_{ij} & \varepsilon_{ij} & \varepsilon_{ij} & \varepsilon_{ij} & \dots & \varepsilon_{ij} \\
\varepsilon_{ij} & \varepsilon_{ii} & \varepsilon_{ij} & \varepsilon_{ij} & \varepsilon_{ij} & \varepsilon_{ij} & \varepsilon_{ij} & \varepsilon_{ij} & \dots & \varepsilon_{ij} \\
\varepsilon_{ij} & \varepsilon_{ij} & \varepsilon_{ii} & \varepsilon_{ij} & \varepsilon_{ij} & \varepsilon_{ij} & \varepsilon_{ij} & \varepsilon_{ij} & \dots & \varepsilon_{ij} \\
\varepsilon_{ij} & \varepsilon_{ij} & \varepsilon_{ij} & \varepsilon_{ii} & \varepsilon_{ij} & \varepsilon_{ij} & \varepsilon_{ij} & \varepsilon_{ij} & \dots & \varepsilon_{ij} \\
\varepsilon_{ij} & \varepsilon_{ij} & \varepsilon_{ij} & \varepsilon_{ij} & \varepsilon_{ii} & \varepsilon_{ij} & \varepsilon_{ij} & \varepsilon_{ij} & \dots & \varepsilon_{ij} \\
\varepsilon_{ij} & \varepsilon_{ij} & \varepsilon_{ij} & \varepsilon_{ij} & \varepsilon_{ij} & \varepsilon_{ii} & \varepsilon_{ij} & \varepsilon_{ij} & \dots & \varepsilon_{ij} \\
\varepsilon_{ij} & \varepsilon_{ij} & \varepsilon_{ij} & \varepsilon_{ij} & \varepsilon_{ij} & \varepsilon_{ij} & \varepsilon_{ii} & \varepsilon_{ij} & \dots & \varepsilon_{ij} \\
0 & 0 & 0 & 0 & 0 & 0 & 0 & \varepsilon_{ii} & \dots & 0 \\
0 & 0 & 0 & 0 & 0 & 0 & 0 & 0 & \dots & 0 \\
\dots & \dots & \dots & \dots & \dots & \dots & \dots & \dots & \dots & \dots \\
0 & 0 & 0 & 0 & 0 & 0 & 0 & 0 & \dots & 0 \\
0 & 0 & 0 & 0 & 0 & 0 & 0 & 0 & \dots & 0 \\
\varepsilon_{ij} & \varepsilon_{ij} & \varepsilon_{ij} & \varepsilon_{ij} & \varepsilon_{ij} & \varepsilon_{ij} & \varepsilon_{ij} & 0 & \dots & \varepsilon_{ij} \\
\varepsilon_{ij} & \varepsilon_{ij} & \varepsilon_{ij} & \varepsilon_{ij} & \varepsilon_{ij} & \varepsilon_{ij} & \varepsilon_{ij} & \varepsilon_{ij} & \dots & \varepsilon_{ii}
\end{bmatrix}$$

Appendix G

Bus Indices for Increasing Elasticity Coefficients

Table G.1 shows the rest of the bus indices which are not displayed in Table 6.21. Only buses with index values different from zero are displayed in Table G.1.

Table G.1: Bus indices for increasing elasticity coefficients for the RTS obtained with the state sampling method, AC OPF and the RTP model considering the largest outage case.

Bus	e_{ii} = -0.1		e_{ii} = -0.3		e_{ii} = 0.4	
	LOLE [hours/year]	*EENS* [MWh/year]	*LOLE* [hours/year]	*EENS* [MWh/year]	*LOLE* [hours/year]	*EENS* [MWh/year]
3	0.0880	0.5928	0.0380	0.4498	0.0800	0.6146
5	0.0020	0.0956	0.0020	0.0930	0.0020	0.0918
6	3.2620	38.9188	3.1980	27.6406	3.1460	22.9342
7	3.4420	249.6365	3.4520	247.9779	3.4820	249.8561
8	0.0100	0.4309	0.0060	0.4003	0.0080	0.4050
9	6.3420	560.6240	3.2120	251.7026	4.1380	390.4580
10	1.8820	3.3522	0.8680	1.1624	1.3020	4.2286
14	6.3340	156.5738	3.2080	64.6992	4.1280	128.4958
15	0.0620	0.0062	0.0180	0.0018	0.0360	0.0038
18	0.3540	0.1652	0.1060	0.1420	0.2240	0.7370
19	6.2900	28.5246	3.1680	10.5822	4.0980	25.2844
20	0.0620	0.0072	0.0200	0.0026	0.0360	0.0062

Appendix H

Additional Examples of Nodal Prices

The case in Figure H.1 shows nodal prices and the price difference when a generator of 350 MW on bus 23 is on outage, and line between buses 8 and 9 is down. A line outage between buses 8 and 9 affects bus 7 in particular. The case in Figure H.2 shows nodal prices and the price difference when a generator of 350 and 155 MW on bus 23 are on outage, and line between bus 13 and bus 23 is down. Bus 13 is most affected in this last case.

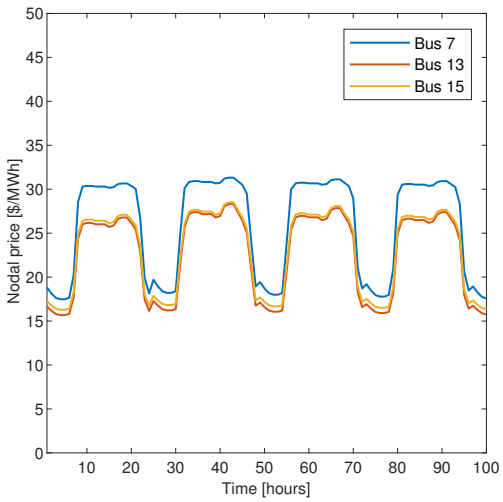

(a) Nodal prices at buses with all components up.

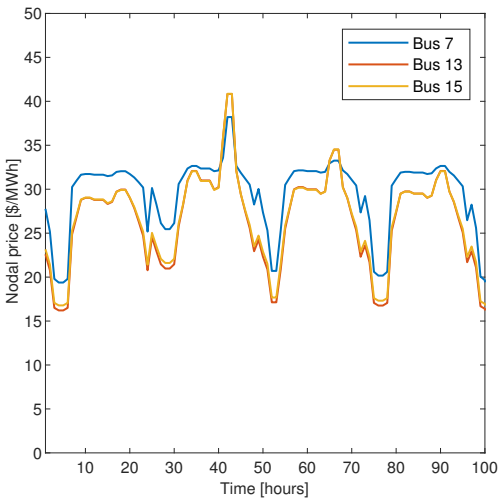

(b) Nodal prices with generator of 350 MW on bus 23 on outage, and line between bus 8 and 9 down.

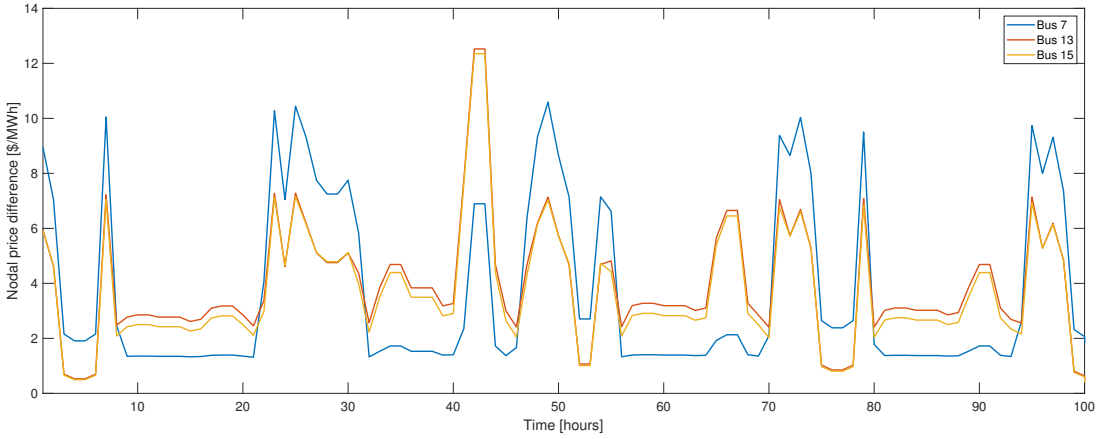

(c) Price difference in nodal prices.

Figure H.1: Varying nodal price difference at different load buses in the RTS. Additional example 1.

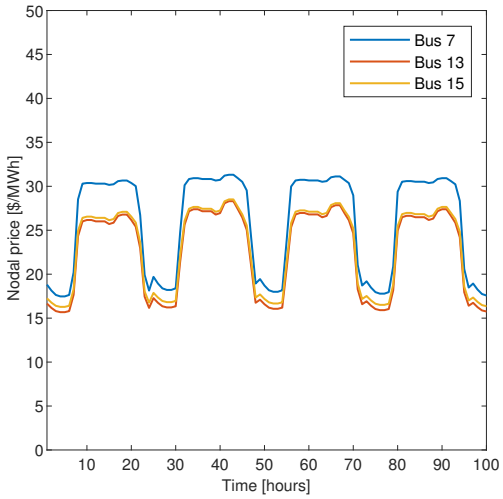

(a) Nodal prices at buses with all components up.

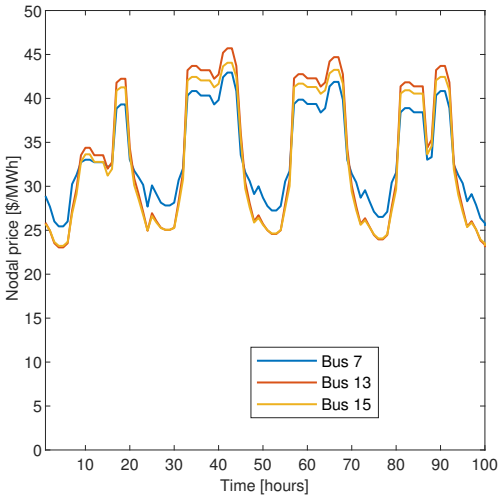

(b) Nodal prices with generator of 350 and 155 MW on bus 23 on outage, and line between bus 13 and 23 down.

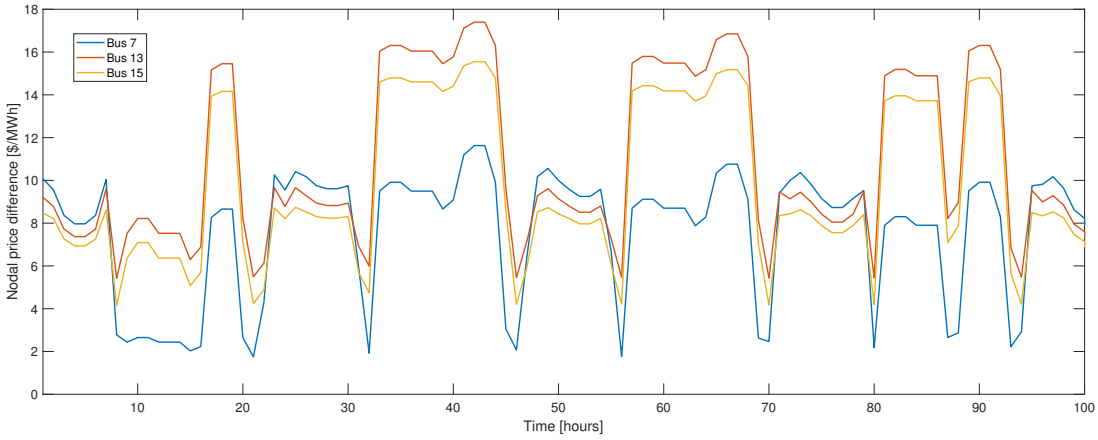

(c) Price difference in nodal prices.

Figure H.2: Varying nodal price difference at different load buses in the RTS. Additional example 2.

Appendix I

Software Codes

(Restricted Public Access)

Anette Solheim

Incorporating Demand Side Response in Power System Adequacy Studies

NTNU
Norwegian University of
Science and Technology